The Dissertation Committee for Kwang Jik Lee Certifies that this is the approved version of the following dissertation :

Investigation of the Photo-Induced Charge Transfer in Organic Semiconductors via Single Molecule Spectroscopy Techniques

Committee:

Paul F. Barbara, Supervisor

Ananth Dodabalapur

Xiaoyang Zhu

Graeme A. Henkelman

Brian A. Korgel

Investigation of the Photo-Induced Charge Transfer in Organic Semiconductors via Single Molecule Spectroscopy Techniques

by

Kwang Jik Lee, B.S.; M.S.

Dissertation

Presented to the Faculty of the Graduate School of
The University of Texas at Austin
in Partial Fulfillment
of the Requirements
for the Degree of

Doctor of Philosophy

The University of Texas at Austin
December, 2009

Dedication

To my parents and my Lord and Savior, Jesus Christ.

Acknowledgements

First of all, I would like to thank my Lord, Jesus Christ, who has always been with me throughout the entirety of these Ph. D. studies. He has been my help and strength so that I could successfully finish this work. I would also like to express my gratitude to my parents for their endless love, prayer, and support for me. I also cannot thank my uncle and aunt enough because they have encouraged and supported me to start and complete Ph.D. studies in the U.S. In addition, I would like to thank all my friends in my church-especially Deacon Lee-for their prayers for me and fellowship we shared in Jesus Christ.

Secondly, I would like to express my gratitude to my supervisor, Prof. Paul F. Barbara, for his enthusiastic guidance and support to my Ph.D. work in his lab. Under his guidance, not only have I learned about how to research with scientific thought, but also about the attitude of a researcher. Paul has been such a kind advisor with deep insights, an encompassing knowledge of science, and an enormous enthusiasm for the field.

Last but not least, I would like to expand my gratitude to my colleagues in Dr. Barbara's group. Sharing the knowledge and the experience as well as the friendship, with all members in Barbara's group has been an enormous help for me to complete my degree. Especially, Dr. Leonid Fredkin, Dr. Josh Bolinger and Dr. Rodrigo Palacios, who are all postdoctoral researchers, helped me greatly with developing the research projects during my Ph.D. studies. I would also thank Yalan and Jenny for the friendship of these last five years we shared as the same-year graduate students.

Investigation of the Photo-Induced Charge Transfer in Organic Semiconductors via Single Molecule Spectroscopy Techniques

Publication No._____________

Kwang-Jik Lee, Ph.D.
The University of Texas at Austin, 2009

Supervisor: Paul F. Barbara

Photo-induced charge transfer which occurs between molecules or different parts of a large molecule is the pivotal process related to performances of organic electronics. In particular, injection of charge carriers into conjugated polymers and dissociation of photo-generated excitons at the heterojunction between a donor and acceptor system are of great importance in determining the luminescence efficiency of organic light emitting diodes (OLEDs) and solar energy conversion efficiency of organic solar cells, respectively. However, the complex nature of organic semiconductors as well as complicated primary processes involved in the functioning of these devices have prevented us from understanding unique characteristics of these processes and thereby engineering better materials for higher performances. In this dissertation, two different types of photo-induced (or -related) charge transfer processes occurring in organic semiconductors were investigated by using single molecule spectroscopy (SMS) techniques to unravel the complexities of these processes. The carefully designed functioning capacitor-like model devices similar to OLEDs and photovoltaic cells were fabricated where isolated single nanoparticles were introduced as an active medium to mitigate the complexities of these materials. We observed that injection of positively charged carriers (holes) into poly[2-methoxy-5-(2'-ethyl-hexyloxy)-1,4-phenylene vinylene] (MEH-PPV) single nanoparticles from the carbazole hole transport layer does not occur in the absence of light. We denoted the observed hole injection in aid of light as the light-induced hole transfer mechanism (LIHT). It was revealed that the charging dynamics are highly consistent with a cooperative charging effect. In addition, the LIHT was proposed as the possible source for the formation of deep trapped hole in organic devices. Local exciton dissociation yields across a nanostructured domain between poly(9,9-dioctylfluorene-*alt*-benzothiadiazole) (F8BT) single nanoparticles and either poly(9,9- dioctylfluorene - co - bis-N,N- (4 -butylphenyl)-bis-N,N-phenyl-1,4-phenylene diamine) (PFB) or poly(9,9-dioctylfluorene-co-N-(4-butylphenyl)diphenylamine) (TFB) film in model photovoltaic devices was also investigated. A wide distribution of exciton dissociation yields was observed from each nanodomain due to the device geometry. The observed hysteresis in fluorescence voltage curve was ascribed to accumulated charges following charge separations. The dynamics of charge separation under the applied electric field was described in more detail.

Table of Contents

List of Tables

List of Figures

Chapter 1: Introduction

1.1 ORGANIC SEMICONDUCTORS (CONJUGATED POLYMERS)

Research on organic electronics that deals with conjugated polymers or small molecules has been growing rapidly due not only to intrinsic interest in molecular electronic materials but also due to the potential commercial impact of these materials [1-4]. As a result, this field, especially bright, high resolution flat-screen displays incorporated with organic light-emitting diodes (OLEDs), is about to have an impact on the commercial market for the first time. Enormous advantages of conjugated polymers such as ease in tuning electric properties by chemical design and synthesis, low cost processing based on low temperature processes, mechanical flexibility, and compatibility with flexible substrates have enabled them to be used as active materials in organic electronics such as OLEDs, organic photovoltaics, and organic thin film transistor (OTFT). However, further understanding in the fundamental physics of conjugated polymers is necessary for continuing progresses and thereby meeting market demand.

The electric properties of conjugated polymers are endowed from their π-conjugated system. Atoms in a conjugated system of an organic compound covalently bond with alternating single and double bonds (e.g., C=C-C=C-C) where π-electrons are not confined to a specific bonding but shared by contiguous atoms instead. These delocalized π-electrons move through π-electrons orbitals which overlap along the polymer backbone. The delocalization of the π-electrons in the p-orbitals of the atoms across the chain increases stability, which results in the lowered overall energy of the molecule [4]. Structures of the poly[2-methoxy-5-(2'-ethyl-hexyloxy)-1,4-phenylene vinylene] (*MEH-PPV*) and [poly(9,9 '-dioctylfluorene-*co*-benzothiadiazole)] which are well known conjugated polymers and also mainly used in this research, are shown in Figure 1.1. One of the unique characteristics of the conjugated polymers is their ability to absorb and emit light. The color of the conjugated polymers results from absorbing certain wavelength of visible light and transmitting or reflecting others. The visible light can be absorbed by chromophores which are the light-absorbing parts of a molecules and quasi-localized with a broad distribution on the polymer chain. When a molecule absorbs a photon of light, an electron in the ground state can be promoted to a higher excited energy level and leaves a hole behind, resulting in the formation of the exciton which is a Coulombically bounded electron-hole pair. The binding energy of the exciton in organic materials, as opposed to that of the inorganic counterpart which is a few tens of meV, is reported to be about one half electron volt [5, 6]. This large binding energy is another characteristic of organic materials and ascribed to their low dielectric constant.

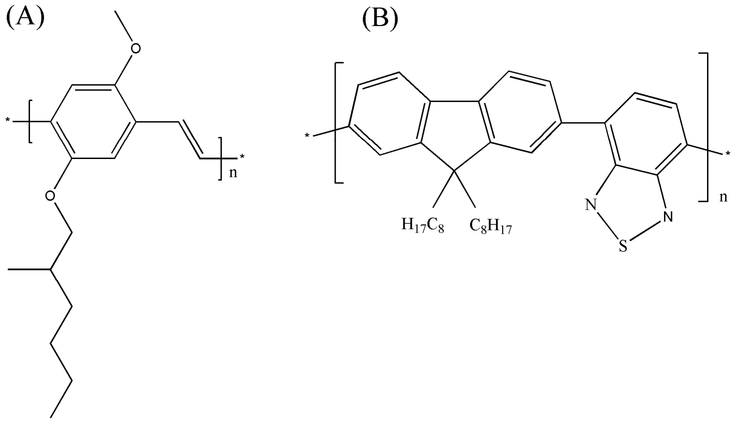

Figure 1.1: Molecular structures of conjugated polymers of (A) MEH-PPV and (B) F8BT

There are a few relaxation pathways for the excited electrons. First, they relax to their ground state while dissipating the photon energy they absorbed in the form of light (radiative relaxation). This luminescence called fluorescence occurs upon absorbing the photon energy. Second, they can decay without emitting light called non-radiative relaxation where the excitation energy absorbed dissipates as heat to the medium. Third, relaxation can occur via intersystem crossing where excited electrons in singlet excited states convert to triplet excitation states, resulting in formation of triplet excitons. This process is then followed by either phosphorescence or a secondary non-radiative relaxation step. Unlike fluorescence, phosphorescence is characterized by their slower radiation process which is due to the quantum mechanically forbidden energy state transition. These processes are summarized as followings:

1. Excitation of molecules: $S_0 + hv_{ex} \rightarrow S_1$
2. Fluorescence: $S_1 \rightarrow S_0 + hv_{em}$
3. Non- radiative relaxation (internal conversion): $S_1 \rightarrow S_0 + heat$
4. Intersystem crossing: $S_1 \rightarrow T_1 + heat$
5. Phosphorescence: $T_1 \rightarrow S_0 + hv_{ph}$
6. Non-radiative relaxation: $T_1 \rightarrow S_0 + heat,$

where, S_0 = ground singlet state, S_1 = lowest excited singlet state T_1 = lowest triplet state, h=Planck's constant, v_{ex} = frequency of excitation light, v_{em} = frequency of emission light and v_{ph} = frequency of phosphorescence light

However, relaxation of the singlet excited state (S_1) can occur through interaction with other molecules or external forces, resulting in fluorescence quenching. For example, hole polarons and impurities in the polymer such as oxygen (O_2) or residual water (H_2O) are well-known fluorescence quenchers [7, 8]. Fluorescence is also quenched by the dissociation of excitons at the heterojunction between two different donor/acceptor type materials. The exciton dissociation can be further facilitated by the help of the applied electric field. Therefore, monitoring the fluorescence quenching could provide useful information regarding physical phenomena occurring inside the polymer. In this research, we monitor fluorescence change of the system under various conditions to investigate important property of the conjugated polymer which is photo-induced charge transfer.

1.2 PHOTO-INDUCED CHARGE TRANSFER IN ORGANIC SEMICONDUCTORS

Charge transfer is the fundamental process occurring between molecules or different parts of a large molecule. Since charge transfer is closely related to the device functions such as luminescence efficiency of OLEDs and solar energy conversion efficiency, it is necessary to understand the nature of the charge transfer process in detail. Here two different types of charge transfer processes which take place in organic semiconductors are discussed.

1.2.1 PHOTO-INDUCED CHARGE INJECTION

Efficient charge injection into conjugated polymers is a central process in achieving organic light emitting diodes (OLEDs) with high performances. Since the first OLED was invented by Tang et al [9], current high efficiency of OLEDs has been achievable by incorporating several additional layers with active light emitting polymers. The roles of these additional layers, which are mainly hole or electron transport (or injecting) layers, are either to help charged carriers being more efficiently injected into the active layer or to balance the number of electron and hole charge carriers injected into the polymer, and thereby increasing the probability of electron-hole recombination, leading to high luminescence efficiency. The barrier for charge carrier injection into an organic semiconductor layer is generally ascribed to the combination of the two factors. The first is the offset of the energy levels between the two polymers. In the case of the hole injection, the difference in the highest occupied molecular orbital (HOMO) energies between a conjugated polymer and a neighboring hole transport layer plays an important role in determining the charge transfer. The other one is the modification of this energy level which is attributed to the surface dipoles or vacuum energy level shift. The accumulation of dipoles at the interfaces causes the bending of the energy band so that it can reduce (or increase) the energy barriers for charge injections.

In the first part of this research, we investigated the injection of hole charge carriers into the single molecule of MEH-PPV polymer via the single molecule spectroscopy (SMS) technique. It is shown that this process is highly related to light such that no hole injection occurs in the absence of the illumination. Injected hole carriers with the aid of light forms either shallowly trapped (mobile) moles or deeply trapped holes. Deep trapped holes are believed to affect the modification of the energy band when accumulated at the interfaces and thereby also the hole injection process. Despite their significant roles in the charge transfer process, deep trapped holes are not well understood how they are formed and why they are so persistent. The observed pronounced hysteresis due to the photo-induced hole injection from the cabazole hole transport layer into the polymer might suggest that the formation of the deep trapped holes are closely related to the photo induced hole transfer process.

1.2.2 PHOTO-INDUCED CHARGE SEPARATION

Photo-induced charge separation which occurs at the heterojunction between the donor and acceptor materials is a very important step in the solar cell mechanism because photon energy absorbed can be converted into potential energy by forming free electron and hole charge carriers through this process. However, due to the large exciton binding energy (~0.5 eV) which is the characteristic of organic semiconductors, it is not easy to dissociate excitons into free charged carriers. It is the internal electric field created by abrupt change in chemical potential energy between two polymers that provides the driving force for the charge separation. Photo-induced charge transfer (separation) occurs in the following sequence: Excitons which were created upon absorbing incident photon energy diffuse to the interfaces between donor and acceptor materials and then undergo charge separation. The electrons move to the acceptor and the holes remain in the donor as a result of the charge separation. However, it is also highly likely that these oppositely charged free carriers meet again and recombine with one another before they reach to corresponding electrodes.

The photo-induced charge separation takes place in the femtosecond time scale (~50 fs) and therefore has been studied using several spectroscopy techniques such as time resolved photoluminescence measurements, absorption spectra measurement and the two-pulse photocurrent correlation technique [10-13]. It has been considered to be a simple single-step electron transfer process from the donor to the acceptor material. However, recently it was reported that charge separation is a much more complicated process involving one or more intermediate states [10-15]. The existence of different types of charge transfer states were reported from several donor acceptor systems. One is characterized by its weak interaction with the ground state and the other is comprised of Coulombically bound germinate polaron pairs which either relax into an energetically favorable exciplex state or undergo charge separation at the interfaces.Since these intermediate states are places where either charge dissociation or also charge trap occurs, the yield of charge separation are believed to be affected by the existence of these states.

The yield of charge separation is also significantly affected by the morphology of the interfaces as well as the size of the nanostructured domains. External quantum efficiencies measured from the same blend system with different morphologies which were obtained by varying the solvent, the temperature of substrates and spin-coating conditions revealed that maximum photovoltaic efficiency of nearly one order of magnitude could be improved by controlling the morphology of the bulk heterojunction polymer film [16]. This change in morphology is also believed to be closely related to the domain size which varies from tens of nanometers or less up to tens of microns [16]. Due to the complexities of organic materials especially at the interfaces, however, a broad distribution of interfacial regions with different photovoltaic efficiencies has been reported.

In the second part of this research, the photo-induced charge separation process which occurs across the nanostructured domains between F8BT and PFB (or TFB) polymers in carefully designed modeled photovoltaic devices was investigated via single molecule spectroscopy (SMS) techniques. The fluorescence intensity quenching as a result of the exciton or geminate-pair dissociation under the applied electric filed was measured, providing useful information regarding the nature of these processes. Especially, we are interested in investigating the charge separation efficiency at the local nanoscale interfacial domain to obtain new molecular level information on the PV mechanisms.

1.3 FV-SMS TECHNIQUES

The tremendous complexity of organic materials has been a barrier to overcome for obtaining a molecular-level understanding of fundamental physics in organic electronics. The complexity for these materials results from a combination of several factors. First, interfacial regions of nanostructure materials have a complex molecular organization. Second, the static morphological disorder as well as the dynamic disorder due to a diverse set of species in nanomaterials such as singlet and triplet excitons, electron and hole polarons and various trapped sites further increases the complexity. At last, the physical process in these materials is intrinsically complex since it involves many individual primary processes. In reality, photoconductive AFM measurements performed on bulk heterojunction photovoltaic devices revealed that local photocurrent varies from area to area, indicating a wide distribution of interfaces with different photovoltaic efficiencies [17-19]. Therefore, a new technique has been required to unravel the complexities observed in these types of materials in order to provide better understanding for fundamental physical processes in organic electronics.

The SMS techniques are techniques which have extensively been utilized in our group as a powerful tool to unravel the complexity of organic materials [7, 8, 10, 20-22]. One good example showing the power of SMS is that the spectra taken from the high molecular weight of multichromophoric system of MEH-PPV single molecules provide a clear evidence for the efficient electronic energy funneling to a small number of low energy sites [23]. In bulk conjugated polymer, however, virtually all the emission occurs from the low energy sites only. Therefore these results nicely demonstrate the ability of SMS to unravel the complex “distribution” of localized emitting states in conjugated polymers. In this research, a complementary SMS tool which is the fluorescence voltage (FV)-SMS technique was used on a carefully designed single molecule hole injection devices as well as a modeled PV device to investigate the photoinduced charge transfer process in organic semiconductors. The core of this technique is that the modulation of fluorescence intensity is used as an indirect evidence for charge injection or charge separation processes.

Since direct electrical measurements of the small number of charges injected per single molecule are exceedingly difficult, an indirect single molecules fluorescence approach was applied in FV-SMS. The study is performed by exciting the single molecules with a laser and then monitoring the bias induced fluorescence intensity modulation to measure the small number of charge carriers injected into a single chain molecule. It was reported from the previous study in our group that one injected hole carrier quenches about 40% of the total fluorescence intensity and additional carriers injected quenches the same portion of the remaining fluorescence intensity. Therefore, complete quenching of the single molecules fluorescence indicates that 7~8 hole carriers are injected into a single molecule, revealing the capability of FV-SMS technique for the precise electric measurement [20, 24]. An example of the fluorescence intensity transient obtained while applying bias is shown as a function of the bias on the top (Figure 1.2 (A)) and the time averaged fluorescence intensity transient derived from the data above is on the bottom in Figure 1.2. The green line above in Figure 1.2 (B) represents one cycle of the applied bias in the experiment. Similarly, the photoinduced charge transfer process was investigated by recording the fluorescence quenching due to the exciton dissociation under the applied electric field.

Studies were performed using two different microscopes. One is an inverted confocal microscope and the other is a home built wide-field vacuum microscope. In both cases, single molecules in device geometry are excited with the 488 nm line of an ion laser while applying a bias using a programmable function generator. The bias induced fluorescence transients are monitored using an APD or CCD camera and synchronized for a better S/N ratio. The schematic of the confocal system and the structure of the hole injection device is shown in Figure 1.3.

1.4 DISSERTATION OVERVIEW

The photo-induced charge transfer process was investigated in this dissertation

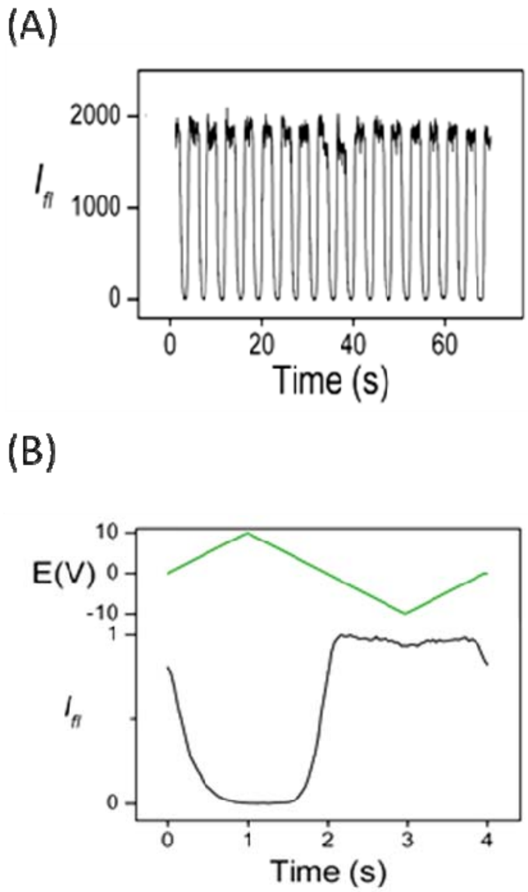

Figure 1.2: (A) Single molecule fluorescence intensity transient obtained while applying the triangular bias across the device. (B) Time averaged fluorescence intensity transient derived from the data shown in (A). The line above represents one cycle of the applied bias (scan rate of 10 V/s) in the experiment.

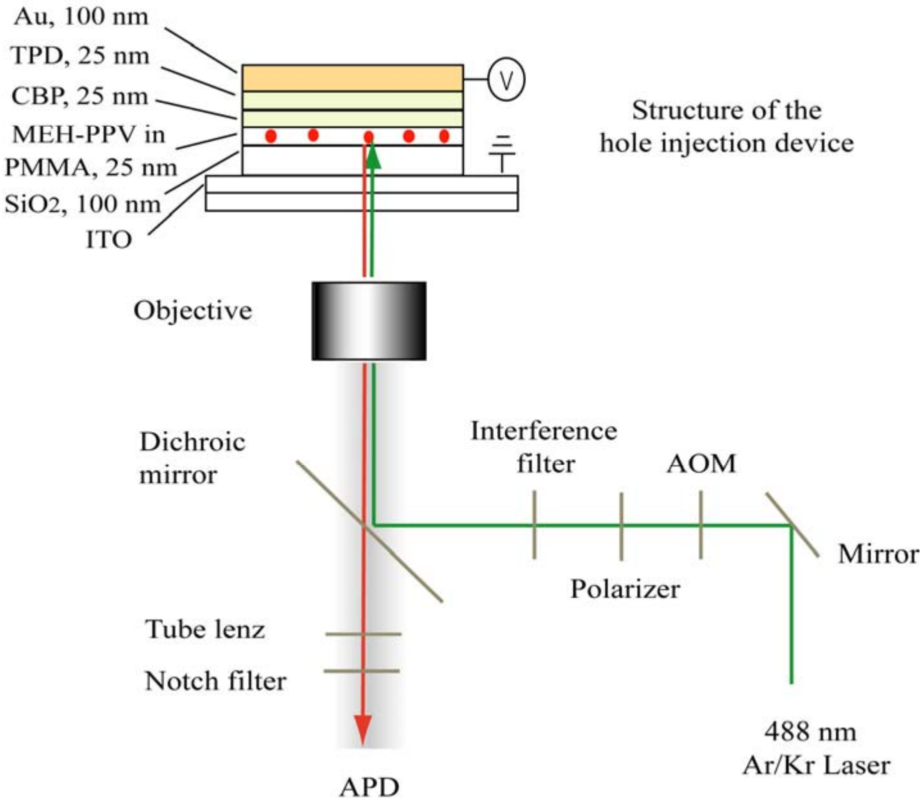

Figure 1.3: Schematic of the structure of the hole-injection device (upper) and experimental setup for the confocal microscope system (below).

which consists of 5 chapters. The first part of it is about photo-induced positive charge (hole) injection into single nanoparticles which include a single chain of molecule and self-assembled nanoaggregates embedded in metal-oxide-semiconductor (MOS) capacitor devices. The second part of it deals with photo-induced charge (exciton) separation at the nanostructured heterojunction between isolated nanoaggregates (donor) and a conjugated film (acceptor) in model photovoltaic devices. Each chapter includes the following contents:

Chapter 1 provides fundamental background knowledge regarding this research. The nature of conjugated polymers with their unique characteristics was described. Especially, two different types of photo-induced charge transfer processes occurring in organic semiconductors were explained with the necessity of new techniques for solving the complexity of these processes. FV-SMS as a powerful tool which can unravel these complexities was introduced followed by the overview of this dissertation.

Chapter 2 includes the work which was published to a journal with the title 'Light-assisted deep-trapping of holes in conjugated polymers'. The injection of hole carriers into a single conjugated polymer chain was investigated using a FV-SMS. Previously unreported light-assisted hole injection was introduced and assigned to a light-induced hole-transfer mechanism (LIHT). In addition, observed results were applied to an image-capturing device approach.

Chapter 3 includes the full paper published to a journal with the title 'Detailed investigation of light induced charge injection into a single conjugated polymer chain'. This chapter is a continuation of the previous chapter. The LIHT mechanism was described in more detail with a comparison with other single conjugated polymer devices or bulk film devices.

Chapter 4 expanded the LIHT mechanism applied to the single chain conjugated polymer system into the self-assembled nanoaggregate system which is almost identical to bulk polymers in morphological states. The observed charging/discharging results were also modeled with device simulations based on a continuum model using a commercial program.

Chapter 5 covers the second part of this research which is photo-induced charge (excitons) separation. It begins with a review over the current issues on the role of charge transfer states involved in the charge separation process. The measurement of local charge separation efficiency occurring across the nanostructured heterojunction domains between F8BT nanoparticle and a PFB (or TFB) conjugated film was described in details with results.

Chapter 2: Light assisted deep-trapping of holes in conjugated polymers

2.1 INTRODUCTION

The nature of positive charge carriers (holes) in organic conjugated polymers remains obscure despite decades of materials and device research [25-33]. Evidence suggests that there are at least two main types of holes, namely shallowly trapped (mobile) holes and deeply trapped holes (DTH) [34-36]. The consequences of positive charge trapping in organic devices are can lead to large enhancement [25, 37] or degradation [38, 39] of device performance. Previous work on organic light emitting diodes (OLEDs) and thin film transistors (TFT's) have shown that deep hole trapping is a common phenomena in organic electronics. Furthermore, DTH may be the cause of the extreme hysteresis that is commonly observed in the current (*i*) vs. voltage (*V*) curves for various types of organic electronics (also known as the bias stress effect). The origin of DTH has been the subject of some speculation with both intrinsic and extrinsic factors being evoked as the source of such trapping. Extrinsic factors include contamination by ion migration from other layers, residual impurities from the synthesis, and diffusion of O_2 and H_2O into the device [34-36, 40-47]. Intrinsic charge trapping theories include mid-gap-state filling, bipolaron formation, interfacial surface sites within the device, and molecular rearrangement [26-28, 30, 32, 37, 38, 48-53].

This paper investigates hole injection from a layer of a carbazole derivative (a strong organic hole-donor), into isolated, single-polymer chains of the conjugated polymer poly(2-methoxy-5-(2'-ethylhexyloxy)-1,4-phenylenevinylene) (MEH-PPV). Hole injection was studied using a fluorescence-voltage single molecule spectroscopy approach that has been developed by the Barbara group. By modulating both the fluorescence excitation light and device bias, it was determined that hole injection from carbazole into single chain MEH-PPV is a purely light driven process, leading to the efficient storage of charge on MEH-PPV. This concept of light induced single molecule charge storage is then adapted to demonstrate a novel image capture device.

2.2 RESULTS AND DISCUSSION

To study hole injection at the carbazole/MEH-PPV interface, multilayered, hole-only devices with a metal-insulator-semiconductor geometry were fabricated as shown in Figure 2.1A (See Materials and Methods). The energetics that govern charge injection and transport in the device are shown in Figure 2.1B, which shows the energy of the highest occupied molecular orbital (E_{HOMO}) relative to the work function of the electrode ($\phi_{\mathrm{ELECTRODE}}$) at positive bias (red-curve) and at zero bias (black curve) as a function of displacement from the gold electrode in the device. These curves were calculated by a commercial simulation program (SimuApsys 2007.3, CrossLight Software Inc.), which is based on a continuum solution of the Nernst and Poisson-Boltzmann equations using empirical parameters for the electronic properties of the materials [54]. The curves were calculated with a very small density of space charges in the device ($<10^{13}$ charges/cm^3), but when the device is allowed to thermally equilibrate, holes flow from the gold anode through an intermediate (Figure 2.1A) hole-transport-layer (HTL) comprised of *N,N'*-Bis(3-methylphenyl)-*N,N'*-diphenylbenzidine (TPD) through the second HTL, 4,4'-Bis(*N*-carbazolyl)-1,1'-biphenyl (CBP), into the conjugated-polymer molecule, which functions as a single-molecule “capacitor”. The simulation predicts about 2 holes per MEH-PPV polymer chain at equilibrium when V=10 V.

The experimental amount and rate of hole injection from the CBP HTL into individual polymer chains was monitored indirectly by single-molecule fluorescence spectroscopy combined with quenching measurements [8, 55, 56]. Single-molecule

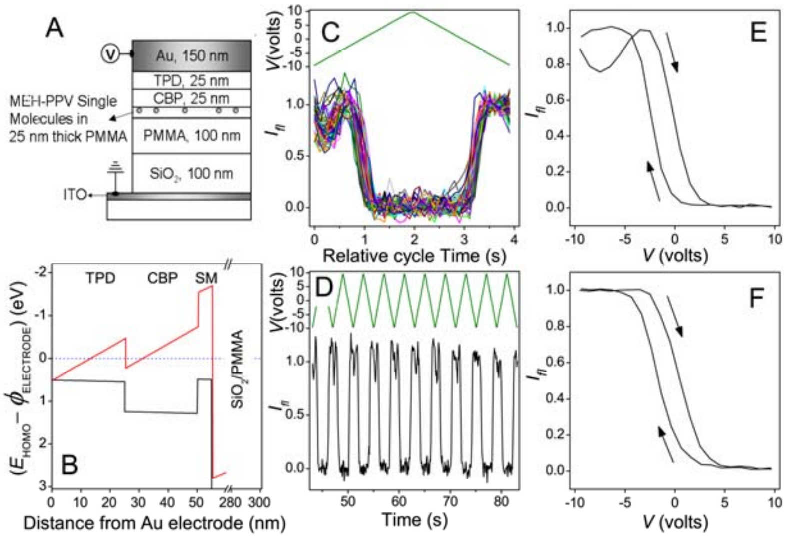

Figure 2.1: (**A**) Hole-injection device structure. (**B**) HOMO energy levels relative to the work function of the hole-injection electrode for the device shown in **A**. The black and red lines are Poisson-Boltzmann simulations at 0V (at equilibrium) and 10V (before charging) respectively. (**C**) Normalized single-molecule fluorescence-intensity trajectories obtained while applying a triangular bias (top green line). (**D**) Ensemble average of ~100 single-molecule normalized fluorescence-intensity trajectories obtained while applying a triangular bias (top green line) (**E,F**) Ensemble average of ~100 single-molecule F-V trajectories obtained at: high vacuum (10^{-5} Pa) (**E**) and 700 Pa of O_2 (**F**). Data shown in panels **C**, **E**, and **F** were obtained by synchronously averaging 25 triangular bias cycles at scan rate of 10 V/s, excitation intensity of 8.4 W/cm^2 (488 nm), and high vacuum (10^{-5} Pa) unless otherwise noted.

transients of the fluorescence intensity, I_{fl}, of the conjugated polymer were recorded as a function of time at constant laser excitation intensity while modulating the bias on the device with a triangle waveform (Figure 2.1C). Figure 2.1D shows the ensemble average of those single particle transients (>95% of the population) that exhibit bias-modulated hole-induced fluorescence quenching due to the injection of several holes. Previous results have shown that one charge induces a quenching of ~ 40%, and each additional charge quenches the remaining emission by a similar amount [8]. The ~ 5% of molecules that did not exhibit bias-modulated hole-induced fluorescence quenching showed a constant intensity for hundreds of bias cycles. The non-modulating fraction of molecules increased for samples that were prepared with thicker PMMA/MEH-PPV layers and therefore are assigned to MEH-PPV molecules that are not in electrical contact with the CBP layer.

Plots of I_{fl} vs. bias (denoted previously by the term fluorescence voltage single molecule spectroscopy, F-V SMS,) are presented for single molecules in Figure 2.2A-C and ensemble averages of the different molecules in Figure 2.1E-F, with arrows indicating the direction (positive or negative going) of the sweep of the bias during the cycle. The I_{fl} vs. bias data were highly reproducible from molecule-to-molecule and were time invariant during the averaging process. The data clearly show that the hole-injection/hole-removal process is highly hysteretic (kinetically controlled) for the fast bias sweep rates of 400 V/s. In contrast, at the slower sweep rate (10 V/s), the quenching dynamics are close to steady state (low hysteresis) for the moderate excitation intensities (~10 W/cm^2), but still hysteretic for the lowest excitation intensities (<0.5 W/cm^2). The switch from steady-state to kinetically controlled charging with increasing sweep rate is especially clear in Figure 2.2D which shows how the bias at which 50% of the intensity drops or recovers ($V_{1/2}$) varies as a function of sweep rate for the positive going

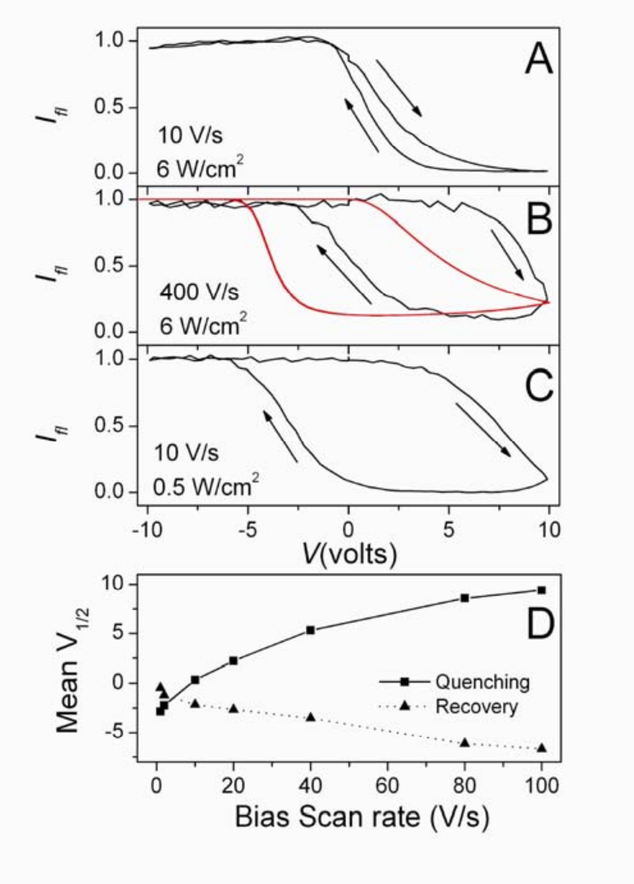

Figure 2.2: (**A, B, C**) Single-molecule fluorescence-intensity trajectories obtained while applying a triangular bias across the device with the scan rate and light intensity indicated in the panels for each transient. Measurements were performed in a confocal fluorescence microscope. The red line in (**B**) represents results from a charging model as described in the text. (**D**) Average $V_{1/2}$ as a function of bias scan rate for 100 molecules with an excitation intensity of 8.4 W/cm^2. Measurements were performed in a wide field vacuum microscope operated at a pressure of 10^{-5} Pa.

(quenching) and negative going (recovery) sweep.

The intensity scale in the Y-axis of these graphs is normalized to the maximum of I_{fl} during the cycle. It was verified that the maximum I_{fl} during the cycle is equivalent to the intensity recorded by holding the sample at negative bias for long times, i.e. it corresponds to a hole-free polymer chain. In addition to the predominant quenching due to hole injection at positive bias, a smaller "intensity dip" is observed in some ensemble averages of the I_{fl} curves at negative bias, e.g. Figure 2.1E. The dip is assigned to the quenching of singlet excitons by triplet excitons in the chains [57] rather than quenching by injected holes. Triplet excitons are more efficiently quenched by holes than singlet excitons [7] consequently at lower hole concentrations (negative bias) triplet quenching occurs but singlet quenching by holes is insignificant. At these biases the concentration of holes in MEH-PPV is sufficiently low, allowing the triplet population to recover and thus result in singlet quenching due to triplets. This is supported by the data in Figure 2.1F which was recorded with a wide-field microscope with a vacuum chamber sample holder. The fluorescence "dip" is absent when the conjugated-polymer molecules are exposed to a small partial pressure of dry oxygen (700 Pa) which quenches triplets by inducing intersystem crossing (see Figure 2.1F) but returns when the oxygen is depleted by evacuating the sample chamber or when the chamber is back filled with nitrogen (not shown).

We assign the injection of holes reported herein to a previously unreported light-induced hole-transfer mechanism (denoted by LIHT) involving light-assisted injection of holes from the CBP layer into single MEH-PPV polymer chains. As shown below, the hole injection apparently involves charge transfer from a CBP hole to a MEH-PPV singlet exciton at the CBP/MEH-PPV interface, perhaps additionally involving the formation of a DTH. Direct evidence that the optical excitation contributes to the charge injection is found in Figure 2.3A, which portrays synchronously averaged I_{fl} vs. time curves for a single molecule recorded with modulation of both the sample bias (square-wave modulated between -6 V and 6 V) and the light intensity (1-s pulse). During the negative bias portion of the cycle (not shown) the sample is allowed to rest with optical excitation for a sufficiently long period to remove all holes. At t = 0 s, the light is switched off and the bias changed to positive, and then at 1.002 s, the excitation is switched on. The I_{fl} vs. t curve begins at unity showing that no charge-injection occurs in the dark despite the positive bias. The depth and rate of the intensity decay (inverse decay time, τ) significantly increases with increasing excitation light intensity, demonstrating that the charge injection processes is light assisted (see below). This is supported by the increase in hysteresis in the I_{fl} vs. t data with decreasing light intensity, as shown by comparing Figure 2.2A with Figure 2.2C.

Further evidence that the charge injection by the LIHT mechanism involves CBP holes is found in Figure 2.3B which shows how τ varies with bias at constant light intensity. Here the bias was scanned slowly in a triangle waveform and the light intensity was pulsed on at a specific voltage during the scan. The decay occurred rapidly over a narrow bias range, so the data in Figure 2.3B (black points) is essentially a study of how the time scale for charge injection occurs as a function of bias. Calculations of the charge density in CBP using the SimuApsys program (see above) simulations predict that the steady-state (equilibrium) charge density of holes D in the CBP and TPD layers is extremely low at negative bias ($<10^{13}$ holes/cm^3) but increases monotonically at 10 V bias to $\sim 10^{18}$ holes/cm^3. Thus, combining information from the simulations and the data in Figure 2.3B, we can plot τ as a function of charge density of the CBP layer (Figure 2.3B, red points), and we can conclude that the charge injection requires both CBP holes and singlet excitons, consistent with the LIHT mechanism. A similar trend is observed

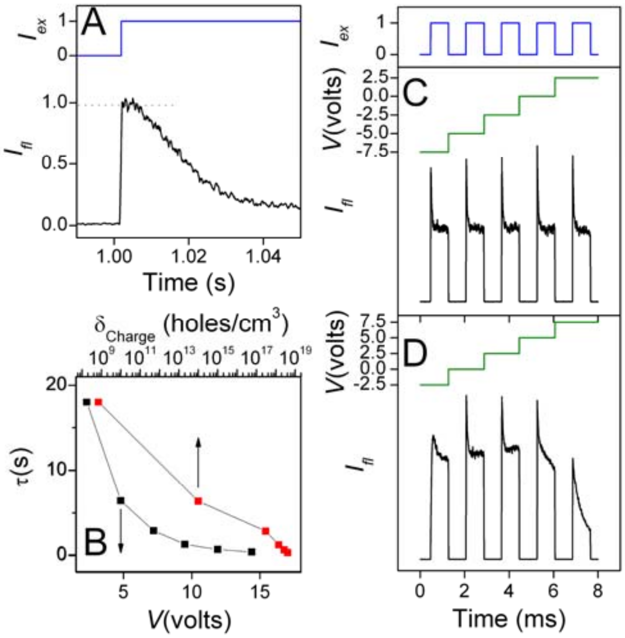

Figure 2.3: (**A**) Synchronously averaged single-molecule fluorescence-intensity time transient (black curve) obtained while applying a 6V bias across the device (t = 0 on the time axis corresponds to the beginning of the positive bias pulse) with the shown light pulse sequence (blue curve). The device was discharged at negative bias between each light pulse cycle (not shown). (**B**) Single-molecule fluorescence decay time constant, τ, as a function of applied bias (black data points) and CBP charge density (red data points) with 0.1 W/cm^2 of excitation intensity. (**C,D**) Fluorescence-intensity transients obtained while modulating the light and bias during each cycle. The light pulse consists of five 200 W/cm^2 intensity pulses as shown by the blue curve. The bias was increased stepwise in 2.5 V increments as shown by the green curves. The black curves are the corresponding single-molecule fluorescence-intensity trajectories where the bias ranged from -7.5 to 2.5 V (**C**) and from -2.5 to 7.5 V (**D**).

for τ vs light intensity at constant bias (results not shown), with τ decreasing with increasing light intensity, further suggesting the light induced nature of the hole injection process.

Figure 2.2B compares the experimental F-V data with kinetic simulations (red-lines) based on a simple version of the LIHT mechanism assuming a hole injection rate which is proportional to the product of the light intensity and the CBP hole density. While many of the qualitative features of the data are addressed by the simulations, the experimental F-V data clearly exhibits a more rapid dependence of the rate of hole-injection on bias and time than predicted by the simulations. In fact, the experimental data has a box-like appearance consistent with a charging process that occurs rapidly over a narrow bias range. While a more sophisticated model that accounts for the density of states of the material may produce better agreement, the deviation from theory and experiment may be due to a cooperative hole injection mechanism. The kinetics of charging the CBP layer may also affect the observed quenching dynamics in these bias sweep experiments. However, the cooperativity model is consistent with the shape of I_{fl} vs t at constant bias and light intensity (Figure 2.3A) which exhibits an induction period over a broad range of conditions, also suggesting cooperative hole injection i.e. the rate of hole injection increases at early times as holes are added.

The single-polymer chain charging process is sufficiently hysteretic that charge can be reproducibly "stored" on a single-polymer chain at intermediate bias (4 V) for long periods (>40 s, in the dark), in analogy to an electronic memory [8]. Results from an imaging version of this experiment are shown in Figure 2.4, where a device with a high concentration MEH-PPV layer is used to capture a simple image, i.e. "UT", which is later read by fluorescence. In this experiment, first the sample is "erased" (discharged) at negative bias during irradiation with a uniform intensity light pulse. This is followed by a “write” stage in which the UT mask is introduced to the beam path and a positive bias is applied during which MEH-PPV molecules in the brighter regions are charged. Finally, the image is “read” at moderate bias with a uniform light pulse. Only the regions that are dark in the “write” stage exhibit bright fluorescence during the read cycle. The sequence was repeated for many minutes by erasing the image at negative bias with a uniform intensity light pulse.

The role of triplets in the charge-injection mechanism was investigated by synchronous modulation of the excitation intensity and electrical bias, see Figures 2.3C and 2.3D. For a bias range too low for charge injection to occur, only intensity modulation due to triplet quenching of singlet excitons is observed associated with triplet population build-up[7]. In contrast for the same molecule with a bias range sufficiently high to inject holes from the CBP layer (Figure 2.3D), quenching due to both triplet excitons and holes is observed but not simultaneously. These data demonstrate that the triplet lifetime is significantly reduced at biases and times before hole-induced fluorescence quenching occurs. It is therefore unlikely that triplets are responsible for the major portion of the LIHT mechanism; rather singlet excitons are the more likely precursor to charge injection.

Various types of devices have shown similar effects as those observed here [25, 37-39]. To test the generality of this phenomenon, devices with a different conjugated polymer were tested. F8BT single molecules in these hole only devices show similar charging properties, but at higher biases, consistent with the higher HOMO energy of F8BT compared to MEH-PPV [58, 59]. Apparently, the thermodynamic barrier for hole injection into a conjugated polymer molecule is overcome through a excited-state charge-transfer mechanism between conjugated-polymer singlet excitons and CBP holes to create a large excess population of shallowly trapped holes. This may be followed by

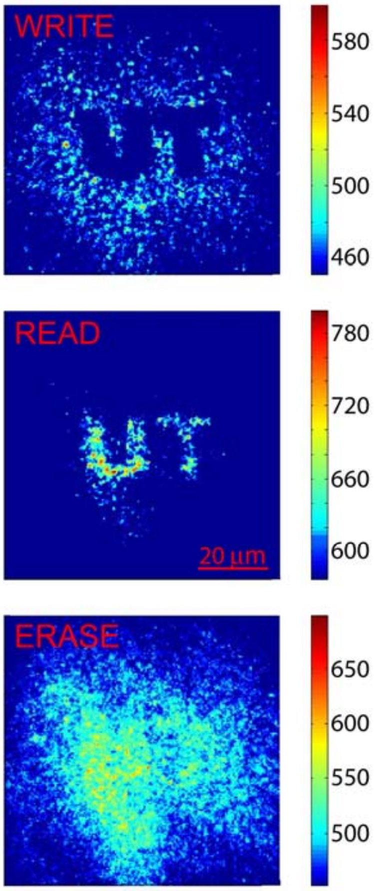

Figure 2.4: Demonstration of image capture using a single-molecule hole-injection device (structure Figure 2.1A) with a relatively high MEH-PPV areal density (>5 molecule/μm^2). Intensity scale bars representing the CCD camera intensity are shown to the right of the images.

thermally activated deep hole trapping [30], or alternatively, light may also participate directly in the trapping process by converting shallowly trapped holes through a photochemical process to DTH, perhaps involving light-induced deprotonation of shallowly trapped holes. With more than 95% of the studied molecules demonstrating identical behavior in a carefully controlled environment (under high vacuum ~10^{-5} Pa), this suggests that the observed trapping phenomena is not due to contamination but it is an intrinsic phenomena of the material, thereby necessitating a more thorough understanding of the mechanism. The apparent observed cooperativity for hole injection implies a dependence of the hole-injection rate on previously injected holes. Perhaps the charging-stress and/or optical "stress" during the early periods of excitation induce a conformational change which lowers the effective E_{HOMO} thereby promoting subsequent charge injection, thus effectively deforming the electronic properties of MEH-PPV. Alternatively, the formation of DTH may be accelerated by hole/hole interaction, perhaps involving bipolaronic like intermediates [27].

2.3 MATERIALS AND METHODS

2.3.1 SAMPLE PREPARATION

The device used for single molecule charge injection was a large area multilayer structure, as shown in Figure 2.1A. The device was fabricated bottom-up on a patterned indium tin oxide (ITO) coated quartz coverslip (Evaporated Coatings, Inc., sheet resistance of 110 Ω/□) using previously described procedures [56], with any changes noted below. Briefly, SiO_2 was deposited by inductively-coupled plasma chemical vapor deposition (ICP-CVD) at 200° C (Oxford instruments, Plasmalab 80plus) for a film thickness of 70 nm as an insulating layer. The remaining device fabrication was performed in a dry N_2 environment (O_2 and H_2O concentrations below 5 ppm). A 100-nm poly(methyl methacrylate) (PMMA, Sigma Aldrich, M_w =101 kg/mol) was deposited by spincoating from toluene (Sigma Aldrich, anhydrous 99.8%) to isolate single molecules of MEH-PPV (Uniax, M_w = 1000 kg/mol) from the SiO_2 layer. PMMA/MEH-PPV layers were deposited by spincoating from toluene with variable thickness (see figure caption), and the MEH-PPV concentration was adjusted to obtain an areal density of ~ 0.5 molecules/μm^2 in the sample unless otherwise noted. Thermal evaporation was used to deposit the hole transport layers, 4,4'-*N*,*N*'-dicarbazole-biphenyl (CBP) (Sigma Aldrich, 98%), and *N*,*N′*-bis(3-methylphenyl)-*N*,*N′*-diphenylbenzidene (TPD) (Sigma Aldrich, 99%), and for the gold electrode (Cerac, 99.99%). Thermal depositions were carried out at 10^{-4} Pa and typical rates were 1 Å/s as measured by a quartz crystal microbalance. Thicknesses for these layers were 25 nm for CBP and TPD and 50 nm for Au. All layer thickness measurements reported here were confirmed by atomic force microscopy (Digital Instruments, Dimension 3100) and/or ellipsometry (J A Woollam Co. Inc.,M-2000). For experiments in the vacuum microscope that were conducted to explore the role of oxygen, a porous 10-nm electrode was used to aid in oxygen diffusion into and out of the sample. All samples for the vacuum microscope were transferred in airtight vessels to minimize exposure to atmosphere prior to entry to the vacuum chamber which was prefilled with ultra high purity argon (Matheson Tri-Gas) or nitrogen (Praxair). For experiments performed in the confocal microscope apparatus, devices were wired and packaged in an inert environment to exclude water and oxygen (see confocal section below).

2.3.2 WIDE-FIELD MICROSCOPE

The experimental apparatus is a home-built wide-field vacuum microscope. The vacuum chamber is equipped with a mechanical rotary pump (Edwards, II3GDT4X) coupled to a turbo-molecular pump (Varian, Turbo-V 81-M) capable of achieving a base pressure of 10^{-5} Pa. The pressure inside the chamber is monitored by a combination of ionization and convection gauges (InstruTech, IGM-410 and CVM-221). Where the effect of oxygen was studied, the chamber was closed off from the vacuum pump using a gate valve, and ultra high purity gases [O_2 (Air Liquide) and N_2 (Praxair)] were introduced into the vacuum chamber in a controlled manner from prefilled glass flasks using a bleed valve. Excitation and fluorescence are coupled into and out of the chamber through a quartz viewport, with all optics except for the microscope objective (Zeiss, LD Achroplan 40x/0.6NA Corr) positioned outside the vacuum chamber. Sample focusing is achieved using a closed-loop piezoelectric drive (Piezosystem Jena, MIPOS 100).

Laser excitation and fluorescence detection are performed in an epi-illumination/detection geometry. The excitation light was provided by a multiline argon ion laser (Melles Griot, 35-LAL-030). The multiline laser beam was spectrally resolved using a prism to spatially isolate the 488-nm line and then further filtered using a narrow pass 488-nm interference filter (Chroma). The beam was then coupled into a single-mode fiber to improve spatial beam quality, expanded to a beam size of ~7 mm ($1/e^2$), and focused on the back aperture of the objective using a AR-coated achromat lens (Edmund Optics, f=400mm). The resulting beam size at the sample was ~65 μm ($1/e^2$). Neutral density filters were employed to attenuate the laser light intensity at the sample over a large range (0.001 to 100 W/cm^2). A quarter-wave plate was introduced to produce circularly polarized light. The fluorescence is separated from the excitation by a dichroic mirror (Chroma, Z488RCD) and a holographic notch filter (Kaiser, SuperNotch-Plus™ 488nm) and imaged onto an electron multiplying CDD (Andor, iXon^{EM}+ DU-897) using an AR coated achromat lens (Zeiss, f=120mm). CCD images were acquired and compiled by the commercially available program Metamorph. For both the linearly scanned and pulsed F-V experiments the timing of the collection of the fluorescence images was synchronized with a time-varying electrical bias *V(t)* applied to the sample by a programmable function generator (Wavetek, 29A). The time dependence of the fluorescence intensity of individual fluorescence "spots", each due to a single MEH-PPV molecule, were determined from a set of acquired images using an image analysis program that was home-written in Matlab. Transients of individual molecules or ensembles of many molecules are time-averaged traces obtained from multiple (25-200) bias cycles unless otherwise noted.

2.3.3 CONFOCAL MICROSCOPE

The apparatus has been explained in detail elsewhere[60] and any changes made are noted below. The experimental apparatus is a modified Axiovert 100 microscope equipped to perform scanning confocal microscopy. The microscope objective used was a Zeiss Achrostigmat 100x/1.25NA oil immersion objective. Excitation was performed with the 488-nm line of an argon ion laser that was intensity modulated by an acoustic optical modulator (IntraAction Corp.). Neutral density filters were employed to reduce the laser light to powers appropriate for single molecule spectroscopy, typically 0.1-12 W/cm^2. A quarter-wave plate was introduced to produce circularly polarized light. The beam was expanded to slightly overfill the back aperture of the objective and then focused to a diffraction-limited spot size of 250 nm on the sample. Stray laser excitation is removed from the fluorescence through the use of a dichroic beamsplitter and a 488-nm notch filter (Chroma). Separate programmable function generators (Wavetek, 29A) were used to control the optical modulation and the applied bias across the single molecule device. Fluorescence emission is detected by an avalanche photodiode (APD) (Perkin-Elmer Single Photon Counting Module) and the transient signal from the detector is recorded with a multichannel scalar (MCS) that is synchronized to both excitation sequence and applied bias. Two separate MCS boards were used; single shot transients were recorded using a Becker Hickl MCS (model PMS-400) to confirm the stability of the single molecule fluorescence emission over the course of the measurement and time-averaged experiments were recorded using a FAST ComTec Gmbh MCS (model MCA-3). All data presented from the confocal microscope are time-averaged transients of a single molecule where the bias sequence has been repeated many times (100-1000 cycles, determined by S/N). The time-averaged transients were either taken directly from the MCS board in accumulation mode or were processed using a home-written Matlab program.

In a typical experiment, a scanning confocal fluorescence-intensity image was acquired to locate a single molecule then the stage was translated such that a single molecule was positioned in the focal area of the microscope to collect the emission transient. Samples were packaged using epoxy and a glass coverslip in a dry nitrogen environment, inhibiting oxygen and water diffusion into the sample. Samples without packaging showed poor photostability and were unsuitable for long-timescale measurements. Due to the high stability of conjugated polymers in an oxygen and water free environment, transients can be acquired for thousands of seconds before photobleaching. All samples were immediately returned to the glovebox following interrogation to further prevent infusion of oxygen and water.

Chapter 3: Detailed investigation of light induced charge injection into a single conjugated polymer chain

3.1 INTRODUCTION

Positive charge carriers (holes) have been broadly reported to be energetically trapped in organic materials and devices. However, the consequences of charge trapping and the nature of the trapping process itself remains poorly defined, despite decades of investigation. For example, the poly(phenylene vinylene) (PPV) class of polymers form shallow and deep traps with energies of 0.1-0.2 and 0.6-0.8 eV, respectively, above the highest occupied molecular orbital levels of these polymers[34-36]. The consequences of positive charge trapping in the layers of organic devices are difficult to predict; indeed large enhancement[25, 37] and degradation[38, 39] of device performance have been reported in different cases. Previous work on devices comprised of conjugated polymers in organic light emitting diodes (OLEDs) and thin film transistors (TFT's) have shown that deep hole trapping is a common phenomena in organic electronics.

Reports of charge trapping in F8BT OLEDs have been observed where the continuous driving of a device resulted in the steadily increasing efficiency of the LED over time[25]. The enhancement was found to persist for up to 24 hours if the device was stored in a nonbiased state. The enhancement was attributed to charge trapping at the hole injection electrode interface where holes becomes deeply trapped. It was further proposed that DTH paired with electrons are responsible for interfacial dipoles that distort the hole transport band sufficiently to allow for tunneling injection of holes and also enhancement of electron injection at the nearby electron injection electrode. In a different example, polythiophene thin-film-transistors (TFTs) have been reported to exhibit current loss due to hole trapping, which reduces the number of mobile carriers in the transistor channel[27, 38]. Using the current-loss as an indirect measurement of hole trapping, it was determined that the stressing rate as defined by the threshold voltage shift was proportional to the initial hole concentration. Electron force microscopy (EFM) measurements performed on pentacene TFT's have shown that trapped holes are highly localized within the device and the rate of formation of these trapped charges are delayed relative to the application of the gate bias and are strongly dependent on the initial concentration of shallow holes.[26, 30]

Several mechanisms for the formation of hole traps have been proposed. Chemical doping of the organic layer has been suggested as a source for DTH. Possible contaminants such as O_2 and H_2O, residual impurities from the synthesis, and ion migration from other layers have been implicated in the formation of trap sites[34-36, 41-45, 61-63]. Others suggest that the trapping occurs due to interfacial surface sites located within the device[37, 52, 64]. A distinct alternative is that the traps are an intrinsic property of the material. Some of the proposed mechanisms for the origin of intrinsic traps include molecular rearrangement, bipolaron formation, and mid-gap-state filling[26-28, 30, 38, 48-50, 65].

We have recently reported that trapped holes can be formed by a light-injected hole transfer mechanism (LIHT) in a single conjugated polymer chain as monitored by fluorescence-voltage single molecule spectroscopy (F-V/SMS) techniques[66]. The light assisted charge injection was shown to be highly cooperative with regard to the number of injected holes, implying the need for the reorganization of the polymer system to accommodate the charge, indeed it was observed that all charge injection into single chain polymers occurs through the light aided injection. The LIHT may be responsible for the poorly understood build up of trapped charge in some organic electronic devices, and this effect may have important consequences for the rate of charge injection and overall device efficiency in OLED device performance. It is interesting to note that the intensities used in our experiments result in excitation rates similar to those witnessed in state of the art OLEDs[66]. Our report may be related to the report of the light driven nature of trap filling in certain conjugated polymers[37], i.e. OLEDs comprised of MEH-PPV films were shown to undergo device enhancement following a brief treatment with white light illumination while being forward biased. This enhancement has been attributed to deep trap filling near the anode and the resulting space charge aided in electron injection into the device by lowering the Schottky barrier present at that interface, helping to balance the mobile carriers in the device, improving recombination in the emitting layer.

In this paper, we present new fluoresce-voltage single molecule spectroscopy (F-V/SMS) results on hole injection into conjugated polymers. We also analyze and discuss the previously reported data from our group in much greater detail.

3.2 EXPERIMENTAL SECTION

3.2.1 SAMPLE PREPARATION

The hole injection devices utilized a large area (1 cm^2) multilayer metal-insulator-semiconductor (MIS) structure as shown in Figure 3.1A. The device was fabricated bottom-up on top of a patterned indium tin oxide (ITO) coated coverslip (Evaporated Coatings Inc., sheet resistance of 110 Ω). The dielectric layer was SiO_2, grown with inductively-coupled plasma chemical vapor deposition (ICP-CVD) (Oxford instruments, Plasmalab 80plus) at 200° C with a thickness of 70 nm through a shadow mask. Poly(methyl methacrylate) (PMMA, Sigma Aldrich, M_w = 101 kg/mol) and poly(2-methoxy-5-(2’-ethylhexyloxy)1,4-phenylenevinylene) (MEH-PPV, Uniax, M_w = 1000 kg/mol) were deposited by spin casting from toluene. The bottom PMMA layer served to isolate MEH-PPV from the SiO_2 layer. Previous work done on a similar system with an

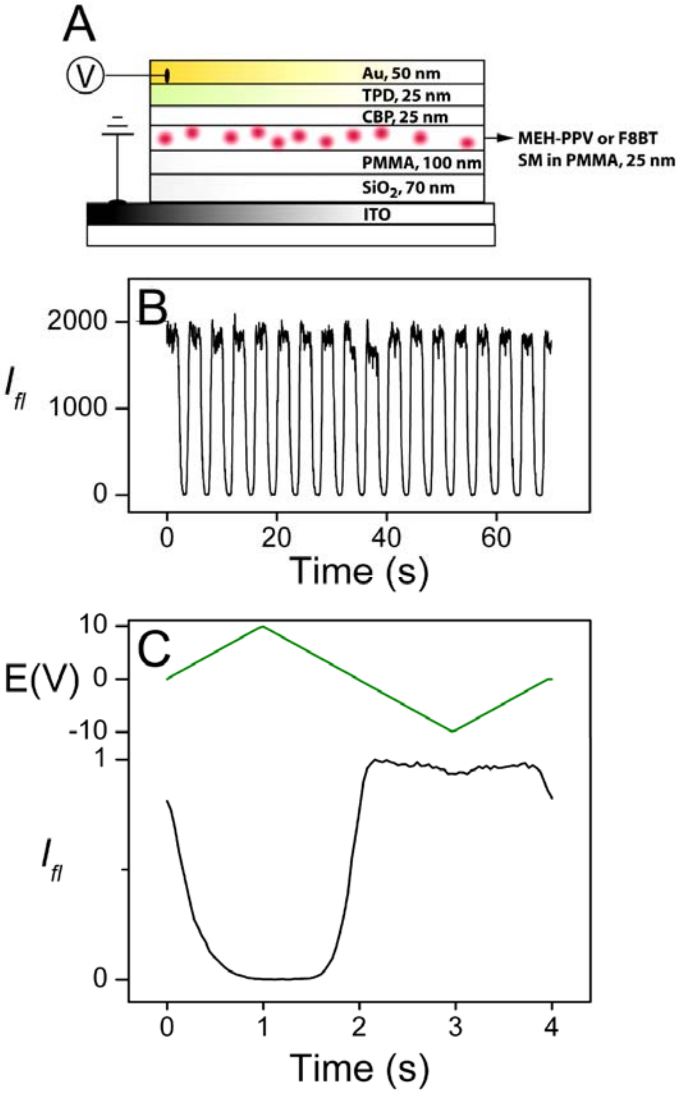

Figure 3.1: (A) Schematic of the hole-injection device structure used in these experiments. (B) Single molecule fluorescence intensity transient obtained while modulating the bias across the device. (C) Time averaged fluorescence intensity transient derived from the data shown in (B). The green line represents one cycle of the applied bias (scan rate of 10 V/s) in the experiment. The presented curve is an average of 40 4-s cycles using a light intensity of 6 W/cm^2.

SiO_2 that was deposited via ebeam evaporation reports an inherent photoinstability of single molecules at the SiO_2 surface. Single chain MEH-PPV was imbedded in a 25-nm thick host matrix of PMMA to prevent aggregation, and the concentration of MEH-PPV was adjusted such that the areal density of the fluorophore was 0.5 molecules/μm^2. The hole transport layers 4,4'-*N*,*N*'-dicarbazole-biphenyl (CBP) (Sigma Aldrich) and *N*,*N*'-bis(3-methylphenyl)-*N*,*N*'-diphenylbenzidene (TPD) (Sigma Aldrich) were employed in these devices. Both hole transport layers were deposited with thermal deposition under high vacuum (10^{-6} Torr) at a rate of 1 Å/s for a thickness of 25 nm for each. Comparison devices were fabricated with 50-nm layers of TPD as the only HTL. Gold was chosen for the top contact and was also thermally deposited with a typical rate of 2 Å/s. Patterning of all the thermally deposited layers was accomplished through the use of shadow masks. The resulting devices contained four independent 15-mm^2 active areas.

All device fabrication was performed in a glovebox environment (O_2 and H_2O concentrations below 5 ppm) except for the SiO_2 deposition where exposure of the substrate to atmosphere was necessary. Devices were wired inside the glovebox using silver paste and then packaged using epoxy and a coverslip. When unsealed the devices were interrogated, the single molecule fluorescence showed a gradual photobleaching whose rate was found to be strongly light dependent. Packaging of the devices lead to enhanced single molecule fluorescence stability, allowing for individual molecules to be studied for more than an hour without significant photobleaching being observed. All devices were immediately returned to the glovebox following interrogation as it was found that devices left out in ambient atmosphere overnight showed single molecule fluorescence decay similar to unsealed samples. This effect has been observed before and is attributed to slow O_2 and H_2O diffusion through the epoxy seal[67].

3.2.2 CONFOCAL APPARATUS

Single molecule microscopy has been previously reported[60] and is only briefly described here. Studies were performed using an inverted confocal microscope (Zeiss, Axiovert 100), and optical excitation was provided with the 488-nm line of a Ar Kr ion laser (Melles Griot, model 35 LTL 835) that was filtered (488 interference filter, Chroma) and attenuated with neutral density filters. Circularly polarized light was used to excite all axes of the molecules in the XY plane and was provided by passing the laser through a quarter-wave plate (CVI Laser). The light was focused to a diffraction limited spot size of 270 nm with a 100X oil immersion objective (Zeiss, Achrostigmat 1.25 NA). Excitation scatter from the sample was filtered using an appropriate dichroic mirror and filter (Chroma, 488 nm notch filter). Fluorescence detection was performed using avalanche photodiodes (APDs) (Perkin Elmer, SPCM-AQR-15). Image acquisition was performed through the use of a closed loop piezoelectric x-y stage (Queensgate, NPS-100A) driven by a computerized controller (RHK, SPM1000). The acquired images were then used to locate single molecules so that the stage could then be moved to excite individual molecules in the device.

Bias modulation of the single molecule device was accomplished with the use of a programmable function generator (Wavetek, model 29A). Light intensity modulation experiments were accomplished through the use of acousto-optical modulators where the input electronic signal to the modulator was provided by another programmable function generator. A master function generator was used to synchronize both the bias generator, the light waveform, and a multichannel scalar board (MCS) that was used to read the output from the APD. Two separate MCS boards were used in this experiment; a Becker Hickl PMS-400 was used to take long-time non-averaged measurements to verify that the fluorescence of the single molecule being irradiated was stable, and a FAST ComTec

Gmbh MCA-3 was used to take time-averaged measurements to achieve high signal to noise.

3.3 RESULTS AND DISCUSSIONS

3.3.1 FV/SMS MEASUREMENTS OF HOLE INJECION

This laboratory introduced FV/SMS techniques as a method to indirectly monitor charge injection via fluorescence quenching in specially designed devices suitable for single molecule spectroscopy[56]. The devices used in FV/SMS are adapted from conventional metal-insulator-semiconductor (MIS) capacitors with single molecule conjugated polymers located at the interface of the semiconductor and the insulator. The semiconductors used are common organic hole transport materials where, upon application of a positive bias, holes are injected from the anode and flow through the HTL to the insulator interface. With a sufficiently high concentration of holes at the insulator interface, controllable injection into the single chain polymer molecules can occur. CBP was chosen for its relatively high ionization potential (IP) of 6.0-6.1 eV[68-70] while TPD has an IP of 5.4 eV[71, 72] and was used to act as an intermediate step between the Au electrode and the CBP HTL. Reversal of the applied bias results in the removal of the accumulated charge, reducing the polymer to its original state. The Au injecting electrode prevents electron injection into the device at the negative biases used in this experiment due to the high work function of gold and the low electron affinity of the HTLs. Since holes are a well documented source of fluorescence quenching in conjugated polymers, the use of single molecule fluorescence microscopy quenching can be used to indirectly monitor charge injection[8, 56, 73-75].

Figure 3.1B and 3.1C demonstrate the effect of a periodic triangular bias applied across one of these CBP MIS devices on the fluorescence of a single molecule. The bias induced quenching is highly reproducible occurring repeatedly for thousands of cycles for a single chain. Consistent with previous results[8, 56, 76], positive bias coincides with fluorescence quenching, while negative bias coincides with fluorescence recovery. The quenching has been assigned to the injection of positive charge from the HTL. It has been shown that one hole induces quenching of ~40% of the original fluorescence intensity for MEH-PPV single molecules of this molecular weight suggesting that the near complete quenching of the single molecule fluorescence is due to the injection of 7-8 charges[8, 74]. The bias dependence of the hole injection rate and yield is attributed to the bias dependence of the concentration of holes at the CBP HTL interface, which decreases tremendously at negative bias in this CBP MIS device. The percentage of molecules in each device that demonstrated bias modulated fluorescence was ~95 % and the observed modulation was highly reproducible from device to device and from molecule to molecule demonstrating good electrical contact between the single conjugated polymer chain and the CBP HTL. The observations reported herein are qualitatively different than previous reports on devices without a good hole injection layer. i.e. CBP. Without this layer the observed fluorescence modulation is apparently due to a pure electric field effect rather than hole injection or in some cases, hole injection due to oxygen and/or mulitphoton ionization. [77-81]

As further evidence that quenching is the result of charge injection, insulating layers of either SiO_2 deposited by ebeam evaporation or poly(isobutyl methacrylate) spun cast from an orthogonal solvent were placed between the MEH-PPV and the CBP HTL. The incorporation of these layers completely arrests fluorescence modulation in the majority of the molecules (<5% of molecules modulate, data not shown), and the few molecules that do show fluorescence modulation in these control devices show erratic modulation behavior suggesting spurious charging and perhaps a pure electric field effect. This supports our conclusion that fluorescence modulation requires electrical contact with the HTL, supporting the idea that modulation is the result of hole injection, not the electric field.

3.3.1.1 SWEEP-RATE/LIGHT DEPENDENCE

Figures 3.2A-C illustrate the dependence of the fluorescence quenching kinetics in the device on the bias scan rate and excitation light intensity. The three F-V curves presented are for the same single molecule under different experimental conditions. Analogous behavior is observed for the vast majority of molecules in the sample and, consequently, the ensemble averaged data (not shown) also are similar to the curves in Figures 3.2A-C. At the slower scan rate of 10 V/s and higher excitation intensity the F-V curves exhibits only a small amount of hysteresis during the bias cycle (Figure 3.2A). The charge injection process is, therefore, close to being kinetically reversible under these conditions. When the excitation intensity is decreased, however, the F-V curve (Figure 3.2C) shows clear evidence of hysteresis consistent with the previous proposal that the charge injection process is light driven[66]. At the faster scan rates and higher excitation intensity hysteresis is also clearly observed (Figure 3.2B). This pure dependence on scan rate may be due to two factors. First, the scan rate may be so rapid that the injection of charges due to light may not be fast enough to keep up with the time varying bias. However, another factor may be slow thermionic charging of the CBP layer. The Schottky barriers to hole transfer across the TPD/CPB heterojunctions may be as large as 0.7 eV according to the HOMO energy offsets[66]. More research will be necessary to distinguish between these two possible explanations for the large hysteresis at the faster scan rates.

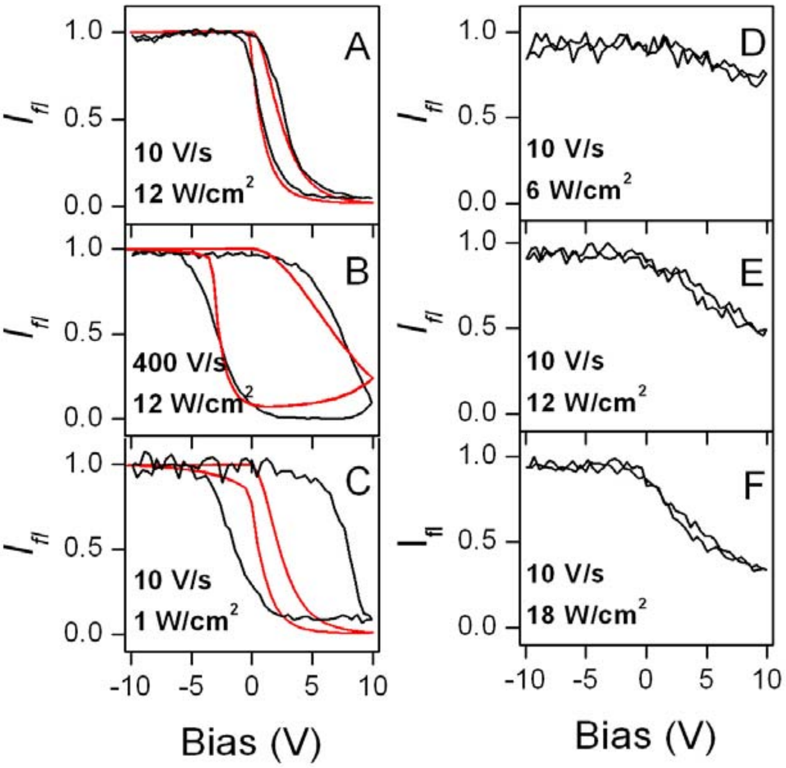

Figure 3.2: (A-C) Time-averaged single-molecule fluorescence-intensity transients (black curves) of MEH-PPV from a CBP device obtained while applying a triangular bias across the device with the bias scan rate and light intensity indicated in the panels for each transient. The red curves represent best fits by the kinetic model detailed in the text. (D-E) Time-averaged single-molecule fluorescence-intensity transients of MEH-PPV from a TPD-only hole injection device obtained while applying a triangular bias. The scan rate and light intensity used for the transients are shown in each panel. Each presented curve is an average of 30-40 cycles. Best fit parameters for: (A) $k_F = 1$, $K = 0.01$, $\varphi_{PC} = 0.6$ (B) $k_F = 1$, $K = 0.005$, $\varphi_{PC} = 0.6$ (C) $k_F = 0.11$, $k_{EXC} = K = 0.015$, $\varphi_{PC} = 0.6$.

3.3.1.2 CPB VS. TPD

F-V/SMS measurements (Figure 3.2B) were performed on TPD only devices with a similar geometry to those of Gesquiere[56]. A comparison of the results to the CBP/TPD devices reveals two important differences. First, for TPD only devices, the quenching depth maxima during a FV scan is light intensity dependent over a large range of biases and scan rates. In contrast, for CBP devices, the quenching depth depth maxima is always close to 100% for all but the lowest excitation intensities. This implies a lower steady-state concentration of injected holes for TPD vs. CBP. This is consistent with energetic considerations (i.e. HOMO energies) for hole transfer across the HTL/MEH-CBP interface which predict that the energetics for hole transfer from TPD into MEH-PPV is isoergic, but exoergic by 0.7 eV for CBP into MEH-PPV. Second, for TPD devices, little or no hysteresis is observed in the fluorescence quenching and recovery for all excitation intensities and scan rates used in this study. The apparent lack of hysteresis in the TPD only device implies more rapid hole injection and ejection rates than that for CBP. This may be due to shallower hole trapping at the TPD/MEH-PPV interface (as compared to than the CBP/MEH-PPV) associated with the energetic of hole transfer across the HTL/MEH-CBP interface.

3.3.1.3 KINETIC MODELING

A light-dependent charging model was developed to simulate the dynamics of the device charging observed for different experimental parameters, i.e. bias scan rate, light intensity, contact resistance, etc. The charge transfer from the Au electrode to the CBP layer is modeled as a diode, resistor and capacitor in series, in analogy to previous circuit treatments involving organic semiconductors[82-85]. The diode is used to model the rectifying properties of the Au/TPD and TPD/CBP interfaces by allowing only hole injection to occur at positive bias and preventing electron injection at negative bias.

When the device is sufficiently forward biased, holes can transfer from the Au electrode to the effective capacitor formed between the CBP layer and ITO electrode with a capacitance of ~1.6 nF, i.e. calculated for a simple parallel plate capacitor model using the geometry of the device.

A differential equation representing the equivalent circuit described above was solved numerically for the application of a triangular wave bias. The result was a Q_c vs. time curve where Q_c represents the charge present on the CBP layer and is used as an input for the empirical rate equation that governs the injection and withdrawal of charge from CBP to single molecule MEH-PPV, detailed below. Hole injection from CBP to single-molecule MEH-PPV is treated as a chemical reaction that is first order in charge concentration at the CBP interface and light intensity. The rate equation is as follows.

$$\frac{dX_{SM}}{dt}=\frac{k_F\cdot k_{EXC}\cdot X_C}{1+\frac{X_{SM}}{\phi_{PC}}}-\frac{K\cdot k_F\cdot k_{EXC}\cdot X_{SM}}{1+\frac{X_{SM}}{\phi_{PC}}}$$

Here X_{SM} is the mean concentration of charges present on a single molecule of MEH-PPV, k_F is the rate constant for charge photoinjection, k_{EXC} is the rate of photoexcitation of the single molecule (which is proportional to the light intensity), X_C is the charge concentration of the CBP layer, ϕ_{PC} is the amount of fluorescence quenching due to one hole on a single MEH-PPV molecule, K is the ratio of the discharge/charge rate constants. This equation was solved using numerical methods, and using the calculated X_{SM}, a Stern Volmer expression was used to convert charge density on the single molecule into fluorescence quenching and plotted against applied bias.

The results of the kinetic simulation are overlayed with the transients presented in Figure 3.2A-C. For these simulations the effective RC time constant for charging the CPB layer was arbitrarily adjusted to <0.1 s ensuring that at the slower scan rates used in our experiments (10 V/s) the kinetics of charging of the CBP is rapid without a large hysteresis. This further ensures that the hysteresis predicted at slow scan rates by this model is due entirely to rate-limiting photoinduced hole-injection. Since neither TPD nor CBP absorb significantly at the wavelength used for optical excitation, light is expected to only accelerate the charging of MEH-PPV through excited state electron transfer and not to increase the charging rate of CBP from the Au/TPD layers.

Qualitatively, some of the features in the experimental data are reproduced in the simulations however; the threshold biases at which quenching and recovery are observed to occur vary greatly with scan-rate speed and the light intensity. This aspect of the experimental F-V curves is not well represented by the model as the dominant effects of changing the input is to affect the charging and discharging rate while the threshold bias remains relatively unchanged with respect to the variable parameters of the simulation. These deficiencies in the model suggest that charge injection is much more complicated, supporting the hypothesis of a cooperative mechanism which enhances charge injection.

3.3.2 BIAS AND EXCITATION INTENSITY DOUBLE MODULATION EXPERIMENTS

To discern the extent of light induced charging for the single molecule devices, fluorescence intensity experiments were performed using square pulses of light at different biases. The plots shown in Figure 3.3 portray the sequence and timing of the light and bias pulses and the resulting fluorescence transient. Light pulses that coincide with negative bias give rise to a fluorescence intensity (after a suitable waiting period) that is assigned to MEH-PPV chains without charges, i.e. completely recovered (unquenched). Light pulses that coincide with positive bias give rise to quenching. The intensity of fluorescence signals at negative bias after a suitable time for discharging and at positive bias just after the pulse is applied are the same within experimental errors, suggesting that no charging in the dark has occurred for the single molecules despite the period of positive bias. The results shown here were taken at a bias of 6V but similar experiments with 10 V also showed no evidence of charge injection without light (data not shown). As a comparison, devices with a 25-nm thick film of bulk MEH-PPV were fabricated and similarly investigated with a multi-bias pulsed fluorescence experiment suitable for monitoring the quenching dynamics from a film of MEH-PPV[86]. The sequence of bias and light pulses used in this experiment as well as the resulting fluorescence transient is presented in Figure 3.4. Figure 3.4A is obtained with constant light illumination while applying the bias shown in the top panel (green curve). It is seen that under constant illumination, as soon as the bias switches from negative to positive, the fluorescence quenches to a level that is 60% of the original fluorescence intensity within 1 second. Figure 3.4B is obtained while using the same bias as shown in 4A, however the light sequence used is as shown (blue curve). The data clearly show that while the sample was in the dark and held at positive bias, MEH-PPV underwent thermionic charge injection, resulting in the fluorescence quenching that is immediately observed upon reillumination of the sample. This suggests that the LIHT mechanism is not required for charging of bulk films.

The difference in quenching mechanisms between the single molecule device and the bulk film may be described by the potential difference in the HOMO energies of the two. Studies of the ionization potentials of pentacene single molecules vs bulk pentacene show an increase in the HOMO energy level of ~1.0 eV for the single molecule as compared to the bulk[87, 88]. If a similar phenomenon occurs for single-chain MEH-PPV, the resulting Schottky barrier may increase to the point where thermionic injection in the single molecule case is slowed to the point of having a negligible effect on the charge injection, leaving only the LIHT as a means for injection.

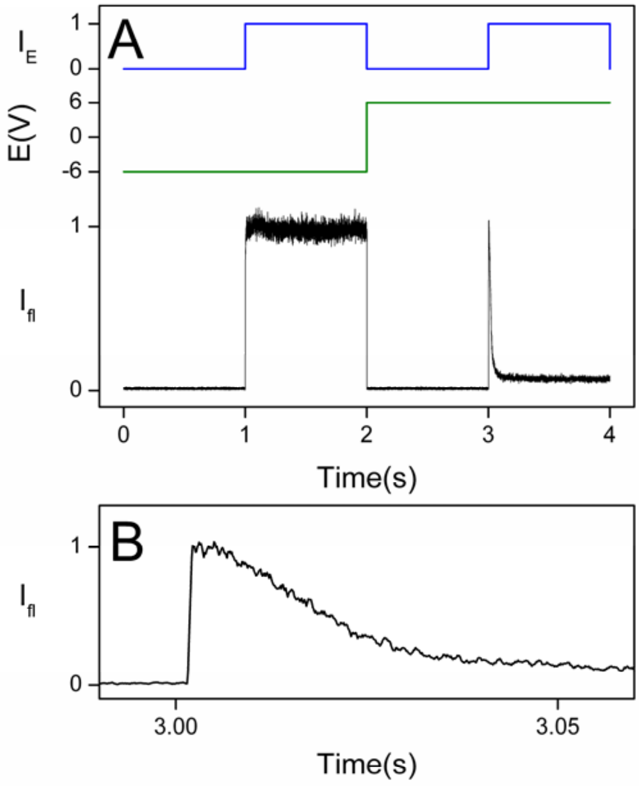

Figure 3.3: (A) Time-averaged single-molecule fluorescence-intensity transient of MEH-PPV (black curve) while simultaneously modulating the applied bias (green curve) and the light (blue curve) as shown. The presented curve is an accumulation of 250 4-s cycles obtained with a light intensity of 0.5 W/cm^2. (B) An expanded axis view of the fluorescence transient shown in (A).

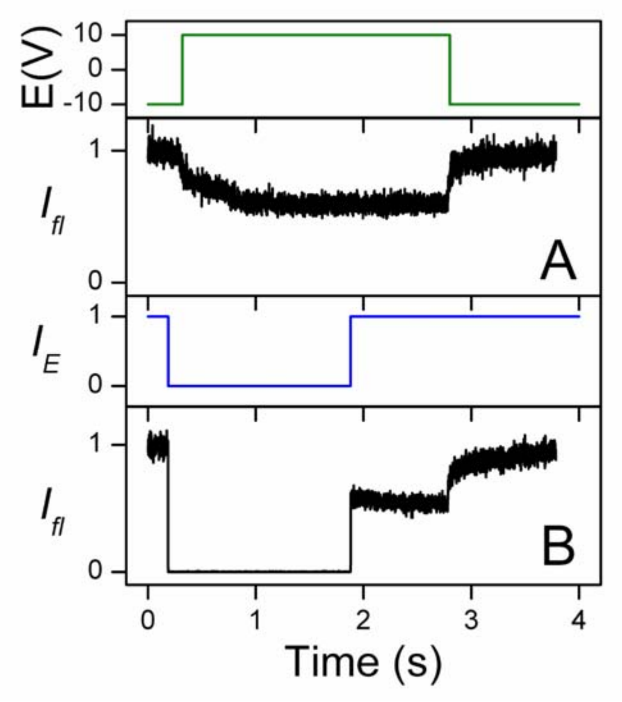

Figure 3.4: Time-averaged fluorescence-intensity transients obtained from an MEH-PPV film device with an applied bias as shown in the upper panel (green curve). The transient shown in panel (A) was acquired with constant light intensity over the course of the entire measurement. The transient in (B) was obtained with a similar applied bias as that of (A) while the light intensity was modulated as shown with the blue curve. Each transient is an average of 4 4-s cycles obtained with a light intensity of 0.1 W/cm^2.

To explore the effect of applied bias on the LIHT process, a series of experiments were performed where a triangular bias with a sweep rate of 20 V/s was applied and a single molecule was irradiated at different potentials along the triangular bias with the same light intensity, effectively probing the influence of the charge density on the CBP layer on the quenching dynamics of single molecules. Transients obtained in this experiment are plotted against the time when the light pulse was initiated ($t-t_0$) and are presented in Figure 3.5. At higher applied bias, it is seen that the rate of quenching increases suggesting that as the CBP layer becomes more charged, the rate of LIHT increases with it. Light intensity was also found to play a similar role in the fluorescence quenching dynamics. As more intense light pulses were used, the fluorescence quenching occurred on a faster time scale; however, regardless of the light intensity used, the quenching depth remained fixed for a given bias. Both of these findings are consistent with the F-V/SMS measurements detailed above and that the LIHT mechanism is comprised of an excited state charge transfer from the exciton of MEH-PPV and holes in the CBP layer.

3.3.2.1 LIGHT-ASSISTED DETRAPPING

The previous section details how light is necessary for the charging process; however, F-V/SMS measurements suggest that light has a less important role in the discharging process however previous work done on organic electronics suggest light may be a powerful tool in trap decharging[28, 37, 38, 89]. A multi-bias pulsed experiment was used to elaborate the role of light in the recovery of charged single molecules. Figure 3.6 presents evidence that light, while not required for the recovery process, significantly enhances it at negative bias. The bias sequence used for this study is detailed in the top panel of Figure 3.6 (green curve). Both transients (black curves) are shown with their respective light pulse sequences (blue curves) in the panels above them.

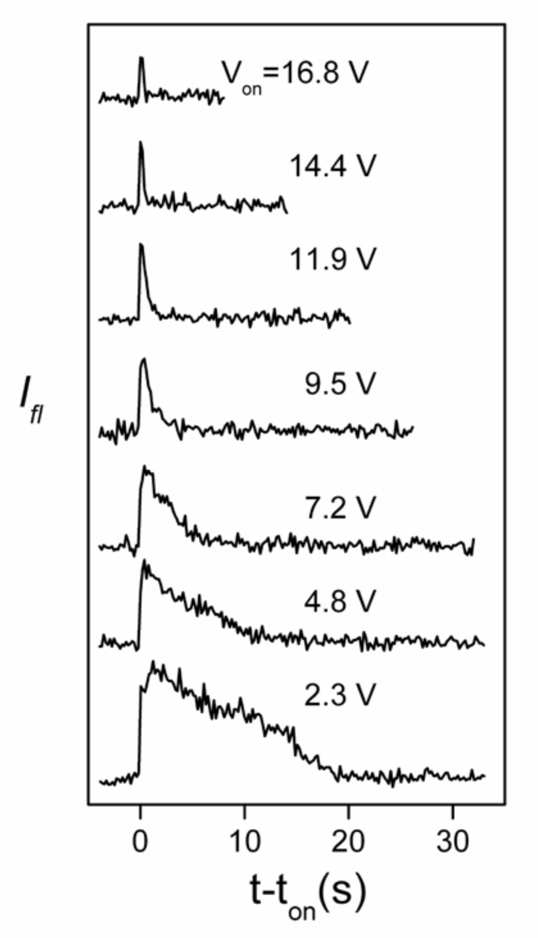

Figure 3.5: Time-averaged fluorescence-intensity transients from a single molecule device. A triangular bias was applied to the device with a scan rate of 20 V/s and the laser excitation intensity (0.2 W/cm^2) being introduced to the sample at different biases. Transients are plotted such that t = 0 corresponds to when the light pulse was initiated. Each curve is an accumulation of 3-5 cycles.

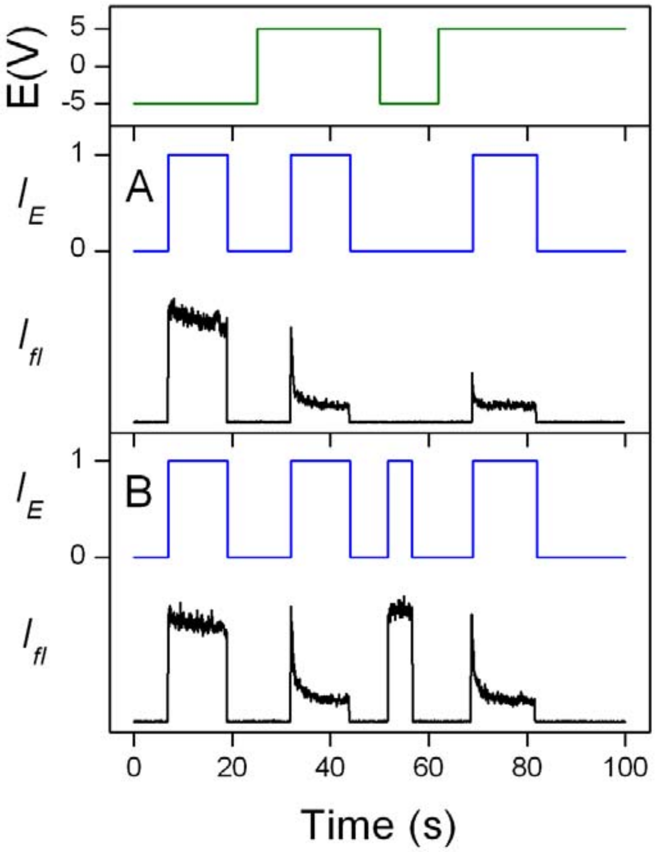

Figure 3.6: Double modulation single-molecule fluorescence-intensity transients (black curves) of a single MEH-PPV molecule. The applied bias for both transients is shown in the top panel (green curve) and the light sequence used is shown directly above each transient (blue curves). Each transient is the accumulation of 10 4-s cycles obtained with a light intensity of 0.5 W/cm^2.

Briefly, the bias sequence was chosen such that that the second period of the negative bias was too short to completely discharge the MEH-PPV molecule as shown by returning the bias back to positive and recharging the molecule. It is seen that when given a short amount of time to discharge, the fluorescence intensity does not fully recover. However, when a brief pulse of light is added to the negative bias, the recovery is shown to be fully complete. Studies performed on charge trapping and bias stress in organic transistors have shown that exposing the system to light of energy above the band gap of the material can greatly enhance the recovery back to the uncharged state of the device.

3.3.2.2 COOPERATIVITY AND CHARGE INCUBATION

Figure 3.3B gives an expanded view of the quenching dynamics observed in the transient from Figure 3.3A. From this, it is seen that the quenching does not occur immediately following sample illumination. Under the conditions used, there exists a 6-ms delay before quenching begins to occur in the molecule which we refer to as charging incubation. To verify that this delay is real and not due to the kinetics of charging the CBP layer, the delay between the beginning of the positive bias and the light pulse was doubled. This showed no discernable effect on the charging incubation period, ruling out the effects of kinetic charging of the CBP layer. From this, two possible explanations of how charge injection occurs becomes viable. The first is that presence of light and charge cause a reorganization of the MEH-PPV single molecule resulting in a lower HOMO energy level similar to that of bulk MEH-PPV. The second is that while light can introduce charge from CBP to MEH-PPV, the charge quickly returns to the CBP layer, and it is only when multiple charges are located in the MEH-PPV that charge becomes trapped, most likely due to bipolaron formation.

3.3.2.3 FAST DOUBLE MODULATION

This laboratory recently introduced fast double modulation experiments similar to those presented here that are designed to monitor the lifetime and behavior of the triplet excitons of single conjugated polymer molecules that also contain of holes[7]. Figure 3.7A shows the fluorescence vs. time curves for a bias range for which no holes are injected in the polymer chain at any point in the sequence. In these experiments, the initial peak in fluorescence intensity at the beginning of each light pulse corresponds to a single chain with no triplets presents. (The dark time period that precedes each light pulse is sufficiently long to ensure the decay of all triplet excitons.) The initial peak in the fluorescence intensity is followed by a decay for each pulse in Figure 3.7A due to the creation of a triplet exciton in the chain which quenchs singlet excitons and reduces the fluorescence intensity, as discussed in detail previously.

Modulation of the device bias sufficient to inject holes while taking these measurements provides information on the nature of hole-triplet interaction. Double modulation experiments were performed on our CBP devices and the results are portrayed in Figure 3.7. In Figure 3.7A, the bias threshold was increase from -7.5 V to 2.5 V in a step-like fashion. The bias range is below the threshold voltage for charge injection into the CBP layer. The results are that only triplet quenching of the singlet exciton occurs, similar to when no bias is applied to the device. In contrast when a bias higher than the threshold of injection is applied as shown in Figure 3.7B, triplet quenching is observed to occur as well as quenching resulting from hole injection from the charged CBP layer. It is interesting to note that consistent with previous results, at higher biases, the peak corresponding to triplet quenching of the singlet exciton disappears followed by a further overall intensity decrease. This is interpreted much like previous reports in that the triplets are more efficiently quenched by holes than the

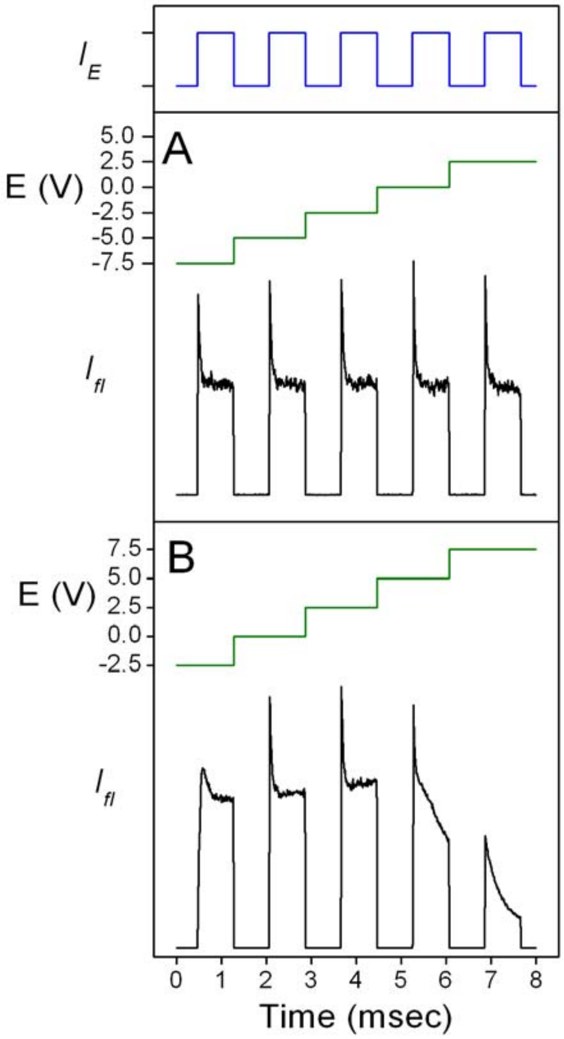

Figure 3.7: Time-averaged fluorescence-intensity transients obtained while modulating the light and bias during each cycle. The light pulse consisted of five 200 W/cm^2 intensity pulses of equal duration as shown by the upper blue curve. The bias was increase stepwise in 2.5 V increments as shown by the green curves. The black curves are the corresponding time-averaged fluorescence intensity transients of the same single molecule where the bias ranged from -7.5 to 2.5 V (A) and from -2.5 to 7.5 V (B) Transients are an accumulation of 1500 8-ms cycles obtained with a laser intensity of 300 W/cm^2.

singlets and thus the initial peak in fluorescence intensity disappears at higher biases. The further overall intensity drop at even higher biases is assigned to quenching of singlet excitons due to the injection of holes. These findings suggest that while holes quenchtriplets before singlets, the mechanism for the quenching of the singlets are most likely unrelated to the triplets. Further studies performed in a vacuum chamber microscope provide more evidence that the quenching observed in these studies is unrelated to the triplet state of the molecule. Oxygen has been observed to be a quencher of triplets, and when a pressure of 5 torr of O_2 was introduced into the vacuum chamber, fluorescence intensity assigned to triplets vanished[7]'[90]. F-V measurements showed little change in the quenching behavior due to the presence of holes, again supporting the idea that triplets are not involved in the LIHT quenching mechanism.

3.3.3 SM F8BT COMPARISON

To determine if the LIHT mechanism is a product of a particular combination of HTL and conjugated single molecule, CBP devices were fabricated with F8BT single molecules to provide a comparison. Bulk F8BT has a much higher HOMO energy (ionization potential) of 5.8-5.9 eV[58, 59] relative to vacuum compared to MEH-PPV and thus it should be more difficult to inject the same number of holes into single-molecule F8BT. Multi-bias pulsed experiment results are shown in Figure 3.8 for a single-molecule F8BT/CBP device. From this it is shown that the charging process for single-molecule F8BT is completely light driven similar to single-molecule MEH-PPV. Similar to MEH-PPV, more intense illumination results in faster fluorescence quenching, but the quenching depth remains fixed for a given applied bias. Also of note, in similar device geometries, an applied bias of 6 V in an MEH-PPV device resulted in near complete quenching of the molecule, suggesting a single molecule has multiple charges isolated on it. At an applied bias of 8 V, the quenching of an F8BT single molecule is

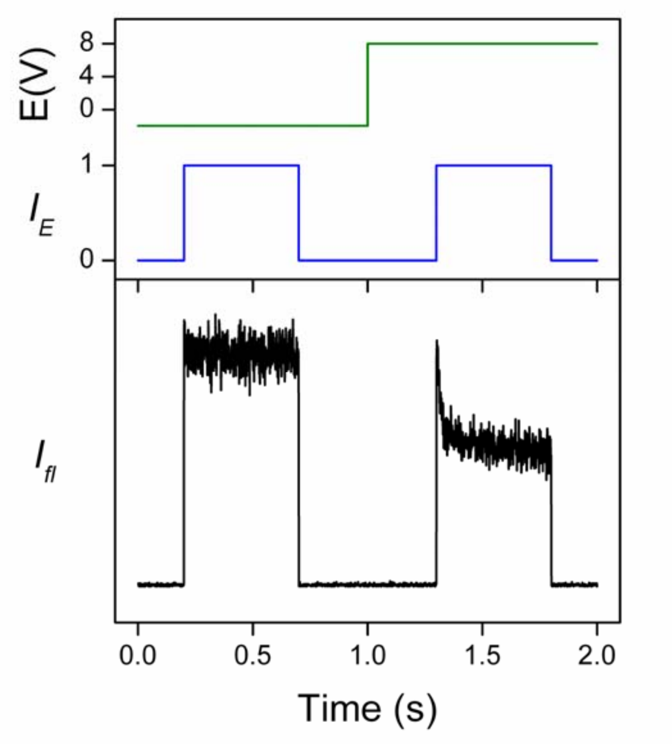

Figure 3.8: Time-averaged fluorescence-intensity transient (black curve) obtained from a single-molecule F8BT device with the applied bias (green curve) and light sequence (blue curve) as shown in the top panel. The presented transient is an accumulation of 20 2-s cycles obtained with a laser intensity of 1 W/cm^2.

~50%, similar to the reported quenching depth of a single hole on an F8BT molecule of similar size[91]. This finding is in agreement with the higher HOMO energy of F8BT relative to MEH-PPV. Also of interest, it appears that the LIHT mechanism is not limited to specific systems, i.e. different single molecule systems can be used as the oxidized species in these devices.

3.4 CONCLUSION

Single-chain conjugated polymers were imbedded at the HTL/insulator interface of an MIS device and hole injection was observed from the HTL using an indirect fluorescence quenching technique. The process was determined to be light dominated with no charging occurring in the dark. This stands in contrast to the thermionic charge injection observed for bulk MEH-PPV films in similar device geometries. This difference is attributed to the possible change in the HOMO energy level and therefore, effective Schottky barrier of a single chain as compared to the bulk film. The single-chain charging dynamics observed further showed evidence of a cooperative effect, suggesting a modification of the polymer chain occurs prior to charge injection. These findings suggest that the optical preparation of trapped charge may have serious implications for the functioning of organic devices.

Chapter 4: Single conjugated polymer nanoparticle capacotors

4.1 INTRODUCTION

The transfer of positive charge (holes) between organic semiconductors across heterojunctions is a central process in organic light emitting displays (OLEDs)[25, 92-95] and other organic electronic devices[96-99]. The energetic barrier for hole injection into a conjugated polymer (CP) layer from an adjacent hole-transport layer (HTL) is generally believed to be controlled by two major factors: the offset of the energy of the highest occupied molecular orbital of the two materials ($E_{\mathrm{HOMO,CP}}-E_{\mathrm{HOMO,HTL}}$) and modifications to this energy due to surface dipoles and other effects which can shift the vacuum level energy.

A closely related issue to charge injection across heterojunctions is the nature of positive charge carriers (holes) in organic conjugated polymers. There are apparently two main types of holes, i.e. shallowly trapped (mobile) holes and the much less well understood and investigated deeply trapped holes (DTH). The extreme hysteresis that is commonly observed in the current (i) vs. voltage (V) curves for various types of organic electronics (also known as the bias stress effect) may be due to the creation and interfacial build-up of DTH[27, 28, 38, 44, 48, 49]. This implies that a build-up of DTH can significantly alter the energetics necessary to inject holes, but the physical and chemical origin of DTH remains obscure despite decades of research[25-31, 50, 61, 64, 65]. One proposal is that DTH are due to the chemical rearrangement/modification of the specific materials[26, 28, 30, 48-50, 61, 65].

We recently have been investigating hole injection from various types of HTL into single polymer chains of the conjugated polymer poly(2-methoxy-5-(2'-ethylhexyloxy)-1,4-phenylenevinylene) (MEH-PPV) as a means of exploring the barriers and rates of hole injection in semiconductor nano domains[100]. Conjugated polymers have potential practical applications in organic electronic devices such as light emitting diodes[25, 101], solar cells[3, 16], field effect transistors[102-104], etc. The experiments employed a device geometry (analogous to the one shown in Figure 4.1a) in which holes are injected into single molecule capacitors from a carbazole derivative (CBP). The experimental amount and rate of hole injection from the CBP HTL into individual, isolated polymer chains was monitored by single-molecule fluorescence spectroscopy using fluorescence quenching as a measure of the charge density in each polymer chain. Direct electrical measurements of charge would be difficult due to the small number of charges injected per single molecule.

Despite the use of HTL/CP combinations, such as CPB/MEH-PPV, that would be expected to exhibit energetically favorable thermal hole injection (see Figure 4.1b), no injection was observed in the dark under positive bias (see Figure 4.1a for the sign convention). This result suggests that the effective E_{HOMO} of single conjugated polymer chains is actually lower than the bulk material, due perhaps to environmental or conformational effects. Interestingly, while no charge injection was observed in the dark, optical excitation of MEH-PPV (producing MEH-PPV excitons) was observed to induce hole injection from the CPB layer. The light-assisted injection of positive charge carriers (holes) was assigned to a light-induced hole-transfer mechanism (denoted by LIHT). The hole injection process involves charge transfer from a CBP hole to a MEH-PPV singlet exciton at the CBP/MEH-PPV interface, perhaps additionally involving the formation of a DTH in MEH-PPV. The molecular level description of the process however has not been established.

This paper describes a continuation of our investigation of hole injection across heterojunction into conjugated polymer nano domains. In this work, we study injection

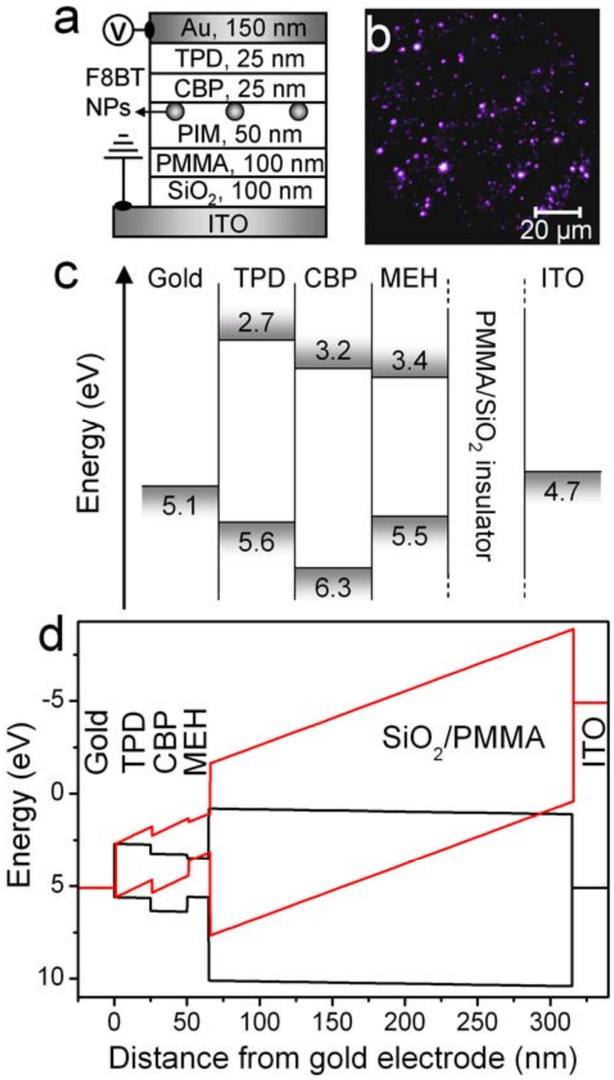

Figure 4.1: (**a**) TPD-CBP hole-injection device containing MEH-PPV NPs. (**b**) Wide-field fluorescence image of a hole injection device. (**c**) Energy diagram of the device shown in a. (**d**) Simulation results for the energy levels of the device shown in a. The black and red lines represent the LUMO (top) and HOMO (bottom) energy levels at 0 V (equilibrium) and 10 V (before significant charging has occurred), respectively.

of holes into single self-assembled MEH-PPV nanoparticles (NPs) comprised of ~10-100 polymer chains per particle and which have a radius in the range of ~10-40 nm. These particles are significantly larger than the single polymer chains that were described above ($r < 7$ nm). Previous spectroscopic studies that compared single polymer chains, conjugated polymer NPs, and bulk thin-films indicate that the morphological state of the conjugated polymer in the NPs and bulk, thin-film forms are similar[105]. In contrast, the single-polymer chains possess a morphology (conformation) with less chain-chain interactions[106-110]. Thus, the investigation of holes into MEH-PPV NPs is a means of determining whether the LIHT process is specific to single polymer chains or more general. In addition, self-assembled conjugated polymer NPs are interesting in their own right, e.g. as alternatives to quantum dots as biological labels[111, 112], and as model systems in electrochemistry[55, 113] and electrogenerated luminescence[114]. This paper explores hole injection into MEH-PPV NPs in devices containing a CBP HTL. As in the study of single polymer chains, injected holes are measured by fluorescence quenching using single particle spectroscopy.

4.2 EXPERIMENTAL

The electrical charging and discharging processes of MEH-PPV NPs were studied in large-area multilayer hole-injection capacitor devices.

4.2.1 DEVICE STRUCTURE AND ASSEMBLY

The general structure of the single-molecule hole-injection device is shown in Figure 4.1a. The device was assembled bottom up on commercial ITO electrodes (Evaporated Coatings, Inc., sheet resistance 50 Ω/□) that were cleaned by successive sonication in trichloroethylene (Sigma-Aldrich, HPLC), acetone (Fisher, HPLC) and methanol (Fisher, HPLC). The SiO_2 insulating layer was deposited by inductively-coupled plasma chemical vapor deposition (ICP-CVD) at 200° C (Oxford instruments, Plasmalab 80plus). The poly(methyl methacrylate) (PMMA, Sigma Aldrich, average MW =101 kg/mol) layer was deposited by spincoating from toluene (Sigma Aldrich, anhydrous 99.8%). The function of this layer was to isolate single nanoparticles of MEH-PPV (Uniax, average MW = 1000 kg/mol) from the SiO_2 layer.

Nanoparticles were prepared by a re-precipitation technique[112-114]. Briefly, a small aliquot of a concentrated solution of MEH-PPV (~1 mg/ml) in tetrahydrofuran is 'flash'-injected into a solution of poly(isobutyl methachrylate) (PIM, Acros, average MW= 300 kg/mol) in cyclohexane. The size of the resulting NPs ($r = 25 \pm 15$ nm) was estimated by comparing the single NP fluorescence intensity distribution to that of a reference NP sample with a known size distribution (measured by Scanning Electron Microscopy). The resulting colloidal suspension is spin-cast to form the PIM/NP layer (10 nm), the NP concentration was adjusted to obtain an areal density of ~ 0.1 particles/μm^2 in the sample.

The device contains two HTLs in series as shown in Figure 4.1a, a layer of 4,4'-*N*,*N'*-dicarbazole-biphenyl (CBP) and a layer of *N*,*N'*-bis(3-methylphenyl)-*N*,*N'*-diphenylbenzidene (TPD). Thermal evaporation was used to deposit the TPD and CBP hole transport layers and the gold electrode (Cerac, 99.99%). Thermal depositions were carried out at $\sim 10^{-4}$ Pa and typical rates were 1-2 Å/s as measured by a quartz crystal microbalance. Layer thicknesses were measured by atomic force microscopy (Digital Instruments, Dimension 3100) and/or ellipsometry (J A Woollam Co. Inc.,M-2000) and are as shown in Figure 4.1a unless otherwise noted. All device fabrication was performed in a glove box (O_2 and H_2O concentration are < 10 ppm and < 1 ppm respectively) except for the SiO_2 deposition.

4.2.2 SINGLE PARTICLE FLUORESCENCE-VOLTAGE (F-V) TECHNIQUE AND EXPERIMENTAL SETUP

The hole charging/discharging processes in individual NP of conjugated polymers in capacitor devices were studied using the previously described fluorescence voltage single molecule spectroscopy, F-V SMS technique[8, 56]. This technique determines indirectly the density of holes in individual florescent molecules or nanoparticles by measuring single-particle florescence quenching. The principle of the technique is based on the well know quenching effect of singlet excitons by hole polarons in organic semiconductors[74].

Two instruments were used to measure the fluorescence intensity of individual NPs in this work: a fluorescence confocal microscope and a wide field vacuum microscope. Both systems have been described in detail elsewhere[100]. In both apparatus the 488-nm line of an argon ion laser was used as the light excitation source, optical excitation and fluorescence collection were done in an epi-illumination/detection geometry. In the wide field instrument, images are recorded with an electron multiplying CCD. The time dependence of the fluorescence intensity of individual NPs, I_{fl}, is determined from a set of fluorescence images using image analysis software home-written in Matlab. In the confocal apparatus images are acquired by raster scanning the sample over a focused laser beam and collecting the resulting fluorescence with an avalanche photodiode. Single molecule transients are then acquired by moving the sample to position a single NP over the focused laser beam. The timing of the collection of wide field images and confocal fluorescence transients were synchronized to a time-varying electrical bias applied to the sample with a programmable function generator. To improve the signal to noise ratio the resultant single particle fluorescence transients are synchronously averaged over several bias cycles (3-20) unless otherwise noted.

For experiments performed in the vacuum microscope set-up, samples were transferred in airtight containers to avoid exposure to atmosphere prior to entry to the vacuum chamber which was prefilled with ultra high purity argon (Matheson Tri-Gas). For experiments performed in the confocal apparatus, samples were packaged inside a glove box to avoid infusion of oxygen and water during data acquisition (for details see ref [100]). The fluorescence intensity of single NPs in these packaged samples was stable for long periods of time (at the excitation intensities used) allowing for individual particles to be studied for several hours without significant photo bleaching being observed. The same was true for unpackaged samples studied at 10^{-5} Pa in the wide-field vacuum microscope set-up.

4.3 RESULTS

4.3.1 SINGLE NP HOLE-INJECTION CAPACITOR DEVICES

Before describing the single particle fluorescence vs. bias experiments it is useful to consider the implications of the device structure on the energetics of charges in the NPs in the device. The device structure and HOMO and LUMO energy levels as a function of distance from the hole injection electrode (gold) are shown in Figure 4.1. The energy levels for the different layers of these materials are shown in black in Figure 4.1c for the bias = 0 case. The HOMO energy level (lower curve) and the LUMO energy level (upper curve) tilt when a positive bias is applied to the device (Figure 4.1c, red curve). As shown in Figure 4.1c, when the device is positively biased (bias convention shown in Figure 4.1a) holes should transfer from the gold electrode to the MEH-PPV nanoparticles due to the higher HOMO energy level. Note that the energy levels in Figure 4.1c have been calculated with a very low concentration of charges in the device HLTs in order to emphasize the effective bias and its effect on the HOMO and LUMO energies before significant charging occurs.

Using typical values from the literature for the materials' properties and results of Poisson-Boltzmann simulations from a commercial program (SimuApsys 2007.3, CrossLight Software Inc.), charges are predicted to transfer from the gold electrode through the TPD and CBP HTL layers into the MEH-PPV nanoparticles (see Figure 4.2, and below for details). In brief, the simulation calculates the numerical, self-consistent solution of the continuity and Poisson-Boltzmann equations in the organic/inorganic layers and at the internal interfaces of the device. The numerical solution is obtained by discretizing space and time, and the dynamic response to a step change in voltage is obtained from a time-dependent iteration sequence.[115] The device structure is modeled with a quasi-2D simulation approach (equivalent to a 3D simulation with a flat z-dependence) in which the single MEH-PPV NP is represented as a 15 x 15 nm rectangular prism located in contact with the CBP layer (see inset on Figure 4.2b). The parameters required as inputs to the simulation are: the mobility (μ), density of states (N) and energy levels (E_{HOMO}, E_{LUMO}) of each organic material and the work functions of the electrode contacts (ϕ_{Au} = 5.1 eV[116]and ϕ_{ITO} = 4.7 eV[117]). The PMMA and SiO_2 materials are described with a "perfect insulator" macro that prevents the flow of charges through their corresponding layers. The initial charge density in the organic materials is assumed to be zero (initial condition).

The density of localized states for all the organic materials was taken as $N = 10^{21}$ cm^{-3} [118, 119] and the rest of the parameters are summarized in Table 1. Figure 4.2 shows the results from the simulations using the model single particle device (Figure 4.2b insert). Figure 4.2a shows the HOMO energy level of the different layers on the device, the black curve (bias = 0 V) was calculated at equilibrium, resulting in a very low

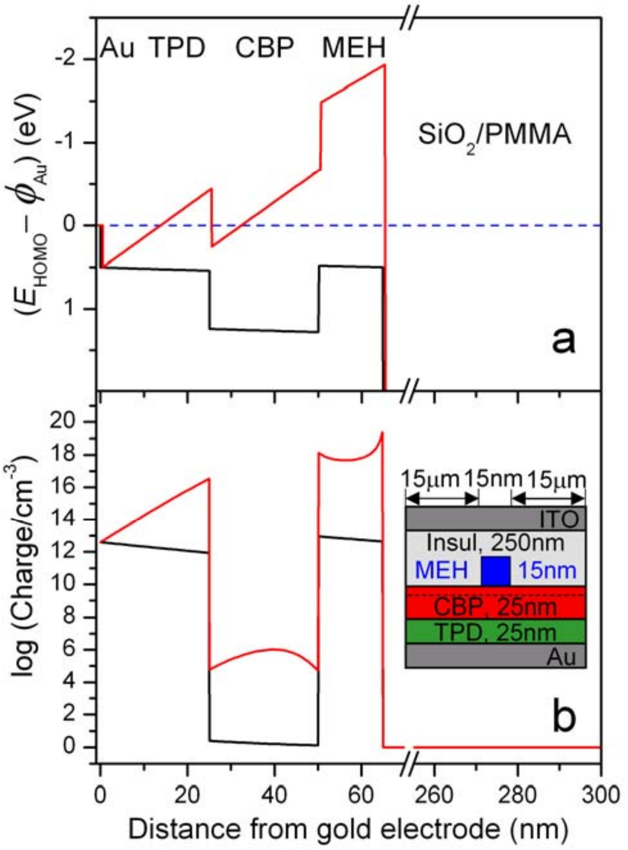

Figure 4.2: Poisson-Boltzmann simulations for a model single-NP hole-injection device. (**a**) HOMO energy levels relative to the work function of hole-injection electrode. The black and red lines were calculated at 0V (at equilibrium) and 10V (before significant charging) respectively. (**b**) Charge density distribution. The black and red lines were calculated at 0V (at equilibrium) and 10V (at equilibrium) respectively. Inset: model device structure. Data presented in (a) and (b) corresponds to a cross section though the middle point of the model device and perpendicular to the electrodes.

Table 4. 1: Parameters used in Simulations

	MEH-PPV	TPD	CBP
E_{HOMO} (eV)	5.9 [a]	5.6 [c]	6.3 [e]
E_{LUMO} (eV)	3.1 [a]	2.7 [c]	3.2[e]
μ_{holes} ($\mathrm{cm}^2\ \mathrm{V}^{-1}\ \mathrm{s}^{-1}$) [g]	$5\ 10^{-5}$ [b]	$3.2\ 10^{-3}$ [d]	$3.8\ 10^{-4}$ [f]
$E_{dep\ holes}$ (V/cm) [g]	$1.6\ 10^{4}$ [b]	$1.5\ 10^{7}$ [d]	$1.5\ 10^{5}$ [f]
$\mu_{\mathrm{electrons}}$ ($\mathrm{cm}^2\ \mathrm{V}^{-1}\ \mathrm{s}^{-1}$) [g]	$3\ 10^{-5}$ [b]	$1\ 10^{-5}$ [d]	$4.4\ 10^{-4}$ [f]
$E_{dep\ electrons}$ (V/cm) [g]	$4.3\ 10^{4}$ [b]	$1\ 10^{8}$ [d]	$2.6\ 10^{6}$ [f]

[a] See ref. [120]
[b] See ref. [59]
[c] See ref. [71, 72]
[d] See ref. [121]
[e] See ref. [122]
[f] See ref. [123]
[g] $\mu = \mu_0$ exp(sqrt(E/E_{dep})), where μ_0 is the mobility at zero field, E is the electric field, and E_{dep} is a parameter that describes the field dependence.

average charge density in the device (< 10^{13} holes/cm^3). Using these initial conditions, the red curve (bias = 10 V) was calculated at early times (< 1 s), before a significant amount of charge is injected. Figure 4.2b shows the charge density distribution of the different layers at 0V (black curve) and at 10 V (red curve) calculated at long times (>10^7 s), when the device has reached equilibrium. According to the simulations, the time scale for reaching charging equilibrium at 10 V is on the order of 100 seconds (not shown). This time is controlled by the energy barriers for a hole transfer across the various Schottky barriers proceeding the MEH-PPV nanoparticles and the charge mobility of the organic layers. The barriers for hole transfer at each of the various interfaces are determined by the HOMO energies from the literature which have an uncertainty of at least 0.5 eV. In addition, the simulations do not take into account interfacial effects such as surface dipoles which usually significantly reduce electron and hole injection barriers[124]. Thus, the actual time scales determined in these simulations are probably in error by orders of magnitude. Nevertheless, the qualitative trends in the simulation are probably realistic since the "sign" of the Schotky barriers is unchanged over the entire range of possible HOMO energies for these materials.

Once the charges reach the nanoparticles, the essentially infinite barrier resulting from the SiO_2 and PMMA insulators block the charge from transferring further to the ITO electrode. Thus the device functions as a series of single particle capacitors in parallel formed by the nanoparticles and the ITO electrode with the PMMA and SiO_2 insulators sandwiched between them. This is shown graphically in Figure 4.2 where steady-state simulations of the E_{HOMO} and hole density as a function of distance from the gold electrode reveal the expected effect for a nanoparticle capacitor connected to the hole injection electrode through the HTL layers. It should be noted that the simulations indicate that for these material types and device geometry, only holes are present at significant concentrations in the device for the applied bias range (-10 to10 V). In particular, the simulations demonstrate that at negative bias most excess charges are removed from the device (not shown).

Under negative bias, the device functions as a simple capacitor formed by the gold and ITO electrodes, albeit with a complicated set of insulating layers between these electrodes. In contrast, at positive bias, after sufficient time is allowed for charge equilibration, the main capacitance is dominated by charges accumulated in the CBP layer (more precisely in a ~ 5 nm region next to the CBP/insulator interface, see dashed area Figure 4.2b inset) and the ITO/electrode. In turn the MEH-PPV nanoparticles are electrically connected to the CBP layer and form additional small capacitors as mentioned above. Note that the charge density as a function of distance within a nanoparticle (Figure 4.2b) is predicted to increase rapidly at the MEH-PPV/PMMA interface in accord with the usual behavior of capacitors with semiconductor electrodes, e.g. a metal-oxide-semiconductor (MOS) capacitor. One implication of this effect is that the fluorescence quenching observed due to hole injection may be complicated by the spatial distribution of the hole density within a particle.

We have taken this effect into account in calculating the fluorescence quenching as a function of bias in Figure 4.3a (red curve). For this purpose, the model NP (15 x 15 nm, see Figure 4.2b inset) was discretized in 5 x 5 nm cells. The normalized fluorescence of each cell (I_{fl}) was calculated using Eq. 1

$$I_{\mathrm{fl}} = 1/[1+(QD/(1-QD))\, C_{\mathrm{holes}}] \qquad (1)$$

where $QD=0.9$ is the normalized fluorescence quenching depth per hole in a cell (5 x 5 nm), and C_{holes} is the discreet number of holes in that cell. The probability of having a discreet number of charges in each cell was calculated using the average charge density in each cell and assuming a Poisson distribution of charges. Using these discreet charge

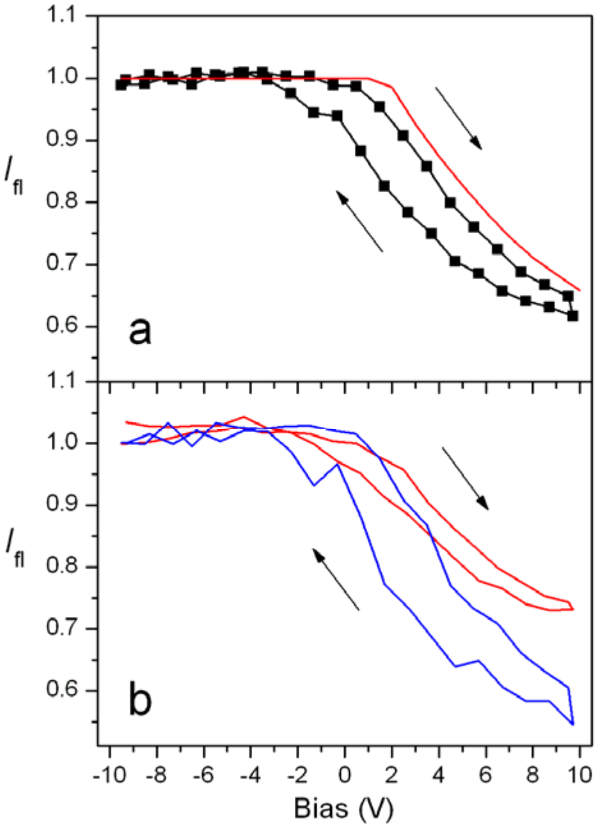

Figure 4.3: (**a**) Ensemble average of 90 normalized single-NP fluorescence-voltage trajectories in a hole-injection device (connected data-points). The data was acquired at a bias scan rate of 0.1 V/sec (direction indicated by arrows) and with an optical excitation intensity of 67 mW/cm^2. The red solid line corresponds to the theoretical F-V values obtained from simulations (see text for details). (**b**) Sub-ensemble average of single-NP F-V curves corresponding to the data shown in a. The red and blue sub ensembles were constructed by sorting the 30 highest and 30 lowest fluorescence intensity NPs.

probabilities and Eq. 1, the normalized fluorescence intensity of each cell was calculated and then averaged over all the cells to give a normalized florescence intensity of the whole model NP.

4.3.2 QUENCHING AS A FUNCTION OF BIAS

Figure 4.3a portrays the ensemble average of the fluorescence intensity of many NPs as a function of bias (Figure 4.3a). In these experiments the charging of individual MEH-PPV NPs is probed by monitoring the fluorescence of the NPs that passes through the transparent ITO electrode. During this time period, a triangular-wave bias was applied to the device at a scan rate of 0.1 V/s. At biases ≤ 0 V the fluorescence intensity is most intense and constant. This intensity is assumed to reflect uncharged nanoparticles and is used to normalize the fluorescence-bias curves. At biases > 2 V, the fluorescence intensity decreases, as mentioned in previous papers[56, 74]. This decrease is assigned to fluorescence quenching resulting from holes in the device. The process specifically involves the quenching of singlet excitons of the conjugated polymer by holes.

The amount of quenching is considerably less than that observed in quenching studies of single conjugated-polymer chains. In this latter case, a single hole has been shown to quench approximately 40% of the fluorescence intensity. For charging studies of single polymer chains in an analogous device architecture to Figure 4.1a, the fluorescence intensity can be quenched at a greater than 99% efficiency[100] indicating the injection of more than 4 holes per single polymer chain. For nanoparticles, in contrast, the quenching efficiency per charge is only <1% for particles of this size range[113] and is highly dependent on the distribution of charges within the NP as discussed below. In agreement with this view, Figure 4.3b shows that large particles, i.e. NPs with high emission intensities (red line), display less quenching as compared to small particles, i.e. NP with low emission intensities (blue line).

The amount of quenching of the NPs shown in Figure 4.3 is also much less than that of similar types of NPs in electrochemical hole injecting cells[113]. In the electrochemistry case, the driving force for hole injection can be made sufficiently high so more than 5000 holes are injected into the nanoparticle and the fluorescence intensity is completely quenched within experimental error. In the dry hole injection devices studied in the present work, the estimation of charges from the fluorescence intensity is complicated by the expected charge distribution within the NP and the approximately 35% quenching observed in Figure 4.3a leads to an estimate of ~16 holes per particle (see below). The effect of bias on quenching is also shown in Figure 4.3a (connected data points). Clearly the amount of hole injection increases as the bias increases due, presumably, to stabilization of the hole in the nanoparticle by an electrostatic capacitance effect. Indeed, simulations predict a quenching depth that agrees qualitatively with experiment as shown in Figure 4.3b (red curve) -however, other experiments indicate that the situation is considerably more complicated since the hole injection process is actually light initiated, see below.

4.3.3 EFFECT OF BIAS SCAN RATE ON FLUORESCENCE QUENCHING

Figure 4.4 portrays the ensemble average of the fluorescence intensity of many NPs as a function of bias at different scan rates. The data indicates that the charging dynamics of the NPs is close to equilibrium, i.e. showing small hysteresis, at the lowest scan rate used in these experiments (0.1 V/s, Figure 4.4c). At scan rates of 10 and 1 V/s, the F-V curves show significant hysteresis indicating that the charging process does not reach equilibrium at these rates.

4.3.4 EFFECT OF OPTICAL EXCITATION INTENSITY ON FLUORESCENCE QUENCHING

Figure 4.5a portrays the ensemble average of the fluorescence intensity of many

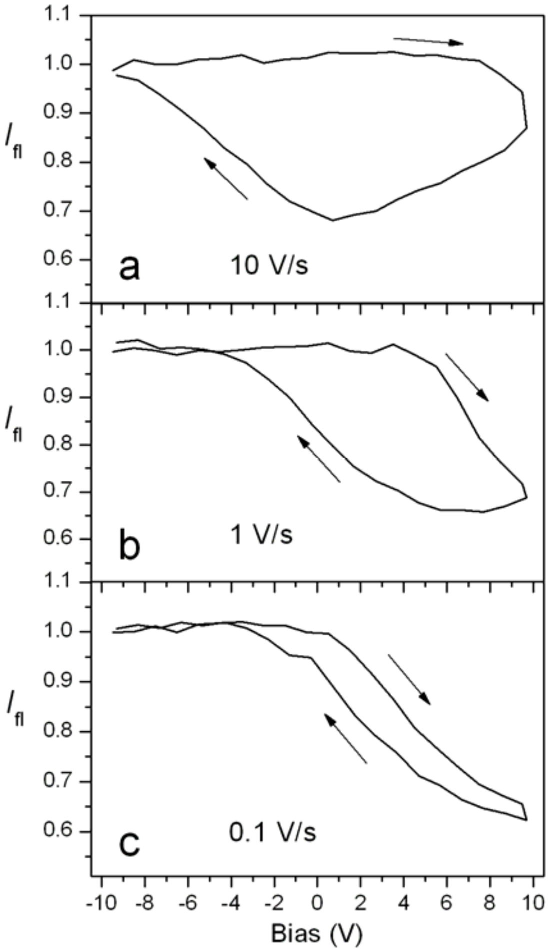

Figure 4.4: (**a-c**) Ensemble average of ~100 normalized single-NP fluorescence-voltage trajectories in a hole-injection device as a function of bias scan rate. Data were obtained at an excitation intensity of 67 mW/cm².

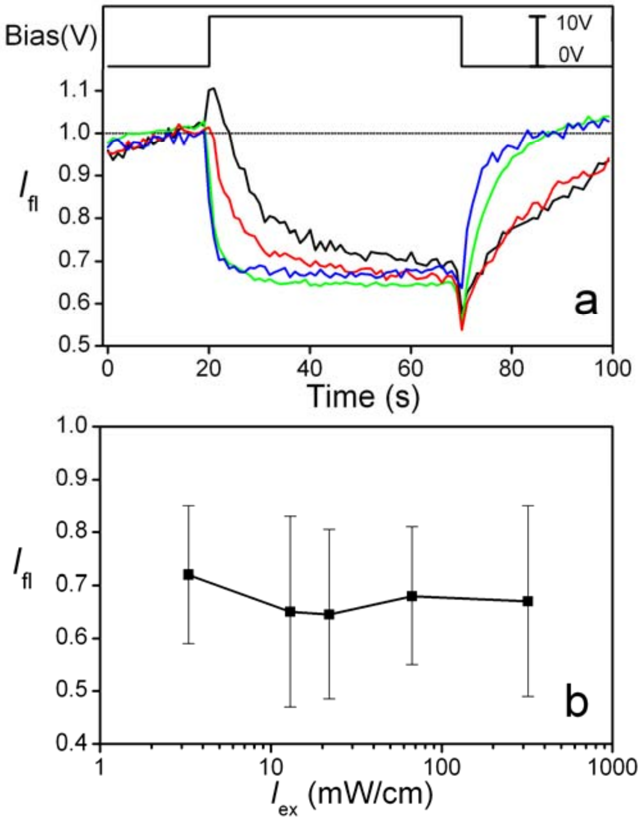

Figure 4.5: (**a**) Ensemble average of ~100 normalized single-NP fluorescence-intensity trajectories in a hole-injection device at different excitation intensities (I_{ex} (mW/cm²): ▬3.3; ▬13; ▬22; ▬67). The data was obtained while applying the bias function shown by the top line. (**b**) Equilibrium normalized fluorescence (time range 60-65 sec) corresponding to the data shown in a. The error bars indicate the standard deviation of the distribution of single NPs equilibrium normalized fluorescence intensity.

NPs as a function of time for different laser excitation intensities. During this time period, a square-wave bias pulse was applied to the device. From these experiments, it is clear that the equilibrium fluorescence quenching of the single NP ensembles are only weakly dependent on excitation light intensity (see Figure 4.5b). Before suggesting possible interpretations for this effect, we consider the dynamics of fluorescence quenching. The fluorescence intensity curves at low light intensity clearly exhibit a build-up of quenching as a function of time. For example, studies performed at the lowest light intensity used (black curve in Figure 4.5a) exhibit a clear delay in quenching. At the higher light intensities, in contrast, the fluorescence quenching is fully established within the time resolution of the experiments. Note that these experiments were performed at very low base pressures (~ 10^{-5} Pa), thus the results in these highly depleted oxygen and water conditions (Figure 4.5a) indicate that the observed single NP charging/quenching is not related to the presence of O_2 and H_2O impurities. The variation of the normalized single-particle florescence quenching depth (error bars in Figure 4.6) and charging/discharging kinetics (not shown) from particle to particle is due to the large size distribution of the MEH-PPV NPs.

The effect of light intensity on the discharging rate is further explored in Figure 4.6 by fluorescence versus time measurements using modulation of both the bias and the optical excitation intensity. These results show that the discharging process of the NPs is also accelerated at higher light intensities. In fact, if charged particles are held in the dark but the bias is made negative, the charge remains in the particles for longer than 0.3 seconds. These data also demonstrate that charging of the NPs at positive bias in the dark occurs at a rate and amount which is too small to be detected by these measurements.

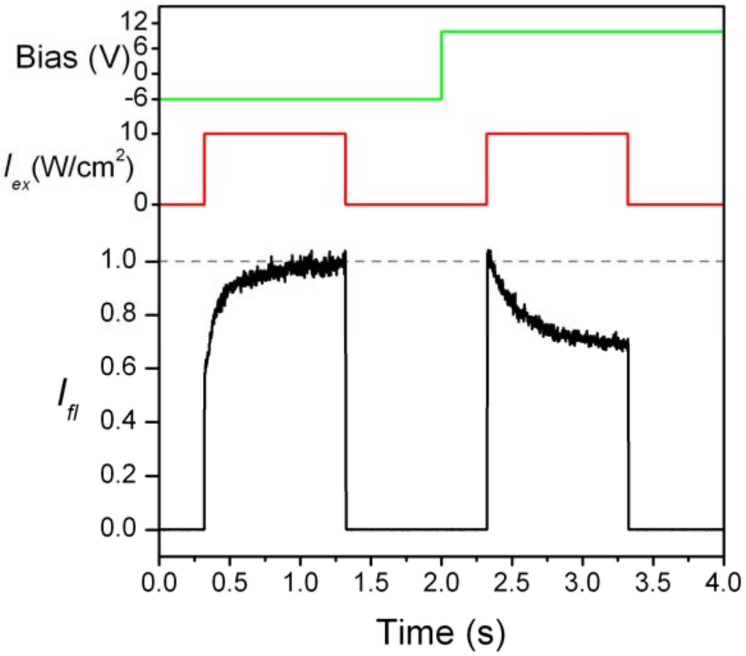

Figure 4.6: (**a**) Single MEH-PPV NP fluorescence-intensity transient (▬) obtained while modulating the light intensity (▬) and electrical bias (▬). The transient was acquired by synchronously averaging 10 sweeps of the shown cycle in a confocal microscope setup[100].

4.4 DISCUSSION

A number of new insights on the nature of hole injection across an organic/organic interface are available by considering the experimental and theoretical results of this paper. The bias dependence of the (fluorescence detected) hole injection process is highly consistent with a mechanism for hole-induced quenching of the MEH-PPV NPs in which hole injection occurs through transfer of holes from the CPB layer into the NP. These results further demonstrate that optical excitation of MEH-PPV is required to transfer holes across the CPB/MEH-PPV interface, presumably involving photo-induced charge transfer from MEH-PPV single excitons and CPB holes.

Interestingly, the amount of hole injection (the number of holes per particle at equilibrium) is independent of the excitation light intensity over a large range, strongly suggesting that while excitation of MEH-PPV is required to accelerate excitation, the amount of charge at steady state under these conditions is probably determined by thermodynamic factors rather than photophysical effects. MEH-PPV excitation is known to accelerate charge transport by a photoconductive mechanism[125, 126] in which MEH-PPV single excitons and MEH-PPV holes interact and induce a transfer of charge from the original position of the hole to the position of the exciton which is thermalized by this process. Such a mechanism could assist the detrapping of holes in MEH-PPV and the transport of holes from the Coulomb well at the insulator side of the NPs which exists at high positive bias. Therefore, a linear dependence on excitation intensity for both the CPB to MEH-PPV hole injection and the return of holes from the NP to the CPB layer could in principle accelerate the equilibration of holes without significantly altering the number of holes per particle at thermodynamic equilibrium.

The proposal that the hole charging of the NPs that is reported in this paper is at thermodynamic equilibrium is highly supported by the qualitative agreement of the amount of quenching as a function of bias observed in the experiment with that predicted by the simulations for the equilibrated particles. The simulations suggest that at thermodynamic equilibrium, the amount of charging of the NPs is controlled by the effective capacitance of the NPs which is determined by many factors, including the geometry of the device, the HOMO energies of the materials, the effective density of states of the different materials, and short-range electrostatic screening effects the CPB/MEH-PPV interface. One important role of the CPB layer in promoting hole injection into the NPs is to function as a nearby reservoir of holes to be injected into the NP in an exothermic process, thus offering a wired connection from the NP to the ITO electrode through the intermediate TPD HTL.

It is highly informative to consider these results in comparison to other recent papers from this laboratory on the injection of holes into *single conjugated polymer chains* from a carbazole HTL[100]. While the results herein show that the amount of quenching only reaches values of approximately 35% for NPs, nearly 100% quenching is observed for single polymer chains[100] which have a radius of approximately 6-7 nm. This can be explained by two factors. First, the simulations show that the charges are piled up on the insulator side of the NPs due to electrostatic screening that causes a decrease in the electric field on the opposite side of the NPs and even in the CPB layer immediately adjacent to the NP. In contrast, for the single polymer chain case, the entire charge region of the chain may be within the quenching distance of the hole, ensuring a much larger amount of quenching at high bias for the single polymer chains. Second, the thin molecular layer in the single polymer case ensures that singlet excitons are created immediately adjacent to the CPB/MEH-PPV interface. In the single polymer chain case therefore, optical excitation affects essentially the entire interfacial region and should be a much greater perturbation on the charge injection process.

Additionally, several insights can be also be made by comparing the results of this paper to recently published results on electrochemical hole injection (oxidation) into single polymer chains[55] and aggregates[113] involving hole injection from an ITO electrode in an electrochemical cell containing a polar solvent and a supporting electrolyte. The number of holes injected per particle observed in the present work at high bias is considerably less than that observed for electrochemical hole injection described previously. This is apparently due to electrostatic considerations. While hole injection in devices in this paper is limited by the effective capacitor formed by the single particle aggregate and the external electrode, in the electrochemical case the negative counter ions of the electrolyte screens the electrostatic repulsion of the holes, allowing for complete charging of the surface of the NPs. Second, since holes are injected in the electrochemical case across an electrochemical double layer whose potential drop is controlled by an external potentiometer using a reference electrode, the Fermi potential at the NP can be scanned over a large range. In fact, the Fermi potential can be scanned over a range sufficient to ensure complete charging of the nanoparticles and ultimately chemical decomposition due to the high degree of oxidation. This is in contrast to the case of the capacitor charging experiment of NPs in which the NP Fermi potential is limited by the NP and CPB capacitance and the HOMO energies of the various layers.

The importance of hole trapping to the processes described in this paper is unclear. It may be that hole trapping is required to achieve the thermodynamic equilibrium that is observed under moderate to high excitation intensities. If this is in fact the case, then the present results imply that optical excitation may accelerate the formation of deeply trapped holes, allowing charging equilibrium to be achieved. This would closely parallel the conclusions of our recent report[100] in which hole injection into single polymer chains requires a cooperative hole induced charging involving a mechanism denoted by LIHT. Further research will be needed, however, in order to establish the actual relationship between the photoinduced charging process for single polymer chains and NPs. It is likely however that both the energetics and kinetics of charge injection from an HTL into an NP involve two factors, i.e. electrostatic interactions and molecular effects, such as the deep trapping of holes.

4.5 CONCLUSION

The hole injection from a CPB HTL into MEH-PPV NPs was investigated by an indirect single-particle fluorescence quenching technique. The results strongly suggest that there is a kinetic barrier for hole injection which limits the injection to slower than the 100 second time scale. This barrier can be overcome with the assistance of optical excitation of the MEH-PPV nanoparticles, achieving a thermodynamic population of injected holes at positive bias. The amount of injected holes at equilibrium is observed to depend upon the bias in a manner highly consistent with device simulations based on a continuum model. Overall, the results demonstrate that the hole injection into nano domains of conjugated polymers is a complex process depending upon molecular interfacial effects and electrostatic interactions.

Chapter 5: Modulation of the Photoinduced Charge Separation at the Nanostructured Heterojunction in Model Photovoltaic Devices

5.1 OVERVIEW OVER CHARGE TRANSFER STATES

5.1.1 PHOTOINDUCED CHARGE SEPARATION IN ORGANIC SOLAR CELLS

Photoinduced charge separation which occurs at the heterojunction between organic materials is one of the most important physical phenomena that influence the overall efficiency of the solar energy conversion. The discovery of efficient charge separation, especially between conjugated polymers and soluble fullerene derivatives, drew great interest in the development of efficient and low-cost organic photovoltaic devices. Several donor/acceptor systems, either between conjugated polymers [127, 128] or conjugated polymer and fullerene based molecules [129, 130] with high charge separation properties, have been employed to realize photovoltaic devices with high performance. The best efficiency of the solar power conversion (~6 %) has recently been reported from the device having a tendem cell structure [131], indicating these materials as a possible candidate for the next generation of organic solar cells. However, there are still many obstacles to overcome to achieve photovoltaic devices with reasonable solar power conversion efficiency for the commercial impact. Even though its advantages over the inorganic counterpart such as high absorption coefficient of conjugated polymers, flexibility of tuning the properties of materials, low fabrication cost and easy processing, poor overlap between the absorption spectrum of the organic chromophores and solar spectrum, low charge mobility and large exciton binding energy (~0.5 eV) in organic materials have retarded the progress in developing solar cells with high efficiencies.

The large binding energy of the Frenkel type excitons typical in organic materials is characteristic of materials with low dielectric constants. Unlike the Wannier excitons in most crystal materials with high dielectric constant which has reduced Coulomb interaction between electrons and holes and thereby a radius much lager than the lattice spacing, Frenkel excitons are delocalized excitons with high Coulombic interaction. The tight-bonding model [132] describes that increased electron-hole Coulomb interactions as well as the reduced exciton size of the Frenkel excitons are due to the less screening effect in organic materials, leading to high localized excitations with a high binding energy. These Frenkel excitons are usually required to reach heterojunction to undergo the charge separation process. The driving force for this process is provided from the energy offset between the highest occupied molecular orbital (HOMO) of the donor and the lowest unoccupied molecular orbital (LUMO) of the acceptor. Since the diffusion length of the excitons in organic materials is typically short (~10 nm), bulk blend systems with the increased interfacial region have been employed to increase the probability of capturing the excitons at the interfaces between donors and acceptors.

Many efforts have been contributed to enhance the solar power conversion efficiency. For instance, tailoring the molecule structure to tune the bandgap of the polymer for harvesting most of the solar spectrum [133, 134], controlling the surface morphology between donor and acceptor for higher charge separation efficiency [135, 136], and engineering the structure of devices for the improved charge transport and contacts have been reported [131, 137]. However, the charge transfer state which is directly related to the charge separation process has not been investigated enough to provide a clear consensus on its role in the charge separation process. Therefore, more research is required to obtain a better understanding of the charge transfer state as well as its effect on the photogenerated charge transfer process. In this review section, two different types of charge transfer states found in various different systems will be introduced with their characteristics. At the end, a quantum chemical model describing the character of these interfacial states will be described in detail.

5.1.2 FORMATION OF TWO DIFFERENT TYPES OF CHARGE TRANSFER STATES

Charge transfer states which are intragap states forming at the heterojunction play important roles in either enhancing or reducing the yield of the charge separation process. The charge separation process has been considered to be a single-step electron transfer process directly from the donor to the acceptor material and yields of this process depend on the local electric field and the density of states for free carriers [138]. However, it has recently been proposed with many evidences that this process involves one or more intermediate steps which are related to the charge transfer states [14, 127, 139, 140]. For example, Morteani et al reported the formation of the Coulombically bound germinate polaron pairs which either relax into an energetically favorable exciplex state or undergo charge separation at a polymer/polymer heterojunction [127]. Another type of the charge transfer state was reported from the polymer/PCBM system which has exhibited the highest power conversion efficiencies to date [139, 140]. The charge transfer states observed in this system were characterized by their interaction with a ground state. The existence of these states is believed to significantly affect the charge transfer process because the dissociation of the excitons is favored in the proximity of a charge transfer state. Furthermore, the probability of capturing excitons at the heterojunction increases in the presence of theses states because the distance of the exciton migration to interfaces decreases, which can reduce recombination loss. On the other hand, they also work as trap sites for the separated charge carriers, resulting in reducing the photocurrent.

Since the charge separation process takes place in the time scale of femtoseconds (~40 fs) [141], optical spectroscopy has widely been used to reveal the electronic interactions, where fluorescence quenching is an indicator of the charge separation. Especially, measurements of the fluorescence intensity quenching due to the exciton or geminate-pair dissociation under the applied electric field provided useful information regarding the nature of these states [127, 139]. The Onsager model which extracts the exciton binding energies using a δ function distribution for the electron hole separation has been used to fit the data collected from the fluorescence measurements under the applied electric field [142]. It calculates the dissociation probability of the excitons (or geminate pairs) in a medium with dielectric constant ε under an applied field F and at temperature T [14, 127, 139]. Estimation of the electron-hole separation within the geminate pair formed at PFB/F8BT heterojunction [14, 127] , calculation of the binding energy of the charge transfer exciton at the heterojunction between MDMO-PPV/PCBM and description of the observed field and temperature dependence of the photocurrent in PPV:PCBM blends using the Onsager model were reported [143]. There are, however, still many issues under the discussion about the formation of this charge transfer state and its role on the charge separation mechanism [139, 143, 144].

5.1.2.1 CHARGE TRANSFER STATES COUPLED TO GROUND STATES IN POLYMER/PCBM SYSTEMS

Recently, the existence of the charge transfer state has been reported from the model photovoltaic blend system between poly[2-methoxy-5-(3',7'-dimethyloctyloxy)-1,4-phenylene vinylene] and [6,6]-phenyl C_{61}-butyric acid methyl ester (MDMO-PPV/PCBM) [139]. An additional low energy emission peak appeared at 840 nm from the direct photoluminescence excitation experiment, indicating that the charge transfer state results from the state interaction with the ground state. The fact that the charge transfer state couples to the ground state in this system is quite different from the exciplex states formed at polymer/polymer heterojunction in that the exciplex state is dissociated or only weakly associated in its ground state [139]. This emission was ascribed to the recombination of electrons and holes at the charge transfer state which is localized to the interfaces between two materials. This state is believed to be involved as an intermediate step in the ultrafast charge separation. Unlike the Frenkel excitons typical of the pristine polymer, it was estimated from the Onsager model where 1.88 nm was used as a fitting parameter for the electron-hole separation distance that the excitons occupying the charge transfer state have smaller binding (130 meV) [139].

More evidence for the formation of a charge transfer state which also coupled to the ground state was provided from the hybrid donor acceptor interfacial region in blend films of poly[9,9-dioctylfluorene-*co*-*N*-(4-methoxyphenyl)diphenylamine] polymer (TFMO) and [6,6]-phenyl-C61 butyric acid methyl ester (PCBM) [10]. Composition dependent additional long wavelength absorption was ascribed to the formation of the charge transfer state. The study of the correlation between the observed long wavelength optical features and charge generation on a series of polyfluorene polymer/PCBM systems revealed that ionization potential of the polymer plays an important role in the formation of the charge transfer state in these systems. On the other hand, the optical gap of the polymer as well as the surface morphology of the blend film turned out to have nothing to do with the formation of a charge transfer state. It was also suggested from the efficient photocurrent generation in the blend films where charge transfer states were observed that this charge transfer state may be closely involved in the charge separation process [10].

5.1.2.2 BOUND INTERMEDIATE STATES IN POLYMER/PCBM SYSTEMS

The formation of the geminate electron hole pair at the polymer-fullerene interface was reported to be closely related to the charge transfer process [144]. This intermediate state which forms directly following the dissociation of the photogenerated excitons is the place where two opposite processes, geminate recombination and complete charge separation, compete against one another. Müller et al studied the exciton dissociation and the geminate charge recombination dynamics using a combination of two-pulse femtosecond spectroscopy with photocurrent detection [144]. It was already reported that these intermediate states were formed in neat conjugated polymer film [145]. Therefore, the question they addressed was whether such bound intermediate states are also relevant in polymer/fullerene blend or not. Two different systems of the MDMO-PPV/PCBM and [methyl-substituted ladder-type poly(*p*-phenylene)] (MeLPPP)/PCBM were chosen to answer the question because of their opposite characteristics of charge dissociation. Their results show that strong geminate recombination was observed from the MeLPPP/PCBM system, resulting in a lower efficiency for photocurrent generation in spite of its high hole mobility. On the other hand, photocurrent with more than one order magnitude higher was exhibited in the MDMO-PPV/PCBM system. The differences in yields of the photocurrent were explained to arise from the different morphology of the film at the heterojunction. The ultrafast anisotropy measurement performed to examine the film morphology exhibited that conjugate segments of MDMO-PPV are stacked with parallel orientation and the initial exciton migration is preferentially of an interchain type. Therefore, in MDMO-PPV geminate polarons relax to delocalized states in ordered domains, which increases the distance of charged carriers within the geminate pair, leading to the lower binding energy and the resulting efficient dissociation. In addition, the close stacking of chain segments in the MDMO-PPV film helps excitons migrate much faster, increasing the probability of capturing the excitons at the interfaces.

5.1.2.3 BOUND INTERMEDIATE STATES IN POLYMER/POLYMER SYSTEMS

Friend group at Cambridge introduced the concept of the formation of the bound intermediate state earlier from the polymer/polymer heterojunction system [127].

Contrary to other systems reviewed thus far where PCBM was present as an electron acceptor, poly(9,9-dioctylfluorene-co-benzothiadiazole) (F8BT) was blended with either poly**(**9,9- dioctylfluorene - co - bis-N,N- (4 -butylphenyl)-bis-N,N-phenyl-1,4-phenylenediamine**)** (PFB) or poly**(**9,9-dioctylfluorene-co-N-(4-butylphenyl)diphenylamine**)** (TFB) in their study. Despite the similarity in the chemical structure of these two materials which involve fluorene in their repeat unit, they show a completely opposite charge separation behavior when blended with F8BT. In practice, the F8BT/PFB is a well known donor/acceptor system for a photovoltaic application due to its high charge separation efficiency while the F8BT/TFB blend is better suited for OLEDs for its high charge recombination property. Therefore, a close scrutiny of these two systems was expected to allow us to understand important clues to how these charge transfer states are related to the observed charge separation efficiency and what physical parameters give rise to that difference.

A simple classification of materials into either one type showing high efficient charge serration or the other having high luminescence quantum yield is not enough because, for example, F8BT has both characteristics when blended with different types of hole acceptor materials. Therefore, it has been required to develop a new description unifying the different excitation dynamics at the polymer heterojunction system. They showed that exciton dissociation occurs in all blend systems followed by the formation of an interfacial geminate charge pair. After that, two processes are present competing against each other: The first process is a regeneration of the bulk exciton through geminate pair recombination. An intermediate heterojunction state which is an exciplex is involved in between the bulk exciton and interfacial geminate pair. Thermal energy of 100~200 meV was suggested as a driving force for these transitions between the different excited states. Therefore, the net charge separation and photoluminescence yields were suggested to be determined by a fine balance of the kinetics of these processes. The other process which competes with geminate pair recombination is a complete dissociation of the geminate pair in aid of the applied electric filed at the heterojunction. The relevant potential energy curves are shown in Figure 5.1 where A and D represent the acceptor (F8BT) and the donor (PFB and TFB), respectively. In this new model, three different excite-states are distinguished as follows: ‘primary excitons’ generated in the bulk upon excitation, ‘exciplexes’ formed by energy transfer from bulk excitons and ‘secondary excitons’ generated via endothermic back electron transfer from the exciplexes [127].

The detailed investigation on a charge separation process was performed using time-resolved photoluminescence measurements, which showed that excitons in these two systems are marginally stable against charge separation and these excitons undergo charge separation at the heterojunction. However, the plotting of the fluorescence quenching data into the Onsager model could be achieved based on the assumption that a geminate pair intermediate forms before an exciplex forms and has a separation distance of 3.1 nm and 2.2 nm for the PFB/F8BT and TFB/F8BT, respectively. The temperature dependence of the fluorescence intensity also exhibited that the ratio of secondary excitons to exciplexes follows an Arrhenius function. The activation energy for the endothermic back transfer towards the bulk exciton was calculated as to be 200 ± 50 meV and 100 ± 30 meV for the PFB/F8BT and TFB/F8BT, respectively. They suggested that different charge separation kinetics between states involved in these two systems originate from the different thermalization distance as well as activation energy.

5.1.2.4 BOUND INTERMEDIATE STATES IN BILAYER POLYMER/POLYMER SYSTEMS

Research on charge-transfer states was further extended from bulk heterojunction blends into the F8BT/PFB bilayer system [14]. Especially, the effect of an applied

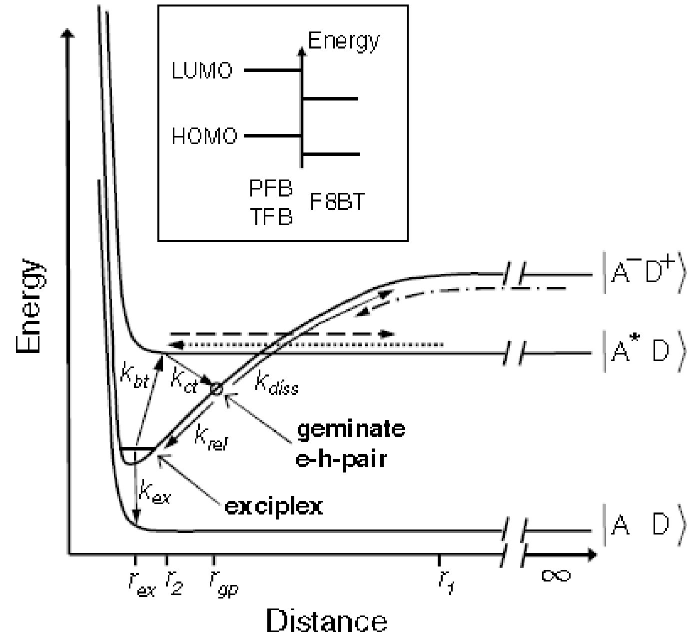

Figure 5.1: Potential energy diagram describing the concept of the formation of the intermediate state at PFB:F8BT vs TFB:F8BT polymer heterojunctions. $|AB\rangle, |A^*B\rangle$ and $|A^-B^+\rangle$ represent the ground state, the excited state and the charge separated state across the heterojunction, respectively. k_{ct}, k_{diss} and k_{rel} represent the rate constant of the geminate pair formation, geminate pair dissociation and relaxation of geminate pair into the luminescent exciplex state, respectively. k_{ex} and k_{bt} represent the rate constant of the exciplex decay and exciplex back transfer to a bulk exciton. The intermolecular distance was used as the X-axis. The inset shows the band offsets at the heterojunction between donor and acceptor polymer [127].

electric field on the charge separation was investigated by measuring the field induced fluorescence modulation at both room and low temperatures. Quenching or enhancement of fluorescence intensity as spectroscopic evidence for charge transfer was found to depend on the direction of an electric field applied. They suggested a simple model describing the observed fluorescence modulation behaviors (Figure 5.2). When heterojunctions formed between two polymers are well aligned in such that the direction of hole transfer coincides with that of an applied electric field, an increase in fluorescence intensity was observed. On the other hand, a change in either the relative orientations of the interface or the direction of an E-field results in a decrease in fluorescence intensity. The observed modulation of exciton dissociation yield under the applied electric field was ascribed to modification of the energy of the charge-transfer state. Therefore, a wide distribution of the charge separation yields was expected to be observed in disordered systems. It was also reported from other researchers that it is possible to control the charge-transfer energetics in donor-acceptor molecules with an external electric field [127, 139]. The field induced fluorescence modulation was also modeled by the interaction between the dipole moment of the charge-separated state and the external field [146].

The temperature dependence of the photoluminescence (PL) electromodulation on the bilayer system was also investigated [14]. Since the thermal repopulation of secondary excitons from exciplexs is almost negligible at low temperature, a comparison of the results collected from low (13K) and room temperature measurements was expected to reveal the thermally assisted nature of the charge separation process. Both measurements exhibited the clear dependence of the fluorescence modulation on the direction of an applied electric field and bilayer orientation as proposed in a simple model shown in Figure 5.2. While the spectra of both quenching and enhancement of the fluorescence intensity (Δ PL) resemble the pure F8BT spectra in shape at low temperature measurement, fluorescence quenching spectra at room temperature varied strongly with emission wavelength and had little resemblance to the pristine F8BT PL spectra [14]. This difference observed was ascribed to the formation of the charge-transfer state at room temperature because of the broad feature of spectra peaking at 650 nm which is identical to exciplex emission in F8BT/PFB blend. It was emphasized that this fluorescence quenching is not due to the dissociation of the exciplex state excitons but due to the geminate pairs on charge transfer state which formed prior to the exciplex state [127]. At low temperature, however, resemblance of spectra between pristine F8BT and the bilayer F8BT/PFB confirmed that changes of exciton emission was responsible for the modulation.

The Onsager's model was used to fit the field induced fluorescence quenching data which exhibited a clear saturation at a high electric field. The value of 2.9 nm as a distance for the geminate pair separation was calculated based on the assumption that the charge pairs are aligned parallel to the applied field with a dielectric constant of 3.2 [14]. Considering the value previously reported in F8BT/PFB bulk heterojunction blends which was 3.1 [127], we can infer that intermediate states for geminate electron hole pairs are similar in both bilayer and bulk heterojunction blend systems.

5.1.3 QUANTUM-CHEMICAL MODELING DESCRIBING THE CHARGE-TRANSFER STATES

The quantum-chemical molecular modeling for these charge-transfer excitations was developed by Huang et al for both F8BT/PFB and F8BT/TFB systems [15]. The charge-transfer exciton in these systems shows sufficient overlap of electron and hole wavefunctions, leading to significant luminescence. This emission state which has been termed 'exciplex' is characterized by an increased radiative lifetime (~100 ns) as well as

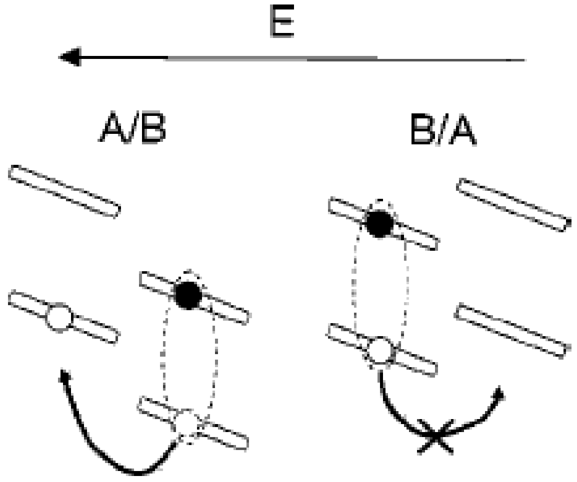

Figure 5.2: A simple model describing the electric-field-induced charge transfer at a heterojunction between polymer A and polymer B [13].

a substantial red-shift. The formation of these states which is usually understood in terms of the redox potential [147] was recently described by the different orientations of the molecules at the heterojunction, resulting in either repulsive or attractive interchain interactions [148]. The calculation of the Coulomb interaction between exciton states on one chain and the ground state on the other done by Sreearunothai et al revealed that the repulsive interaction leads to a blue-shift emission, whereas the attractive interaction prefers forming the exciplex state, resulting in enhanced charge separation [148]. Similar descriptions of exciplex that match experiments very well were produced experimentally in the model proposed by Huang et al [15]. However, for the F8BT/PFB system, this model revealed the existence of the energetically similar but non-emissive charge-transfer states, explaining why this system has low fluorescence quantum efficiency. Thus this founding provided a general framework for the description of electron-hole capture or separation at heterojunctions.

The detailed calculation was done by calculating the polarization energy induced by the presence of F8BT on the PFB exciton as varying the relative displacements of the PFB chain from the F8BT backbone. The results exhibited that either attractive or repulsive interactions appear as a result of the different orientations of the interacting chains. This is in quite good agreement with previously reported Sreearunothai's work [148]. While the charge interactions give rise to a red-shift of the PFB electronic transition under the attractive configurations, a blue-shifted PFB optical transition was shown in the repulsive configuration. In addition, it was observed that a pronounced charge-transfer occurs between the partial negative charges on the BT unit of F8BT and a neighboring positively charged triarylamine group of PFB in the attractive configuration.

The characteristics of the lowest singlet excited states such as excitation energy, radiative lifetime and charge redistribution were also calculated as a function of displacements along the molecule backbone. In F8BT/PFB cases, three distinct regimes were revealed. The first electronic transition occurred at an energy of ~2.3 eV and with a lifetime of 1~2 ns in the first regime. These values are comparable to the experimental values for F8BT excitons. In the second regime, excited states with a calculated prolonged lifetime up to a few hundred nanoseconds were identified. This increased radiative lifetime is similar to characteristics of exciplex states. For the last regime, the lowest excited state was identified as polaron-pair excited states. This state is characterized by a much longer lifetime and smaller oscillator strength, but similar excitation energy to that of the exciplexes.

The same calculation was performed on F8BT/TFB systems, revealing that three different regimes also exist. For the first two regimes, they were almost identical to those of F8BT/PFB system. The first electronic transition occurred at an energy of ~2.46 eV and with a radiative lifetime of ~1.5 ns. This electronic excitation also had a dominant excitonic character. In the second regime, calculated long lifetime of a few hundred nanoseconds indentify this state as emissive exciplexes. However, in the last regime, the calculation shows that lowest excited state which is referred to charge transfer-exciton state had a characteristic which cannot be clearly classified as either excitons or exciplexes because both localized and charge-transfer excitations contribute to its wavefunction. As compared to exciplex state, the charge-transfer state in this regime shows a much lower intermolecular charge transfer character.

5.2 INTRODUCTION

The photo-induced charge transfer rate, which is an important factor affecting the overall efficiency of organic electronic devices such as organic light emitting diodes (OLEDs), organic thin-film transistors (OTFTs) and organic photovoltaics, has been reported to be significantly affected by an applied electric-field (or bias potential). As an important technique to investigate the nature of the field induced exciton dissociation as well as exciton interactions with polarons in conjugated polymers, measurements of the fluorescence intensity enhancement or quenching upon applying bias potential have been widely utilized [14, 20, 24, 127]. In practice, the electric field induced fluorescence intensity dynamics of a phenyl-substituted poly(phenylene-vinylene) (PhPPV) due to the modulation of the rate of exciton dissociation [149] and efficient singlet exciton quenching of poly[2-methoxy-5-(2'-ethyl-hexyloxy)-1,4-phenylene vinylene] (MEH-PPV) due to the interaction with injected hole polarons from hole transport layers are reported, respectively [20, 24]. However, the tremendous, complex nature and physics of these conjugated polymers occurring, in particular, at heterojunctions between two different materials have severely limited their molecular-level understanding.

The complexities of these materials are ascribed to the combination of the following factors: First, the interfacial regions of nanostructure materials have been reported to exhibit complex molecular organization [150, 151]. Second, the static morphological disorder (heterogeneity) in nanomaterials resulting from the presence of a broad distribution of interfacial regions further increases the complexity due to variations in the alignment of the energy bands of the highest occupied molecular orbital (HOMO) and lowest occupied molecular orbital (LUMO) [17, 152]. Third, the PV process itself is very complex since it involves several individual primary processes (light absorption, exciton diffusion, charge transfer and charge collection) as well as a diverse set of species such as singlet and triplet excitons, polarons and deeply trapped holes. Fourth, dynamic disorder due to the presence of these species, in particular, when they are present in close proximity, also leads to the further complexity. Recent photoconductive atomic force microscope (AFM) measurements [17, 152, 153] revealed, as a consequence of these complexities, a broad distribution of interfacial regions with different PV efficiencies, indicating the necessity of the new molecular level technique rather than ensemble average tools to explore the charge transfer process occurring in small local nanodomains.

The fluorescence-voltage SMS technique was first introduced in this group to study charge injection in device environments which are similar to organic LEDs, memory cells and photovoltaic devices [20, 154]. In FV-SMS, fluorescence intensities of each individual single molecule (or particle) are recorded as a function of the bias applied across the device. This technique is analogous in several ways to the widely used conventional current vs. voltage measurements. However, the enormous advantage of the FV-SMS technique over the conventional IV measurement is that it allows us to unravel the complex nature of conjugated polymers or complicated processes occurring in organic devices by mitigating factors contributing to the complexities mentioned above. In reality, the measurement of the small number of charges injected per single nanoparticle (or molecules), which is impossible to directly measure with bulk measurement methods, was reported by indirectly monitoring the fluorescence quenching in specially designed devices [20, 24, 155]. In this research, a new experimental tool, a home-built vacuum wide-field microscope, coupled with FV-SMS as a powerful tool to unravel the complex nature and physics of organic materials, was introduced on a model photovoltaic device (Figure 5.3A) composed of nanostructured binary composites of the organic semiconductors either F8BT/ poly-(9,9'-dioctylfluorene-*co*-bis-*N*,*N'*-(4-butylphenyl)-bis-*N*,*N'*-phenyl-1,4-phenylenediamine (PFB) or F8BT/ poly(9,9-dioctylfluorene-*co*-*N*-(4-butylphenyl) diphenylamine) (TFB). The F8BT nanoparticle systems employed in this nanostructured heterojunction are expected to have enormous advantages over the F8BT bulk film because the necessity to transport charge across the bulk film, the poorly defined nature of the Fermi potential profile within the film and complicated interfacial dipoles could be ignored in the nanoparticle system while they still keep the same nature of organic semiconductors with bulk polymers. In addition, the donor/acceptor interfaces studied here are oriented in a precise direction relative to the applied electric field which greatly simplifies the analysis of the effect of electric field on the energetics and yields of charge separation and related processes.

The F8BT/PFB is well known as a photovoltaic donor/acceptor system for its high charge separation efficiency as opposed to F8BT/TFB which is better suited for OLEDs due to its high charge recombination property [127]. Negatively separated charge carriers remain in a F8BT single-assembled nanoparticle while positively charged carriers move to the energetically favorable bottom PFB (or TFB) layers following exciton dissociation in individual isolated nanodomains in this prototype of capacitor-like device. Fluorescence intensity modulation as a result of these charge separation processes under the applied electric field used as an indirect indicator showing charge separation yields. Different charge separation property between two polymers was studied with different excitation intensities.

To differentiate an electric field induced fluorescence modulation from fluorescence quenching by the interaction of excitons with injected hole polarons from the hole transport layer at positive bias, the device structure was modified where the bottom PFB (or TFB) layer was replaced with an inert PMMA polymer. This modified device structure is also identical to that of the previously studied hole injection devices, except that self-assembled MEH-PPV nanoaggregates were replaced with F8BT nanoaggregates. Therefore, it further allows us to compare the nature of hole injection of these two different conjugated polymers. Other comparison devices, such as charge separation only device where the hole transport layer was replaced with an organic

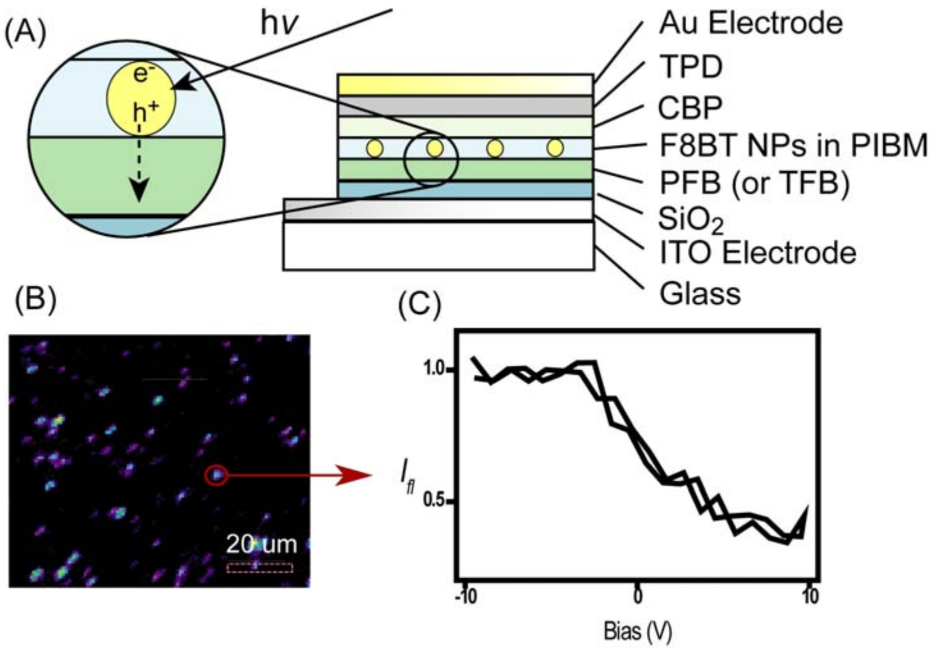

Figure 5.3: (A) The structure of the model photovoltaic device and the expanded view of the heterojunction of the nanostructured binary composites of the organic semiconductors (F8BT/PFB). The arrows indicate the absorption of the photo energy *hv* and the direction of charge flow upon charge dissociation, respectively. (B) The fluorescence image showing individual F8BT nanoparticles in a model device and (C) corresponding fluorescence intensity vs. bias plot of an individual F8BT nanoparticle as shown in (B).

insulating layer (Figure 5.6A) and the device of F8BT single molecules rather than nanoparticles (Figure 5.6B), were also investigated. A wide range of excitation intensities as well as bias scan rates were applied to study the kinetics of photoinduced charge dissociation and charge injection processes.

5.3 EXPERIMENTAL

Research has been performed using FV-SMS coupled to a home-built vacuum wide-field microscope with the optical excitation provided by the 488-nm line of an ArKr ion laser on isolated donor/acceptor nanodomains in the model photovoltaic devices.

5.3.1 DEVICE FABRICATION

The model photovoltaic device shown in Figure 5.3A was fabricated as the following: The dielectric layer of SiO_2 (70 nm) was grown with inductively coupled plasma chemical deposition (ICP-CVD) (Oxford instruments, Plasmalab 80plus) on top of a patterned indium tin oxide (ITO) coated coverslip at 200 ^{O}C following consecutive cleaning processes of the ITO electrodes with sonication in trichloroethylene (Sigma-Aldrich, HPLC), acetone (Fisher, HPLC) and methanol (Fisher, HPLC) for at least 20 min for each step. A 100 nm thick of the hole acceptor layer of PFB (American dye source Inc., average MW =60 kg/mol) (or TFB, (American dye source Inc., average MW =34 kg/mol)) was deposited by spincoating from toluene on top of the ITO.

Electron acceptor F8BT (American dye source Inc., average MW = 70 kg/mol) nanoparticles were prepared from the precipitation method as illustrated in Figure 5.4A [22]. The 12 μL of F8BT solution in tetrahydrofuran (THF) with an optical density of 4 was injected into a 2 mL solution of poly(isobutyl methacrylate) (PIBM) (Acros, Mw = 300 kg/mol) in cyclohexane while stirring the solution. The size of the self-aggregates is estimated about 25 ± 15 nm for radius based on the intensity comparison with a reference nanoparticle sample with a known size distribution. The histogram of the size distribution of the nanoparticles obtained from this method is also shown in Figure 5.4B.

The resulting colloidal solution was spin-cast on top of the hole acceptor layer to form the heterojunctions where nanoparticles are embedded in the host matrix of a 25 nm thick PIBM layer and are in good contact with the hole accepting layer from the bottom. Both PFB (or TFB) and PIBM were dissolved in orthogonal solvent for each other in order to prevent an erosion problem. To confirm the morphology of interfaces between two polymers, the atomic force microscope (AFM, Digital instruments, Dimension 3100) study was performed. Cyclohexane which is the solvent for the PIBM was dropped on top of the rotating PFB film which was previously deposited on a coverglass. The thickness of the PFB film before and after a drop of cyclohexane was almost identical. Though the surface roughness of the film increased after a drop of cyclohexane as shown in Figure 5.5, the variations in the film roughness is acceptable considering the size of nanoparticles compared to the dimension of the scanned image. Thicknesses of each layer, which were confirmed by the AFM analysis, were also precisely controlled by adjusting the concentration of the solution and the spinning speed of the spin-coater.

The hole transport layers (HTL) of 4,4’-N,N’-dicarbazole-biphenyl (CBP) (Sigma Aldrich, 98 %) and N,N’-bis(3-methylphenyl)-N,N’-diphenylbenzidene (TPD) (Sigma Aldrich, 99 %) were thermally deposited with thermal deposition under high vacuum (10^{-6} Torr). The deposition rate was 1 Å/s and the thickness of each layer was controlled to be 25 nm. Gold (Cerac, 99.99%), as a top electrode, was thermally deposited consecutively under the same conditions as those used for HTL depositions. For the deposition of both HTL and gold, electrode shadow mask was used for the patterning of all the layers. Then completed devices were wired for electrical measurements using

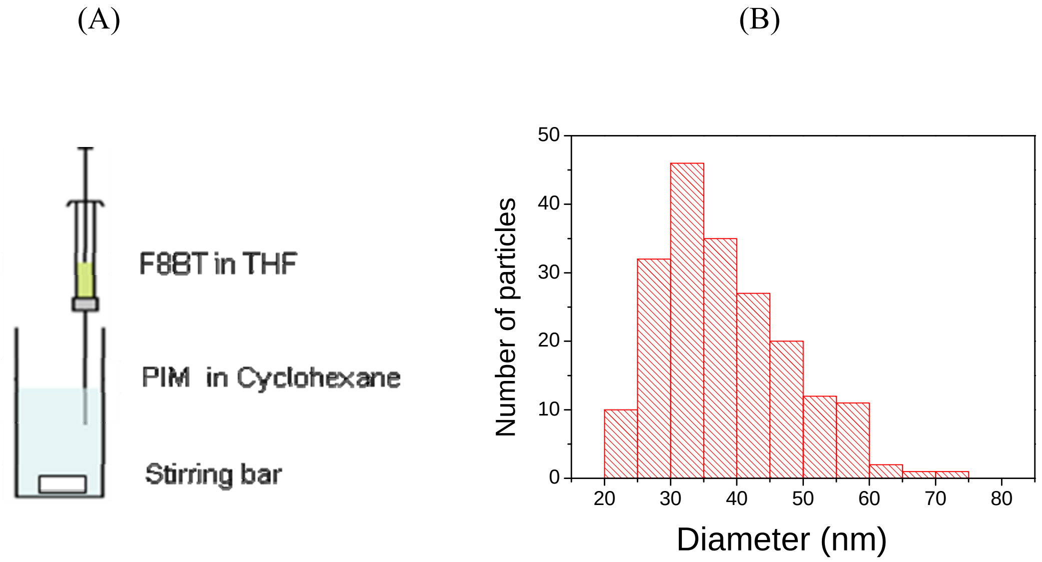

Figure 5.4: (A) The illustration showing the setup of the precipitation method for nanoparticle synthesis and (B) the size distribution of nanoparticles prepared in this method. The average diameter was ~38 nm with a standard deviation of ~10 nm.

silver paint. All the processes for the device fabrication except the deposition of the dielectric layer were performed inside the glovebox (MBraun, O_2 and H_2O concentrations below 5 ppm) to prevent devices from being exposed to oxygen or water which are well known sources for photobleaching of the conjugated polymers. It is inevitable for short time exposure of the device to air after SiO_2 deposition. All measurements were performed under high vacuum (10^{-7} Torr) pressure.

Other comparison devices (Figure 5.6) were fabricated by modifying the structure of the previously mentioned standard device shown in Figure 5.3. For devices used to specifically study the hole injection effect (without charge separation), the bottom PFB (or TFB) layer was replaced with the same thickness of the inner polymer layer of poly(methyl methacrylate) (PMMA) (Sigma Aldrich, Mw = 101 kg/mol). All others except the newly introduced bottom PMMA layer are the same as the structure shown in Figure 5.3. To study only the effect of the charge separation, blocking of hole injection was tried by replacing the CBP and TPD hole injection layers with a new dielectric polymer polyhydroxystyrene (PHS, polyscience, Mw = 20 kg/mol) (Figure 5.6A). The PHS was reported to have good dielectric properties when incorporated as an insulating layer in organic field-effect transistors (TFTs). In addition, PHS was chosen because it is dissolved in ethyl acetate which is orthogonal solvent for the bottom hole accepting polymer PFB (or TFB). However, the AFM study indicated that ethyl acetate completely washes out the bottom PIBM matrix. Therefore, the PHS dielectric layer was spin coated from ethyl acetate on top of the F8BT nanoaggregates layer where nanoparticles are isolated without the PIBM matrix layer (Figure 5.6A). In addition, devices with F8BT single molecules (Figure 5.6B) instead of nanoparticles were fabricated in a little bit different geometry of the device structure where F8BT single molecules were also directly embedded in the hole accepting PFB film.

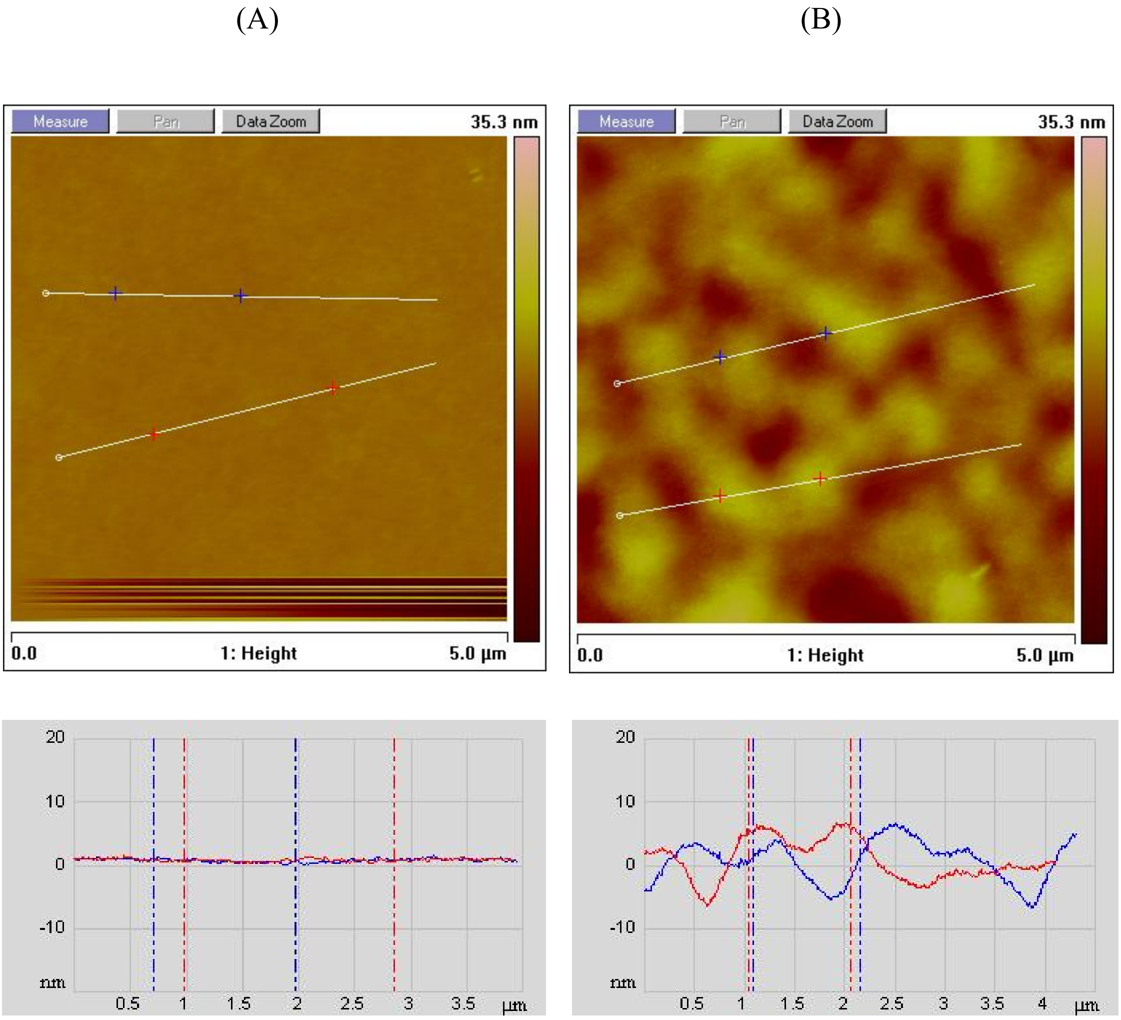

Figure 5.5: AFM images showing the surface morphology of (A) the pure PFB film and (B) a drop of cyclohexane on PFB film while spin casting. Line-scanning data below show the roughness of the surface, which are 0.24 nm and 2.70 nm (rms), respectively, corresponding to the image above.

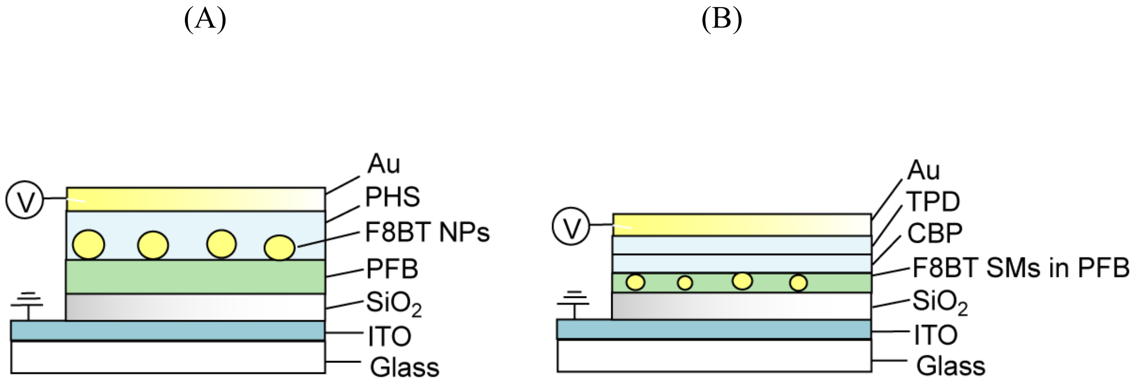

Figure 5.6: Other device structures studied as control devices. (A) The charge separation only device and (B) the F8BT single molecule device

5.3.2 HOME-BUILT WIDE FIELD VACUUM MICROSCOPE

The experimental apparatus is a home-built wide field vacuum microscope which was recently designed and built to study the effects of atmosphere on the performance of organic devices. This microscope is equipped with a mechanical rotary pump coupled to a turbo-molecular pump and is capable of reaching a base pressure of 10^{-7} Torr. A combination of vacuum gauges (InstruTech IMG-410 and CMV-221) were used to monitor the pressure inside the chamber [155]. The schematic of this microscope is shown in Figure 5.7.

All optics are located outside the chamber with the exception of the long working distance microscope objective (Zeiss LD Achroplan 40x/0.6NA Corr). A quartz view port window which was wedged with an anti-reflecting coating to mitigate the reflected emission couples the excitation and fluorescence into and out of the chamber. Fluorescence excitation is provided by the 488-nm line of a multi-line Ar ion laser (Melles Griot, 543 series). The laser line is spatially dispersed using a prism and further spectrally isolated using a 488-nm interference filter (Chroma). Laser intensity is attenuated with neutral density filters to intensities appropriate for single molecule spectroscopy. Fluorescence intensity is collected and stray excitation light is rejected with a dichroic mirror (Chroma, Z488RCD) and a holographic notch filter (Kaiser, SuperNotch-Plus, 488nm) [155].

This microscope system was slightly modified for this research purpose. Since the size of nanoparticles is estimated based on their relative fluorescence intensity, a flat field excitation rather than the Gaussian profile beam is required for precise fluorescence intensity comparisons. Therefore, the Pi beam shaper (MolTech GmbH, piShaper6_6_VIS)_which converts the Gaussian profile beam into a flat excitation beam was introduced where a flat beam is achievable only when a Gaussian beam of 6 mm in

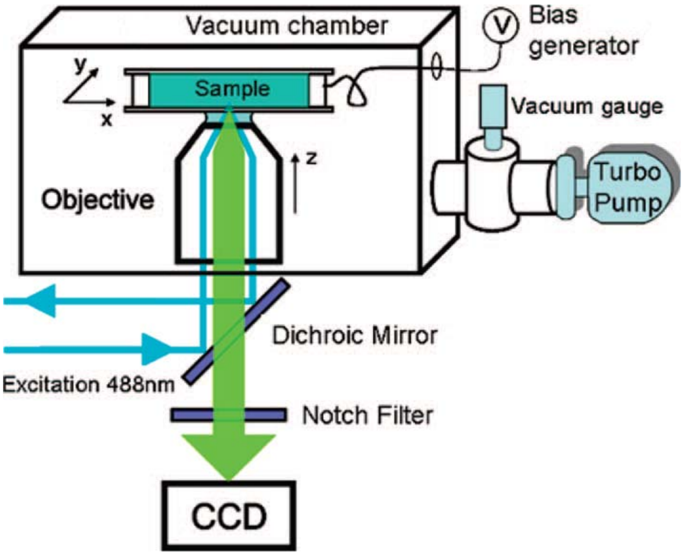

Figure 5.7: The schematic of the home-built wide field vacuum microscope [155].

diameter passes through the Pi beam shaper. The diameter of the Gaussian beam was adjusted using a beam expander (Blue Hill Optical Technologies, BXZ-532-2-8X 532nm Zoom Beam Expander). The beam size was measured using a method where a razor blade was placed on the beam path and fluorescence intensity was measured as a razor blade receded from the beam path. The derivative of the fluorescence intensity profile recorded as a function of the razor blade position gave rise to the Gaussian profile and a beam diameter was determined where the intensity of the profile falls to the $1/e^2$ of the maximum intensity of the Gaussian profile. In addition, the second beam expander was introduced after the Pi beam shaper to enlarge the beam diameter in order to obtain a much larger excitation area. Furthermore, the piezoelectrical actuator (Piezosystem jena GmbH) which was specially designed for vacuum applications and coupled with the voltage amplifier (NV40/1CL E), was also attached to the vacuum wide-field microscope to achieve precise fine focusing of the image. Precise controlling of the image focus with the nm resolution and the maximum motion of 500 μm was achievable using the piezo actuator. The piezoelements were controlled by the voltage amplifier with an integrated measuring system. The communication between computer and voltage amplifier was achieved by using a standard interface line.

5.3.3 APPARATUS AND SOFTWARE

The vacuum wide-field microscope image of nanoparticles (Figure 5.3B) was acquired by collecting fluorescence intensities upon illuminating nanoparticles using the 488-nm line of an ArKr ion laser. The fluorescence intensity was collected on an electron multiplying (EM) CCD detector array (Andor, iXon-DU-897) with the commercially available program Metamorph (Molecular Devices, 1992-2007, Version 7.1.0.0). Highest sensitivity of the EMCCD detector was achieved with the deepest cooling and lowest clock induced charge parameters. In addition, the fast frame rate (34.5 fps) of the

EMCCD detector further allows noises arising from clock induced charges to be reduced. The pixel size of the detector and active pixels are 16 μm and 512x512, respectively. All parameters for the image acquisition such as exposure time per pixel, total number of frames for an image, and the value of the EM gain were adjusted using the Metamorph program. The amount of EM gain was controlled in real time and used to amplify the incoming signal. This Metamorph program was also used as an analysis tool for the collected images.

To achieve images with higher signal to noise (S/N) ratio, collected signals were synchronously averaged for the period of measurements. For the bias modulation experiments, a time varying triangular bias was applied to the sample by a programmable function generator (Wavetek, 29A) with the optical excitation. Synchronization was achieved as follows: Two function generators were coupled with the EMCCD detector and the Metamorph software. The software commands the CCD camera to send a signal to the master function generator which subsequently triggers the other function generator for the bias application. The timing for the synchronization was monitored using an oscilloscope (company, model). Then collected signals were synchronously averaged with the corresponding applied bias for better signals.

For the analysis of the images collected, a home-written Matlab routine was used to find the individual bright spots (due to the single nanoparticles) in the CCD images and to calculate the integrated fluorescence intensities of the spots. The time dependence of the fluorescence of individual spots was determined from a set of acquired images and it was ensemble averaged and/or synchronously averaged over several bias cycles as needed (Figure 5.3C). Analysis of the ensemble average data for all molecules collected as well as each individual nanodomain is enabled using this program by selecting either whole area or the specific area we are interested in. In addition, nanoparticles could be sorted into groups based on their fluorescence intensities, allowing study for the size dependent behaviors.

5.4 RESULTS AND DISCUSSION

An isolated F8BT/PFB single nanodomain indicated in the circle of the image (Figure 5.3B) and the corresponding time averaged fluorescence transient as a function of the applied bias (Figure 5.3C) were obtained using a vacuum wide-field microscope with a FV-SMS technique applied on a simplified model photovoltaic device (Figure 5.3A). The migration of separated charged carriers to energetically favorable directions, which is toward the PFB layer for holes and the F8BT nanodomain for electron carriers, following exciton dissociation upon illumination is illustrated in an extended view of the heterojunction between donor/acceptor polymers (Figure 5.3A). This photoinduced charge separation is ascribed to the energy offset of the HOMO (donor) and LUMO (acceptor) energy level and is responsible for the initial decrease in fluorescence intensity in the absence of an applied electric field.

We studied electric field effects on charge separation efficiency at each individual donor/acceptor interface of model photovoltaic devices. The square-wave bias pulse was applied to the device and corresponding ensemble averaged fluorescence intensity modulations for 77 interfaces and each individual fluorescence intensity transient for 7 selected interfaces were recorded as a function of time in Figure 5.8 and Figure 5.9, respectively. To rule out the effect of the domain size on exciton dissociation efficiency due to the different distances required for excitons to migrate to heterojunctions for dissociation, molecules in the range of similar sizes were selected. The individual transients shown in Figure 5.9A and the histogram representing the quenching depth of each transient for all 77 interfaces reveal a wide distribution of quenching depth, indicating charge separation efficiency varied from domain to domain. In addition, the degree of distribution of quenching depth varied from device to device, further supporting the heterogeneity of this process. However, the observed heterogeneity was incapable of being resolved in ensemble averaged data (Figure 5.8).

The observed heterogeneity of the local exciton dissociation yield had been expected from the calculation based on the quantum-chemical modeling for the charge transfer excitations occurring between PFB and F8BT [15]. The calculation of the Coulomb interaction between excited states on one chain and the ground state on the other done by Sreearunothail et al also revealed that the different orientations of the molecules at the heterojunction could lead to different charge separation yields due to the different attractive or repulsive interchain interactions[148]. In reality, the recent photoconductive AFM measurements performed on the organic photovoltaic blends showed heterogeneity of the yield of the local exciton dissociation via mapping local photocurrents [17, 152, 153]. Therefore, the result shown in Figure 5.9 is clear spectroscopic evidence of the heterogeneity of a local yield of exciton dissociation in a conjugated donor/acceptor system. The difference in yields of electric field induced quenching from particle to particle is believed to result from the variation of the morphologies which give rise to different interchain interactions.

To further study the electric field induced charge dissociation process, FV-SMS measurements were performed by applying a triangular bias across the F8BT/PFB device at the bias scan rate of 10 V/sec with an excitation intensity of 40 mW/cm^2. The results of the time-averaged ensemble averages of FV-SMS transient data were shown as a function of the applied bias in Figure 5.10A. Rather than symmetrical-like fluorescence quenching at maximum electric field intensity from both positive and negative directions, which is what we expected, overall fluorescence intensity decreases with different rates as

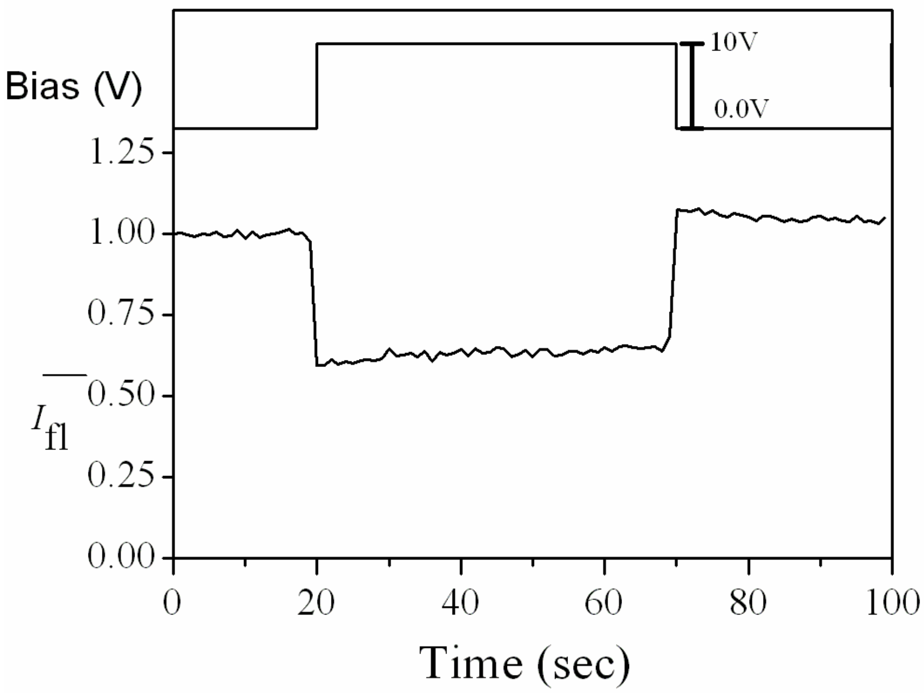

Figure 5.8: Ensemble averaged fluorescence intensity transient taken from the 77 individual isolated F8BT/PFB heterojunction nanodomains. The data were obtained while applying the square–wave bias pulse as shown above at the excitation intensity of 40 mW/cm^2.

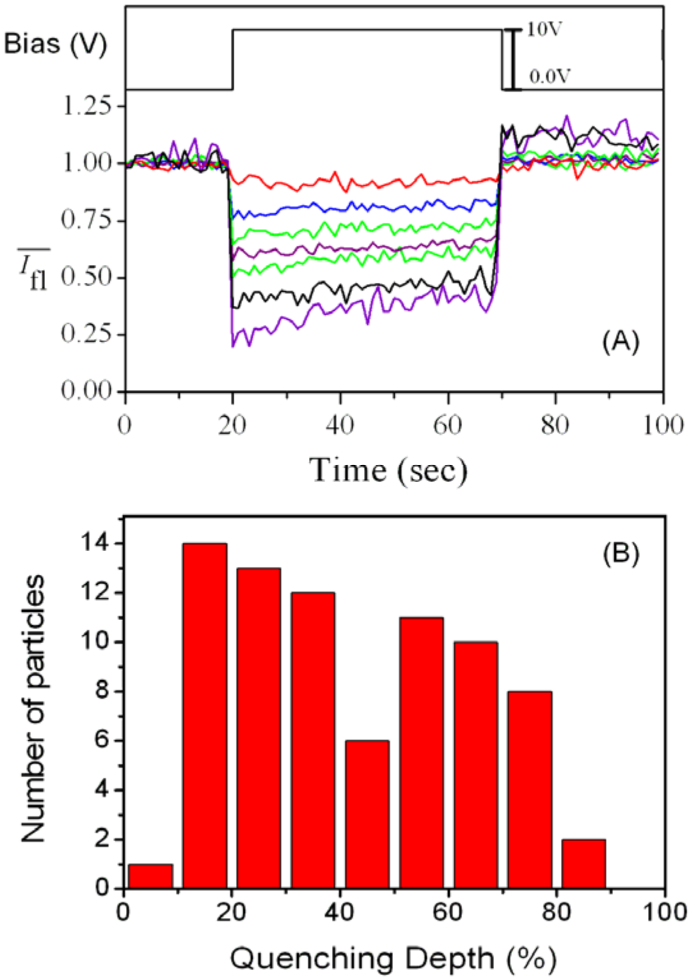

Figure 5.9: (A) The individual fluorescence intensity transients taken from the selected 7 F8BT/PFB heterojunction domains among the 77 interfaces shown in Figure 5.8. (B) The histogram represents a wide distribution of the fluorescence modulation depth for the 77 heterojunction domains.

triangular bias was scanned from negative 10V to positive 10 V. In addition, it is also revealed that large amounts (~45%) of fluorescence quenching occurred at 0 volt, meaning that HOMO-LOMO energy offsets and built-in internal potential significantly contribute to the yield of the exciton dissociation for the F8BT/PFB system. Asymmetric fluorescence quenching behavior observed here is believed to be due to the precisely well aligned heterojunction direction relatively to the applied electric field. Under the positive bias, the diffusion direction of positively separated hole carriers coincides with that of the electric field, while they are opposite with one another under the negatively applied bias, counterbalancing or even increasing the fluorescence intensity by suppressing the exciton dissociation. Similar results were reported from studies with the bilayer of F8BT/PFB film devices where devices with a different order of layers (F8BT/PFB and PFB/F8BT) were fabricated and constant electric field was applied to each device [14]. Enhancement and decrease in fluorescence intensity was observed, depending on the direction of the electric field and device types.

Another unignorable factor giving rise to fluorescence modulation is exciton quenching by injected holes at positive bias. To estimate how much it contributes to total fluorescence modulation observed here, changes in fluorescence intensity under both positive and negative electric field relative to that at the built-in voltage were calculated from the data shown in Figure 5.10A and resulting date points which are connected with solid lines were drawn as a function of electric field in Figure 5.10B. The results indicates that the modulation depth obtained while applying forward bias is slightly bigger than that caused by the fluorescence recovery at reverse bias sweep. To further study the contribution of the exciton quenching by injected holes to total fluorescence intensity modulation, the same measurements were done but at three orders of magnitude lower excitation power than before. According to the LIHT mechanism described in

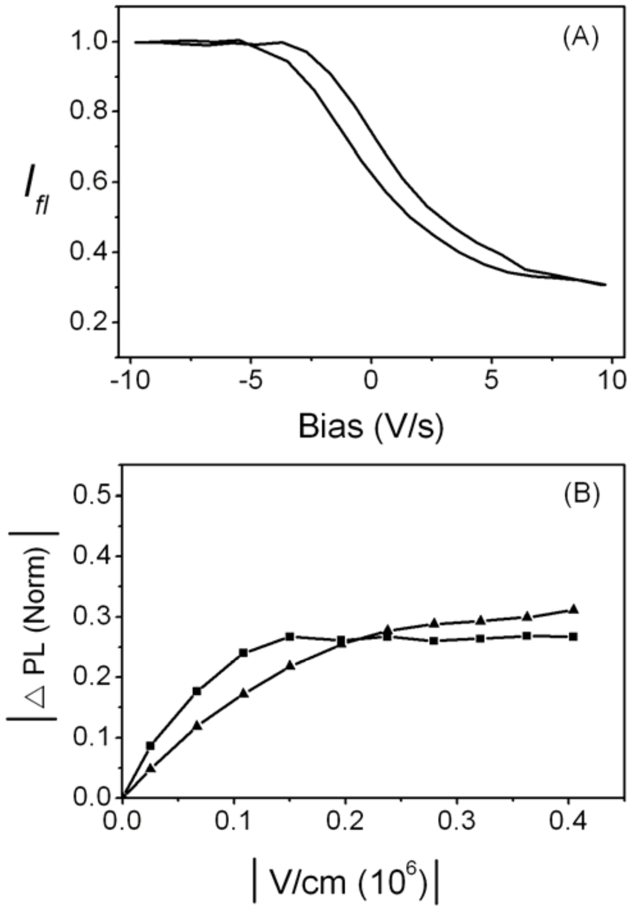

Figure 5.10: (A) Ensemble averages of fluorescence intensity transients of F8BT nanoaggregates plotted vs. applied bias at the scan rate of 10 V/s at excitation intensity of 40 mW/cm^2. (B) Change in fluorescence intensity verses applied electric field from the data shown in (A) for forward (triangle) and reverse (square) E-field.

previous chapters, hole injection from the CBP hole transport layer into F8BT nanoaggregate is expected to be ignorable at this low excitation intensity. In reality, no fluorescence quenching was observed from the device where the bottom PFB layer was replaced with an inert PMMA film in order to study only the exciton-polaron quenching (Figure 5.11 F). However, when the PFB layer was introduced again, fluorescence modulation reappeared as shown in Figure 5.11 E. Therefore, the analysis of fluorescence quenching at oppositely applied electric fields as well as the results of fluorescence modulation at very low excitation intensity indicates that the portion of exciton-polaron quenching is not significant.

Although the contribution of exciton quenching by hole polarons to overall quenching magnitude is not pronounced, it is believed to affect the quenching dynamics as exhibited in Figure 5.10B. While early saturation of the fluorescence intensity is reached at reversely applied electric field, a continuous fluorescence decrease with a slow quenching rate is observed under the forward applied electric field. The early part of the fluorescence change which shows an almost linear behavior in response to the forward electric field is dominated by excitons undergoing field induced charge separation. The further increase in quenching with much slower rates, especially at higher electric field regime, is believed to be due to a slow hole charging effect from the CBP hole transport layer into F8BT nanoaggregates which will be discussed later. On the other hand, quick fluorescence recovery under the existence of the reversely applied electric field only is ascribed to the reduced charge dissociation rates.

To investigate differences of charge dissociation properties for the F8BT/PFB and F8BT/TFB systems, the same FV-SMS measurements were performed with a wide range of excitation laser powers. At excitation intensities lower than 40mW/cm^2, two different donor/acceptor systems showed similar quenching behaviors except the initial fluorescence intensity of F8BT nanoparticles before normalization, which is not shown here, was about 10 % weaker for the F8BT/PFB system, supporting the fact that yields of charge separation in PFB/F8BT is more efficient than those of F8BT/TFB. However, at the excitation intensities above 40 mW/cm^2, fluorescence quenching depth started to decrease as the excitation intensity increases. In addition, clear hysteresis appeared first from the F8BT/PFB at 350 mW/cm^2 (Figure 5.11B) and then from both at 4.4 W/cm^2 (Figure 5.11 A).

Decrease in quenching depth is ascribed to the increased population rate of photogenerated exciton, which overwhelms the exciton depopulation rate caused by both exciton dissociation at heterojunctions and hole charging from the CBP layer. In addition, increased electrostatic repulsion by the accumulation of the large amount of positive charged carriers in a PFB layer as a result of efficient exciton dissociations further reduces the efficiency of the charge separation. The accumulation of the hole carriers is also believed to be responsible for the appearance of the hysteresis.

Kinetics of the charge separation process was further studied by applying triangular biases with different scanning rates at the excitation intensity of 350mW/cm^2. The results shown in Figure 5.12 exhibit that fluorescence varies gradually in response to the change in scan rates, resulting in less quenching depth at slower scan rates. At the excitation intensity used here, it is complicated to differentiate only the charge separation process from other factors such as hole accumulations and hole charging, requiring the assumption that different behaviors mainly result from the different scan rates. Therefore, the dependence of the quenching depth on applied bias scan rates means that charge dissociation process is kinetically controlled rather than steady state reaction. It is might be due to the increased rate of exciton population in F8BT domains. However, recoveries of fluorescence in a similar way with one another under the reverse bias scan indicates

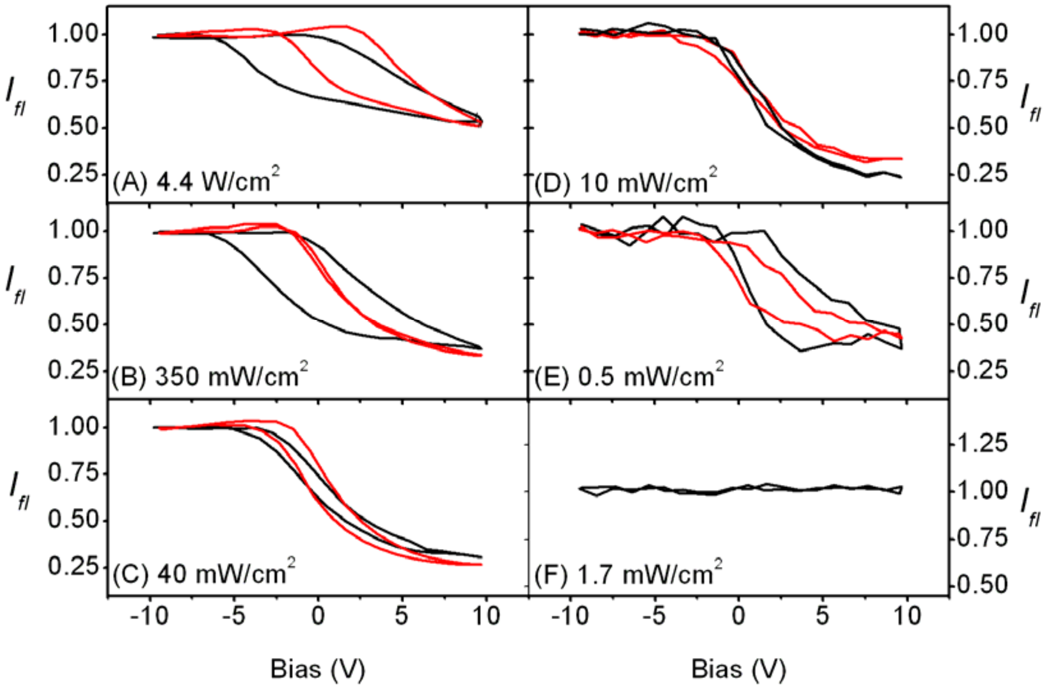

Figure 5.11: (A~E) Ensemble averaged fluorescence intensities for F8BT/PFB (black) and F8BT/TFB (red) systems were plotted as a function of bias at the scan rate of 10 V/s under the different excitation intensities. (F) Ensemble averaged fluorescence intensity was obtained from the F8BT/PMMA system.

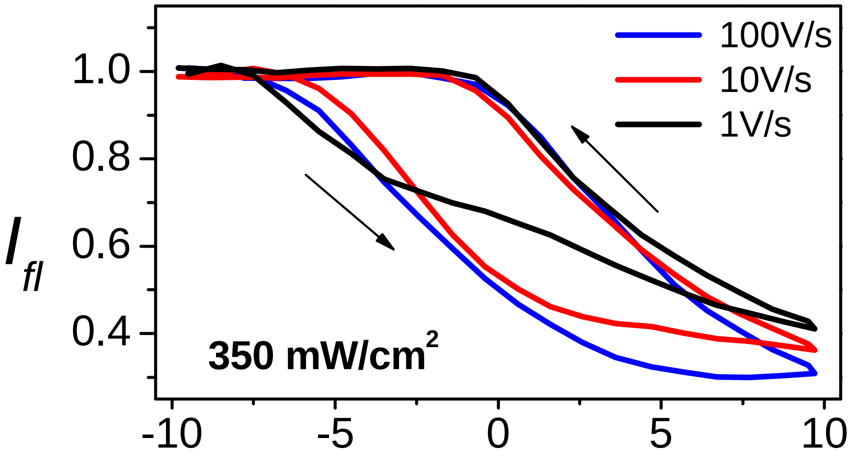

Figure 5.12: Ensemble averages of fluorescence intensity obtained at different scan rates with excitation intensity of 350 mW/cm^2 were plotted with arrows, indicating the direction of the bias sweep during the cycle.

that rates of the reduction in an electric field induced exciton dissociation process are not scan rate dependent.

To investigate the role of fluorescence quenching by interaction between photogenerated excitons and thermally injected positive hole carriers on the total fluorescence modulation, hole injection only devices were fabricated by introducing an inert PMMA layer instead of a hole acceptor PFB layer. The FV-SMS results shown in Figure 5.13 reveal quite different fluorescence modulation behaviors in response to the applied bias. First of all, we observed that almost no fluorescence quenching occurs at lower excitation intensity (Figure 5.13C, Figure 5.11F) which coincides with previously reported light induced hole transfer (LIHT) process on MEH-PPV single aggregates [22]. Interestingly, fluorescence quenching is also seen at negative bias where holes are extracted out of the device. This unexpected behavior is believed to be the result of slow processes of hole charging and discharging, resulting in fluorescence fluctuation as well as hysteresis. The higher barrier for hole injection due to the lower HOMO level of the F8BT nanoparticles compared to that of the previously studied MEH-PPV may prevent hole from being efficiently injected from the HTL.

The data obtained to study the effect of the scan rate on charging kinetics where hysteresis disappears at slow scan rate also supports that it is a slow process. However, at higher excitation intensities, even though the data exhibit a different degree of hysteresis, total fluctuation depth remains almost the same as around 30%. The total fluorescence quenching depth obtained from the F8BT/PFB model photovoltaics does not seem to reflect this additional quenching depth originated from the charging effect. Instead, less fluorescence quenching was observed at higher excitation laser intensity (Figure 5.11A), even though charging is more efficient at this condition. We think, in addition to the accumulated charges in PFB layer which prevent further exciton dissociation, that

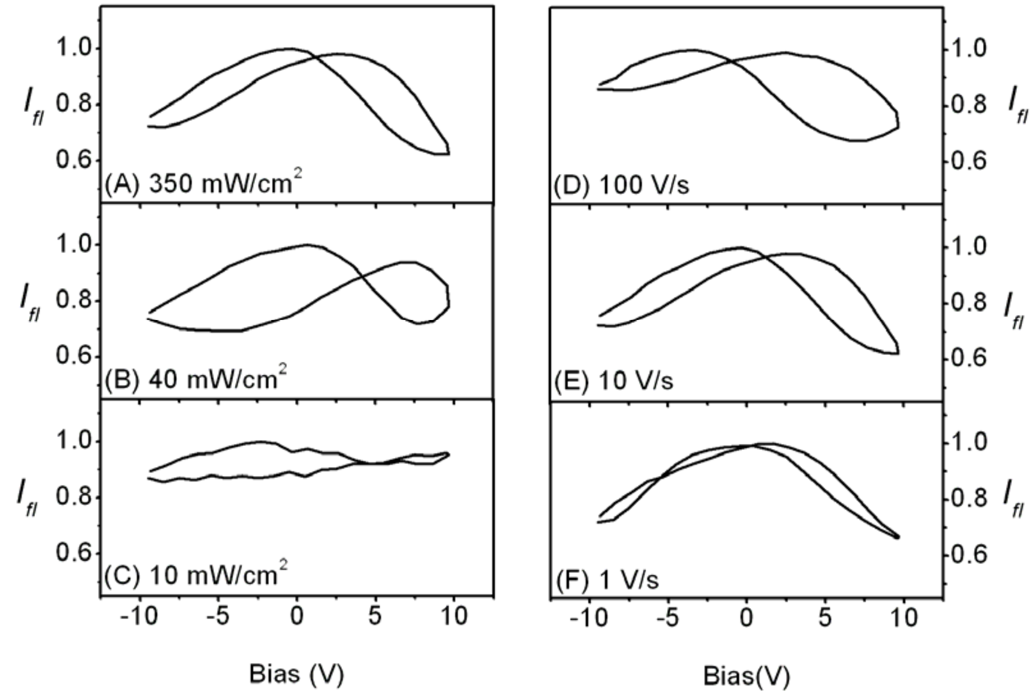

Figure 5.13: (A~C) Ensemble averages of fluorescence intensity for the F8BT/PMMA device was plotted as a function of bias at the different excitation intensities under the same scan rate (10 V/s) and (D~E) at the same excitation intensity (350 mW/cm^2) under different scan rates.

injected hole carriers which may recombine with the remaining electrons in the F8BT nanodomains upon charge dissociation, are responsible for the observed discrepancy in fluorescence quenching depth. However, the recombination between injected holes and remaining electrons in F8BT nanodomains requires further research to confirm this hypothesis.

As another comparison device, a new device structure was devised to study the effect of the charge separation only on the fluorescence modulation. The organic dielectric material of PHS which endowed the organic thin film transistor with good dielectric properties [156] was newly introduced in place of CBP and TPD hole injecting layers by spin casting on top of the F8BT nanoparticles (Figure 5.6A). However, we could not succeed to achieve this structure of devices because of the problem of erosion of the bottom layer against the solvent (ethyl acetate) for PHS. The fluorescence intensity measurements and AFM analysis performed on this device reveals that the bottom PIBM layer was completely washed out while depositing the upper PHS layer so that no F8BT aggregates exist. Even though PHS was tried to directly deposit on top of the self-isolated nanoparticles without the PIBM matrix, it again turned out that F8BT nanoparticles rarely remain. The FV-SMS result obtained from these few remaining nanodomains exhibits there is no fluorescence modulation in response to the bias. This result is believed that the remaining molecules have very poor contact with the bottom PFB layer, resulting in no charge separation under the applied electric field. Therefore, to achieve the complete hole block devices, the new technique of crosslinking of the bottom layer might be required.

As the last type of devices, the F8BT single molecule device was designed (Figure 5.6B). Assuming the shape of the F8BT single molecule to be a cubic and the density of the F8BT polymer (Mw = 70 kg/mol) is 0.8 g/L, the size and the volume of the cubic were roughly calculated to be about 5.1 nm for each side of the cubic and 140 nm^3, respectively. In this structure of devices, the F8BT single molecules are directly embedded in a bottom PFB layer rather than the upper PIBM matrix. Therefore, the PFB layer in this structure of devices works as the hole acceptor as well as the matrix for the single molecules. Though the direction of both charge separation and diffusion are not precisely oriented to a specific way in this device geometry, interfaces between each domain are able to be defined very well without any erosion issues. Therefore, this system is analogous to the bulk heterojunction system with the much less concentration of F8BT.

However, this type of single molecule devices was also not feasible for study of the charge dissociation process due to the following two reasons: first, relatively high background emission from PFB as well as weak emission from F8BT single molecules prevents donor/acceptor interfaces from being recognized. Second, unexpected significantly intense background emission, especially at negative bias, was observed. It turns out that the high emission from matrix was ascribed to the keto defect sites which are commonly found from polyfluorene-type material [157, 158]. It is reported that keto defect can be generated as main channel of the photo(or electro) oxidative degradation process [157]. Though we couldn’t further study the charge dissociation process from this type of the device, this approach demonstrates the possible side effect we might get from this donor/acceptor systems.

5.5 CONCLUSION

The FV-SMS technique reveals that local yields of the photoinduced charge dissociation occurring across the isolated interface between F8BT nanoaggregates and the PFB (or TFB) thin film are highly area dependent. Spectroscopic evidence for the heterogeneity in the nature of charge separation yield was clearly demonstrated.

Fluorescence quenching from the F8BT/PFB system was mainly ascribed to the charge dissociation under the applied electric field rather than exciton quenching by injected holes from HTL. The accumulated charges in the hole acceptor layers, especially at higher excitation intensity, are believed to be responsible for the observed hysteresis shown in the FV-SMS results. In addition to the electric field and hole charging, luminescence as a result of the recombination between separated electrons and injected holes is suggested a possible factor affecting the fluorescence intensity modulation. From the charge injection devices, it was confirmed that the LIHT mechanism was applied to the F8BT nanoparticle system. However, as opposed to MEH-PPV, pure hole injection into F8BT nanoaggreagtes was very slow process.

References

1. Al-Ibrahim, M., et al., *The influence of the optoelectronic properties of poly(3-alkylthiophenes) on the device parameters in flexible polymer solar cells.* Organic Electronics, 2005. **6**(2): p. 65-77.

2. Thompson, B.C. and J.M.J. Frechet, *Organic photovoltaics - Polymer-fullerene composite solar cells.* Angewandte Chemie-International Edition, 2008. **47**(1): p. 58-77.

3. Yu, G., et al., *Polymer Photovoltaic Cells - Enhanced Efficiencies Via a Network of Internal Donor-Acceptor Heterojunctions.* Science, 1995. **270**(5243): p. 1789-1791.

4. Jerry, M., *Advanced Organic Chemistry reactions, mechanisms and structure*. 3rd ed. 1985, New York: John Wiley & Sons, inc.

5. Someya, T., H. Akiyama, and H. Sakaki, *Enhanced binding energy of one-dimensional excitons in quantum wires.* Physical Review Letters, 1996. **76**(16): p. 2965-2968.

6. Walck, S.N., T.L. Reinecke, and P.A. Knipp, *Exciton binding energy in T-shaped semiconductor quantum wires.* Physical Review B, 1997. **56**(15): p. 9235-9238.

7. Gesquiere, A.J., S.-J. Park, and P.F. Barbara, *Hole-Induced Quenching of Triplet and Singlet Excitons in Conjugated Polymers.* Journal of the American Chemical Society, 2005. **127**(26): p. 9556-9560.

8. Park, S.-J., et al., *Charge Injection and Photooxidation of Single Conjugated Polymer Molecules.* Journal of the American Chemical Society, 2004. **126**(13): p. 4116-4117.

9. Tang, C.W. and S.A. Vanslyke, *Organic Electroluminescent Diodes.* Applied Physics Letters, 1987. **51**(12): p. 913-915.

10. Benson-Smith, J.J., et al., *Formation of a ground-state charge-transfer complex in polyfluorene/[6,6]-phenyl-C-61 butyric acid methyl ester (PCBM) blend films and its role in the function of polymer/PCBM solar cells.* Advanced Functional Materials, 2007. **17**(3): p. 451-457.

11. Hallermann, M., S. Haneder, and E. Da Como, *Charge-transfer states in conjugated polymer/fullerene blends: Below-gap weakly bound excitons for polymer photovoltaics.* Applied Physics Letters, 2008. **93**(5): p. 053307.

12. Morteani, A.C., et al., *Exciton regeneration at polymeric semiconductor heterojunctions.* Physical Review Letters, 2004. **92**(24): p. 247402.

13. Muller, J.G., et al., *Ultrafast dynamics of charge carrier photogeneration and geminate recombination in conjugated polymer : fullerene solar cells.* Physical Review B, 2005. **72**(19): p. 195208.

14. Dhoot, A.S., et al., *Electromodulation of photoinduced charge transfer in polyfluorene bilayer devices.* Applied Physics Letters, 2004. **85**(12): p. 2256-2258.

15. Huang, Y.S., et al., *Electronic structures of interfacial states formed at polymeric semiconductor heterojunctions.* Nature Materials, 2008. **7**(6): p. 483-489.

16. Arias, A.C., et al., *Photovoltaic performance and morphology of polyfluorene blends: A combined microscopic and photovoltaic investigation.* Macromolecules, 2001. **34**(17): p. 6005-6013.

17. Coffey, D.C., et al., *Mapping local photocurrents in polymer/fullerene solar cells with photoconductive atomic force microscopy.* Nano Letters, 2007. **7**(3): p. 738-744.

18. Leever, B.J., et al., *Spatially resolved photocurrent mapping of operating organic photovoltaic devices using atomic force photovoltaic microscopy.* Applied Physics Letters, 2008. **92**(1): p. 013302.

19. Mihailetchi, V.D., et al., *Photocurrent generation in polymer-fullerene bulk heterojunctions.* Physical Review Letters, 2004. **93**(21): p. 216601.

20. Bolinger, J., et al., *Detailed Investigation of Light Induced Charge Injection into a Single Conjugated Polymer Chain.* Journal of Physical Chemistry C, 2008. **112**(47): p. 18608-18615.

21. Gesquiere, A.J., et al., *Single Molecule Spectroscopy of Organic Dye Nanoparticles.* Nano Letters, 2005. **5**(7): p. 1321-1325.

22. Palacios, R.E., et al., *Single conjugated polymer nanoparticle capacitors.* Chemical Physics, 2009. **357**(1-3): p. 21-27.

23. Barbara, P.F., et al., *Single-molecule spectroscopy of conjugated polymers.* Accounts of Chemical Research, 2005. **38**(7): p. 602-610.

24. Bolinger, J.C., et al., *Light-assisted deep-trapping of holes in conjugated polymers.* Proceedings of the National Academy of Sciences of the United States of America, 2009. **106**(5): p. 1342-1346.

25. Seeley, A.J.A.B., et al., *Trap-assisted hole injection and quantum efficiency enhancement in poly(9,9' dioctylfluorene-alt-benzothiadiazole) polymer light-emitting diodes.* Journal of Applied Physics, 2004. **96**(12): p. 7643-7649.

26. Muller, E.M. and J.A. Marohn, *Microscopic evidence for spatially inhomogeneous charge trapping in pentacene.* Advanced Materials (Weinheim, Germany), 2005. **17**(11): p. 1410-1414.

27. Salleo, A. and R.A. Street, *Kinetics of bias stress and bipolaron formation in polythiophene.* Physical Review B: Condensed Matter and Materials Physics, 2004. **70**(23): p. 235324/1-235324/8.

28. Lang, D.V., et al., *Bias-dependent generation and quenching of defects in pentacene.* Physical Review Letters, 2004. **93**(7): p. 076601/1-076601/4.

29. Campbell, A.J., D.D.C. Bradley, and H. Antoniadis, *Dispersive electron transport in an electroluminescent polyfluorene copolymer measured by the current integration time-of-flight method.* Applied Physics Letters, 2001. **79**(14): p. 2133-2135.

30. Jaquith, M., E.M. Muller, and J.A. Marohn, *Time-resolved electric force microscopy of charge trapping in polycrystalline pentacene.* Journal of Physical Chemistry B, 2007. **111**(27): p. 7711-7714.

31. Coffey, D.C. and D.S. Ginger, *Time-resolved electrostatic force microscopy of polymer solar cells.* Nature Materials, 2006. **5**(9): p. 735-740.

32. Sinha, S. and A.P. Monkman, *Delayed recombination of detrapped space-charge carriers in poly[2-methoxy-5-(2 '-ethyl-hexyloxy)-1,4-phenylene vinylene]-based light-emitting diode.* Journal of Applied Physics, 2005. **97**(11): p. 114505.

33. Schmechel, R. and H. von Seggern, *Electronic traps in organic transport layers.* Physica Status Solidi a-Applied Research, 2004. **201**(6): p. 1215-1235.

34. Giebeler, C., et al., *Optical studies of electric fields in poly(2-methoxy-5-ethyl(2(')-hexyloxy) para-phenylene vinylene) light-emitting diodes.* Applied Physics Letters, 1999. **74**(24): p. 3714-3716.

35. Feller, F., D. Geschke, and A.P. Monkman, *Decay of space charge in conjugated polymers measured using pyroelectric current transients.* Journal of Applied Physics, 2003. **93**(5): p. 2884-2889.

36. Meier, M., et al., *Determination of trapping parameters in poly(p-phenylenevinylene) light-emitting devices using thermally stimulated currents.* Journal of Applied Physics, 1998. **84**(1): p. 87-92.

37. Yakimov, A.V., V.N. Savvate'ev, and D. Davidov, *The role of traps in polymer-based light-emitting devices.* Synthetic Metals, 2000. **115**(1-3): p. 51-56.

38. Salleo, A. and R.A. Street, *Light-induced bias stress reversal in polyfluorene thin-film transistors.* Journal of Applied Physics, 2003. **94**(1): p. 471-479.

39. Gundlach, D.J., et al., *Solvent-induced phase transition in thermally evaporated pentacene films.* Applied Physics Letters, 1999. **74**(22): p. 3302-3304.

40. Northrup, J.E. and M.L. Chabinyc, *Gap states in organic semiconductors: Hydrogen- and oxygen-induced states in pentacene.* Physical Review B, 2003. **68**(4): p. 041202.

41. Rep, D.B.A., et al., *Mobile ionic impurities in organic semiconductors.* Journal of Applied Physics, 2003. **93**(4): p. 2082-2090.

42. Zilker, S.J., et al., *Bias stress in organic thin-film transistors and logic gates.* Applied Physics Letters, 2001. **79**(8): p. 1124-1126.

43. Gomes, H.L., et al., *Analysis of deep levels in a phenylenevinylene polymer by transient capacitance methods.* Applied Physics Letters, 1999. **74**(8): p. 1144-1146.

44. Matters, M., et al., *Bias-stress induced instability of organic thin film transistors.* Synthetic Metals, 1999. **102**(1-3): p. 998-999.

45. Goldmann, C., D.J. Gundlach, and B. Batlogg, *Evidence of water-related discrete trap state formation in pentacene single-crystal field-effect transistors.* Applied Physics Letters, 2006. **88**(6): p. 063501/1-063501/3.

46. Kagan, C.R., A. Afzali, and T.O. Graham, *Operational and environmental stability of pentacene thin-film transistors.* Applied Physics Letters, 2005. **86**(19): p. 193505.

47. Jurchescu, O.D., J. Baas, and T.T.M. Palstra, *Electronic transport properties of pentacene single crystals upon exposure to air.* Applied Physics Letters, 2005. **87**(5): p. 052102.

48. Chang, J.B. and V. Subramanian, *Effect of active layer thickness on bias stress effect in pentacene thin-film transistors.* Applied Physics Letters, 2006. **88**(23): p. 233513/1-233513/3.

49. Gomes, H.L., et al., *Bias-induced threshold voltages shifts in thin-film organic transistors.* Applied Physics Letters, 2004. **84**(16): p. 3184-3186.

50. Kadashchuk, A., et al., *Charge-carrier trapping in polyfluorene-type conjugated polymers.* Journal of Applied Physics, 2005. **98**(2): p. 024101/1-024101/8.

51. Muller, J.G., et al., *Precursor states for charge carrier generation in conjugated polymers probed by ultrafast spectroscopy.* Physical Review Letters, 2002. **88**(14): p. 147401.

52. Lupton, J.M., et al., *Time delayed electroluminescence overshoot in single layer polymer light-emitting diodes due to electrode luminescence quenching.* Journal of Applied Physics, 2001. **89**(1): p. 311-317.

53. Vorotyntsev, M.A. and J. Heinze, *Charging process in electron conducting polymers: dimerization model.* Electrochimica Acta, 2001. **46**(20-21): p. 3309-3324.

54. APSYS, User's Manual and Reference Manual, Version 2007.3, Crosslight Sofware Inc., 2004-2005.

55. Palacios, R.E., et al., *Single-Molecule Spectroelectrochemistry (SMS-EC).* Journal of the American Chemical Society, 2006. **128**(28): p. 9028-9029.

56. Gesquiere, A.J., S.J. Park, and P.F. Barbara, *F-V/SMS: A new technique for studying the structure and dynamics of single molecules and nanoparticles.* Journal of Physical Chemistry B, 2004. **108**(29): p. 10301-10308.

57. Gesquiere, A.J., et al., *Single Molecule Modulation Spectroscopy of Conjugated Polymers.* Journal of Physical Chemistry B, 2005. **109**(25): p. 12366-12371.

58. Fung, M.K., et al., *Distinct interfaces of poly (9,9-dioctylfluorene-co-benzothiadiazole) with cesium and calcium as observed by photoemission spectroscopy.* Journal of Applied Physics, 2003. **94**(9): p. 5763-5770.

59. Chua, L.L., et al., *General observation of n-type field-effect behaviour in organic semiconductors.* Nature, 2005. **434**(7030): p. 194-199.

60. Yip, W.T., et al., *Classifying the photophysical dynamics of single- and multiple-chromophoric molecules by single molecule spectroscopy.* Journal of Physical Chemistry A, 1998. **102**(39): p. 7564-7575.

61. Northrup, J.E. and M.L. Chabinyc, *Gap states in organic semiconductors: Hydrogen- and oxygen-induced states in pentacene.* Physical Review B, 2003. **68**(4): p.041202.

62. Kagan, C.R., A. Afzali, and T.O. Graham, *Operational and environmental stability of pentacene thin-film transistors.* Applied Physics Letters, 2005. **86**(19): p. 193505.

63. Jurchescu, O.D., J. Baas, and T.T.M. Palstra, *Electronic transport properties of pentacene single crystals upon exposure to air.* Applied Physics Letters, 2005. **87**(5): p. 052102.

64. Sinha, S. and A.P. Monkman, *Delayed recombination of detrapped space-charge carriers in poly[2-methoxy-5-(2 '-ethyl-hexyloxy)-1,4-phenylene vinylene]-based light-emitting diode.* Journal of Applied Physics, 2005. **97**(11): p. 114505.

65. Muller, J.G., et al., *Precursor states for charge carrier generation in conjugated polymers probed by ultrafast spectroscopy.* Physical Review Letters, 2002. **88**(14): p. 147401.

66. Bolinger, J.C., et al., *Light-assisted deep-trapping of holes in conjugated polymers.* Proceedings of the National Academy of Sciences of United States of America, 2009, **106**(5): p. 1324-1346.

67. Burrows, P.E., et al., *Reliability and Degradation of Organic Light-Emitting Devices.* Applied Physics Letters, 1994. **65**(23): p. 2922-2924.

68. Wang, Y., et al., *Enhancement of iridium-based organic light-emitting diodes by spatial doping of the hole transport layer.* Applied Physics Letters, 2005. **87**(19): p. 193501.

69. Baldo, M.A., M.E. Thompson, and S.R. Forrest, *High-efficiency fluorescent organic light-emitting devices using a phosphorescent sensitizer.* Nature, 2000. **403**(6771): p. 750-753.

70. Matsusue, N., et al., *Charge carrier transport in an emissive layer of green electrophosphorescent devices.* Applied Physics Letters, 2004. **85**(18): p. 4046-4048.

71. Liang, C.J., et al., *Improved performance of electroluminescent devices based on an europium complex.* Applied Physics Letters, 2000. **76**(1): p. 67-69.

72. Hong, Z.R., et al., *Rare earth complex as a high-efficiency emitter in an electroluminescent device.* Advanced Materials, 2001. **13**(16): p. 1241-1245.

73. McNeill, J.D., et al., *Near Field Spectroscopic Investigation of Fluorescence Quenching by Charge Carriers in Pentacene-Doped Tetracene.* Journal of Physical Chemistry B, 2004. **108**(31): p. 11368-11374.

74. Yu, J., et al., *Efficient exciton quenching by hole polarons in the conjugated polymer MEH-PPV.* Israel Journal of Chemistry, 2004. **44**(1-3): p. 127-132.

75. Palacios, R.E., et al., *Spectroelectrochemistry Studies of the Charging and Discharging of Single Conjugated-Polymer Nanoparticles.* Nature Materials. Submitted., 2006.

76. Lee, Y.J., et al., *Probing a molecular interface in a functioning organic diode.* Applied Physics Letters, 2005. **87**(5): p. 051906/1-051906/3.

77. Schindler, F., et al., *How single conjugated polymer molecules respond to electric fields.* Nature Materials, 2006. **5**(2): p. 141-146.

78. Smith, T.M., et al., *Electric field effects on internal conversion: An alternative mechanism for field-induced fluorescence quenching of MEH-PPV and its oligomers in the low concentration limit.* Journal of Physical Chemistry C, 2007. **111**(27): p. 10119-10129.

79. Smith, T.M., et al., *Electrofluorescence of MEH-PPV and Its Oligomers: Evidence for Field-Induced Fluorescence Quenching of Single Chains.* Journal of Physical Chemistry B, 2006. **110**(15): p. 7732-7742.

80. Hania, P.R., D. Thomsson, and I.G. Scheblykin, *Host matrix dependent fluorescence intensity modulation by an electric field in single conjugated polymer chains.* Journal of Physical Chemistry B, 2006. **110**(51): p. 25895-25900.

81. Hania, P.R. and I.G. Scheblykin, *Electric field induced quenching of the fluorescence of a conjugated polymer probed at the single molecule level.* Chemical Physics Letters, 2005. **414**(1-3): p. 127-131.

82. Devine, R.A.B., et al., *X-ray irradiation effects in top contact, pentacene based field effect transistors for space related applications.* Applied Physics Letters, 2006. **88**(15): p. 151907/1-151907/3.

83. Berleb, S., W. Brutting, and G. Paasch, *Interfacial charges and electric field distribution in organic hetero-layer light-emitting devices.* Organic Electronics, 2000. **1**(1): p. 41-47.

84. Berleb, S., W. Brutting, and G. Paasch, *Interfacial charges in organic hetero-layer light emitting diodes probed by capacitance-voltage measurements.* Synthetic Metals, 2001. **122**(1): p. 37-39.

85. Lindner, T., G. Paasch, and S. Scheinert, *Hysteresis in organic field-effect devices. Simulated effects due to trap recharging.* Journal of Applied Physics, 2005. **98**(11): p. 114505/1-114505/9.

86. Hieda, H., et al., *Fluorescence quenching induced by injected carriers in organic thin films.* Thin Solid Films, 1998. **331**(1,2): p. 152-157.

87. Friedlein, R., X. Crispin, and W.R. Salaneck, *Molecular parameters controlling the energy storage capability of lithium polyaromatic hydrocarbon intercalation compounds.* Journal of Power Sources, 2004. **129**(1): p. 29-33.

88. Amy, F., C. Chan, and A. Kahn, *Polarization at the gold/pentacene interface.* Organic Electronics, 2005. **6**(2): p. 85-91.

89. Devine, R.A.B., *Influence of bias stressing and irradiation on poly-three-hexylthiophene based field effect transistors.* Journal of Applied Physics, 2006. **99**(8, Pt. 1): p. 083701/1-083701/5.

90. Fradkin, L., et al., Factors Controlling Hole Injection in Single Conjugated Polymer Molecules. Joournal of Physical Chemistry A, 2008. 113(16): p. 4739-4745.

91. Lammi, R.K. and P.F. Barbara, *Influence of chain length on exciton migration to low-energy sites in single fluorene copolymers.* Photochemical & Photobiological Sciences, 2005. **4**(1): p. 95-99.

92. Friend, R.H., et al., *Electroluminescence in conjugated polymers.* Nature (London), 1999. **397**(6715): p. 121-128.

93. Moons, E., *Conjugated polymer blends: linking film morphology to performance of light emitting diodes and photodiodes.* Journal of Physics-Condensed Matter, 2002. **14**(47): p. 12235-12260.

94. Zhang, X.J. and S.A. Jenekhe, *Electroluminescence of multicomponent conjugated polymers. 1. Roles of polymer/polymer interfaces in emission enhancement and voltage-tunable multicolor emission in semiconducting polymer/polymer heterojunctions.* Macromolecules, 2000. **33**(6): p. 2069-2082.

95. Salaneck, W.R., et al., *Conjugated Polymer Surfaces and Interfaces: Electronic and Chemical Structure of Interfaces for Polymer Light Emitting Devices.* 1996. 150 pp.

96. Zhu, X.Y., *Charge Transport at Metal-Molecule Interfaces: A Spectroscopic View.* Journal of Physical Chemistry B, 2004. **108**(26): p. 8778-8793.

97. Cahen, D. and A. Kahn, *Electron energetics at surfaces and interfaces: Concepts and experiments.* Advanced Materials, 2003. **15**(4): p. 271-277.

98. Halls, J.J.M., et al., *Charge- and energy-transfer processes at polymer/polymer interfaces: A joint experimental and theoretical study.* Physical Review B: Condensed Matter and Materials Physics, 1999. **60**(8): p. 5721-5727.

99. Fahlman, M., et al., *Electronic structure of hybrid interfaces for polymer-based electronics.* Journal of Physics-Condensed Matter, 2007. **19**(18).

100. Bolinger, J., et al., *Are the Electronic Properties of Conjugated Polymers Deformable?* Science, submitted, 2008.

101. Guo, T.F., et al., *High-performance polymer light-emitting diodes utilizing modified Al cathode.* Applied Physics Letters, 2005. **87**(1): p. 013504.

102. Scheinert, S. and G. Paasch, *Fabrication and analysis of polymer field-effect transistors.* Physica Status Solidi a-Applied Research, 2004. **201**(6): p. 1263-1301.

103. Muratsubaki, M., et al., *Field-effect transistors based on poly(p-phenylenevinylene) derivatives.* Chemistry Letters, 2004. **33**(11): p. 1480-1481.

104. Zaumseil, J., R.J. Kline, and H. Sirringhaus, *Electroluminescence imaging and microstructure of organic light-emitting field-effect transistors.* Applied Physics Letters, 2008. **92**(7).

105. Grey, J.K., et al., *Size-dependent spectroscopic properties of conjugated polymer nanoparticles.* Journal of Physical Chemistry B, 2006. **110**(51): p. 25568-25572.

106. Yu, J., D.H. Hu, and P.F. Barbara, *Photophysics of conjugated polymers unmasked by single molecule spectroscopy.* Springer Series in Chemical Physics, 2001. **67**(Single Molecule Spectroscopy): p. 114-129.

107. Hu, D., J. Yu, and P.F. Barbara, *Single-Molecule Spectroscopy of the Conjugated Polymer MEH-PPV.* Journal of the American Chemical Society, 1999. **121**(29): p. 6936-6937.

108. Hu, D.H., et al., *Collapse of stiff conjugated polymers with chemical defects into ordered, cylindrical conformations.* Nature, 2000. **405**(6790): p. 1030-1033.

109. Yu, J., D. Hu, and P.F. Barbara, *Unmasking electronic energy transfer of conjugated polymers by suppression of O2 quenching.* Science (Washington, D. C.), 2000. **289**(5483): p. 1327-1330.

110. Vanden Bout, D.A., et al., *Discrete intensity jumps and intramolecular electronic energy transfer in the spectroscopy of single conjugated polymer molecules.* Science (Washington, D. C.), 1997. **277**(5329): p. 1074-1077.

111. Wu, C., et al., *Energy Transfer Mediated Fluorescence from Blended Conjugated Polymer Nanoparticles.* Journal of Physical Chemistry B, 2006. **110**(29): p. 14148-14154.

112. Szymanski, C., et al., *Single Molecule Nanoparticles of the Conjugated Polymer MEH-PPV, Preparation and Characterization by Near-Field Scanning Optical Microscopy.* Journal of Physical Chemistry B, 2005. **109**(18): p. 8543-8546.

113. Palacios, R.E., et al., *Charging and discharging of single conjugated-polymer nanoparticles.* Nature Materials, 2007. **6**(9): p. 680-685.

114. Chang, Y.-L., et al., *Electrogenerated Chemiluminescence of Single Conjugated Polymer Nanoparticles.* J. Am. Chem. Soc. submitted, 2008.

115. Apsys, user's manual and reference manual, version 2007.3, Crosslight Sofware Inc., 2004-2005.

116. *CRC Handbook of Chemistry and Physics*. 86th ed, ed. D.R. Lide. 2005, Boca Raton (FL): CRC Press.

117. Tokito, S., K. Noda, and Y. Taga, *Metal oxides as a hole-injecting layer for an organic electroluminescent device.* Journal of Physics D-Applied Physics, 1996. **29**(11): p. 2750-2753.

118. Arkhipov, V.I., et al., *Effect of doping on the density-of-states distribution and carrier hopping in disordered organic semiconductors.* Physical Review B: Condensed Matter and Materials Physics, 2005. **71**(4): p. 045214/1-045214/7.

119. Davids, P.S., I.H. Campbell, and D.L. Smith, *Device model for single carrier organic diodes.* Journal of Applied Physics, 1997. **82**(12): p. 6319-6325.

120. Kim, Y.G., et al., *Variable band gap conjugated polymers for optoelectronic and redox applications.* Journal of Materials Research, 2005. **20**(12): p. 3188-3198.

121. Ruhstaller, B., et al., *Transient and steady-state behavior of space charges in multilayer organic light-emitting diodes.* Journal of Applied Physics, 2001. **89**(8): p. 4575-4586.

122. Hill, I.G. and A. Kahn, *Organic semiconductor heterointerfaces containing bathocuproine.* Journal of Applied Physics, 1999. **86**(8): p. 4515-4519.

123. Matsusue, N., Y. Suzuki, and H. Naito, *Charge carrier transport in red electrophosphorescent emitting layer.* Japanese Journal of Applied Physics Part 1-Regular Papers Brief Communications & Review Papers, 2006. **45**(7): p. 5966-5969.

124. Crispin, X., et al., *Characterization of the interface dipole at organic/ metal interfaces.* J Am Chem Soc, 2002. **124**(27): p. 8131-41.

125. Sitch, C.D., D.A. Halliday, and A.P. Monkman, *Steady State Photoconductivity in Conjugated Polymers.* Materials Research Society Symposium Proceedings, 2001. **665**: p. C8.17.1-C8.17.5.

126. Barth, S., et al., *Extrinsic and intrinsic dc photoconductivity in a conjugated polymer.* Physical Review B, 1997. **56**(7): p. 3844-3851.

127. Morteani, A.C., et al., *Exciton regeneration at polymeric semiconductor heterojunctions.* Physical Review Letters, 2004. **92**(24): p. 247402.

128. Snaith, H.J., et al., *Charge Generation Kinetics and Transport Mechanisms in Blended Polyfluorene Photovoltaic Devices.* Nano Letters, 2002. **2**(12): p. 1353-1357.

129. Hoppe, H., et al., *Photovoltaic action of conjugated polymer/fullerene bulk heterojunction solar cells using novel PPE-PPV copolymers.* Journal of Materials Chemistry, 2004. **14**(23): p. 3462-3467.

130. Kim, K., et al., *Roles of donor and acceptor nanodomains in 6% efficient thermally annealed polymer photovoltaics.* Applied Physics Letters, 2007. **90**(16): p. 163511.

131. Kim, J.Y., et al., *Efficient Tandem Polymer Solar Cells Fabricated by All-Solution Processing.* Science, 2007. **317**(5835): p. 222-225.

132. Scholes, G.D. and G. Rumbles, *Excitons in nanoscale systems (vol 5, pg 683, 2006).* Nature Materials, 2006. **5**(11): p. 920-920.

133. Kroeze, J.E., et al., *Contactless Determination of the Photoconductivity Action Spectrum, Exciton Diffusion Length, and Charge Separation Efficiency in Polythiophene-Sensitized TiO2 Bilayers.* The Journal of Physical Chemistry B, 2003. **107**(31): p. 7696-7705.

134. Wong, W.-Y., et al., *Tuning the Absorption, Charge Transport Properties, and Solar Cell Efficiency with the Number of Thienyl Rings in Platinum-Containing Poly(aryleneethynylene)s.* Journal of the American Chemical Society, 2007. **129**(46): p. 14372-14380.

135. Arias, A.C., et al., *Vertically segregated polymer-blend photovoltaic thin-film structures through surface-mediated solution processing.* Applied Physics Letters, 2002. **80**(10): p. 1695-1697.

136. Chiesa, M., et al., *Correlation between Surface Photovoltage and Blend Morphology in Polyfluorene-Based Photodiodes.* Nano Letters, 2005. **5**(4): p. 559-563.

137. Shrotriya, V., et al., *Efficient light harvesting in multiple-device stacked structure for polymer solar cells.* Applied Physics Letters, 2006. **88**(6): p. 064104-3.

138. Peumans, P. and S.R. Forrest, *Separation of geminate charge-pairs at donor-acceptor interfaces in disordered solids.* Chemical Physics Letters, 2004. **398**(1-3): p. 27-31.

139. Hallermann, M., S. Haneder, and E. Da Como, *Charge-transfer states in conjugated polymer/fullerene blends: Below-gap weakly bound excitons for polymer photovoltaics.* Applied Physics Letters, 2008. **93**(5): p. 053307.

140. Ohkita, H., et al., *Charge Carrier Formation in Polythiophene/Fullerene Blend Films Studied by Transient Absorption Spectroscopy.* Journal of the American Chemical Society, 2008. **130**(10): p. 3030-3042.

141. Sariciftci, N.S., et al., *Photoinduced electron transfer from a conducting polymer to buckminsterfullerene.* Science, 1992. **v258**(n5087): p. p1474(3).

142. L.Onsager, Phys.Rev., 1938. **54**: p. 554.

143. Mihailetchi, V.D., et al., *Photocurrent generation in polymer-fullerene bulk heterojunctions.* Physical Review Letters, 2004. **93**(21): p. 216601.

144. Muller, J.G., et al., *Ultrafast dynamics of charge carrier photogeneration and geminate recombination in conjugated polymer : fullerene solar cells.* Physical Review B, 2005. **72**(19): p. 195208.

145. Yan, M., et al., *Spatially indirect excitons as primary photoexcitations in conjugated polymers.* Physical Review Letters, 1994. **72**(7): p. 1104.

146. Hilczer, M., S. Traytak, and M. Tachiya, *Electric field effects on fluorescence quenching due to electron transfer.* The Journal of Chemical Physics, 2001. **115**(24): p. 11249-11253.

147. Weller, A., *The Exciplex.* 1975, New York: Academic. 23-38.

148. Sreearunothai, P., et al., *Influence of Copolymer Interface Orientation on the Optical Emission of Polymeric Semiconductor Heterojunctions.* Physical Review Letters, 2006. **96**(11): p. 117403-4.

149. Lupton, J.M., C. Im, and H. Bassler, *Fast field-induced dissociation and recombination of optical excitations in a pi-conjugated polymer.* Journal of Physics D-Applied Physics, 2003. **36**(10): p. 1171-1175.

150. McNeill, J.D. and P.F. Barbara, *NSOM investigation of carrier generation, recombination, and drift in a conjugated polymer.* Journal of Physical Chemistry B, 2002. **106**(18): p. 4632-4639.

151. Bout, D.A.V., et al., *Near-field optical studies of thin-film mesostructured organic materials.* Accounts of Chemical Research, 1997. **30**(5): p. 204-212.

152. Douheret, O., et al., *Nanoscale electrical characterization of organic photovoltaic blends by conductive atomic force microscopy.* Applied Physics Letters, 2006. **89**(3): p. 032107.

153. Leever, B.J., et al., *Spatially resolved photocurrent mapping of operating organic photovoltaic devices using atomic force photovoltaic microscopy.* Applied Physics Letters, 2008. **92**(1): p. 103302.

154. Gesquiere, A.J., S.-J. Park, and P.F. Barbara, *F-V/SMS:A New Technique for Studying the Structure and Dynamics of Single Molecules and Nanoparticles.* The Journal of Physical Chemistry B, 2004. **108**(29): p. 10301-10308.

155. Fradkin, L., et al., *Factors Controlling Hole Injection in Single Conjugated Polymer Molecules.* Journal of Physical Chemistry A, 2009. **113**(16): p. 4739-4745.

156. Sandberg, H.G.O., et al., *Insulators and device geometry in polymer field effect transistors.* Organic Electronics, 2005. **6**(3): p. 142-146.

157. List, E.J.W., et al., *The role of keto defect sites for the emission properties of polyfluorene-type materials.* Synthetic Metals, 2003. **139**(3): p. 759-763.

158. X.H. Yang, F.J., D. Neher, P.V. Lawson, J.-L. Bréas, E. Zojer, R. Gütner, P. Scanduicci de Freitas, M. Forster, U. Scherf,, *Suppression of the Keto-Emission in Polyfluorene Light-Emitting Diodes: Experiments and Models.* Advanced Functional Materials, 2004. **14**(11): p. 1097-1104.

Vita

Kwang Jik Lee was born in Busan, Korea on May 07, 1976, the son of Sung Je Lee and Il Suk You. After graduating from the Busan Jung Ang High school in 1995, he started his undergraduate study in Korea University, Seoul, Korea on the same year. He graduated with a Bachelor degree of Science in Material Science and Engineering in 2002. During his undergraduate study, he had also served his military service for 30 months in the Republic of Korea Air Force (ROKAF) from 1997 to 1999. Before he went abroad for his Master study at Texas A&M University with funding from the government institute (Korea Science and Engineering Foundation (KOSEF)), he had one year research experience in the National Lab (Korea Institute of Science and Technology (KIST)) in Seoul, Korea. In 2003, He joined the Dr. H.-J Sue group in the Material division under the Mechanical Engineering Department at Texas A&M University, College Station, Texas. He completed his study with the Master degree of Science in Mechanical Engineering in 2005 and then entered his doctoral program in Material Science and Engineering of the University of Texas at Austin under the guidance of Prof. Paul F. Barbara.

Permanent address: 39-40 Dae yeon Dong, Nam Gu, Busan, Korea, 608-023

This dissertation was typed by Kwang-Jik Lee.